2019

Development, Validation, and Utilization, of a Long-term Nearshore Synthetic Wave Record

Sergio A. Pena
University of North Florida, sergiopd93@gmail.com

DEVELOPMENT, VALIDATION AND UTILIZATION OF A LONG-TERM NEARSHORE SYNTHETIC WAVE RECORD

By

Sergio Pena

A Thesis submitted to the Department of Civil Engineering

in partial fulfillment of the requirements for the degree of

Master of Science in Civil Engineering

UNIVERSITY OF NORTH FLORIDA

COLLEGE OF COMPUTING, ENGINEERING AND CONSTRUCTION

July 2019

The thesis "Development, Validation and Utilization of a Long-Term Nearshore Synthetic Wave Record" submitted by Sergio Andres Pena in partial fulfillment of the requirements for the degree of Master of Science in Civil Engineering has been

Approved by the thesis committee: **Date**

_____ _____

Dr. William R. Dally, Ph.D., P.E.
Thesis Advisor and Committee Chairperson

_____ _____

Dr. Don Resio, Ph.D.

_____ _____

Dr. Christopher J. Brown, Ph.D., P.E.

Accepted for the School of Engineering:

_____ _____

Osama Jadaan, Ph.D.
Director of the School of Engineering

Accepted for the College of Computing, Engineering, and Construction:

_____ _____

William Klostermeyer, Ph.D.
Dean of the College of Computing, Engineering, and Construction

Accepted for the University of North Florida:

_____ _____

John Kantner, Ph.D.
Dean of the Graduate School

DEDICATION

This thesis is dedicated to my family for their continued encouragement and motivation.

To Angela, thank you for always standing by my side. You constantly inspire me to become the best version of myself.

AKNOWLEDGEMENTS

I would like to express my gratitude to everyone who helped make this thesis a reality. I want to thank my supervisor, Dr. William Dally for his encouragement and guidance. Thank you for teaching me the importance of comparing "apples to apples," I am extremely grateful for your insight and your patience. A special thanks to Dr. Don Resio, Professor and Director of the Taylor Engineering Research Institute (TERI), whose support was instrumental to the completion of my master's degree. I would also like to thank Dr. Christopher Brown for serving on my master's thesis committee. I am extremely grateful for your helpful and meticulous feedback. A sincere thank you to Surfbreak Engineering Inc. and Dr. Zarillo at FIT for providing essential the essential data used in this thesis. Lastly, I want to thank everyone in the Coastal Engineering department at UNF, including Mrs. Hollis Klein and fellow graduate students, for valuable assistance and advice along the way. This study was funded by the Taylor Engineering Research Institute (TERI).

TABLE OF CONTENTS

LIST OF TABLES

LIST OF FIGURES

ABSTRACT

The need for a consistent and accurate production of long-term nearshore wave record is discussed. With multiple decades of offshore hindcasts and long, continuous data sets available, it is possible to create a nearshore synthetic wave record. The Brevard County coastline offers an area with a high quality 62-year long offshore hindcast, as well as an 11-year long and nearly continuous high-resolution nearshore wave record to compare with model performance. This thesis presents the steps in the development and performance of the synthetic nearshore wave record produced. A novel approach was used to compare, validate and calibrate this type of data which included using quantile-quantile plots and bin-averaged scatter plots. In a comparison between two reputable deep-water hindcasts (MSC50 and Wavewatch III), it was found that Wavewatch III significantly underpredicts wave heights in the higher range (>8m). At the nearshore STWAVE proves to be a simple, robust and fast way to create a nearshore wave record. Root mean squared error (0.272m-0.317m) and modified index of agreement (0.697-0.646) values for significant wave height show promising results for overall model performance with the currently available hindcast. Possible future improvements could be made by modifying the offshore hindcast to have finer grid resolution and further studying different friction models for the nearshore wave transformation model. Overall, the use of the MSC50 hindcast, to drive STWAVE at the nearshore, exhibits good agreement with ADCP data and analysis for significant wave heights can be used with confidence. Currently, no long-term trends can be resolved with the available record at the location used herein, yet more years of data/hindcasts in the future could provide more evident trends in wave climate change.

Chapter 1: Introduction and Background

1.1 The Need for Long-Term Nearshore Wave Information

The nearshore is generally defined as the region between the shoreline and the depth where waves induce sediment motion on the sea floor (Dean and Dalrymple, 2004). Wave information in this region is used on a regular basis by coastal engineers and scientists for, e.g. 1) design of coastal structures such as jetties, seawalls, groin fields, and breakwaters, 2) design and performance assessment of beach nourishment projects, 3) development of sediment budgets for inlet and shoreline management, 4) establishing Coastal Construction Control Lines (CCCLs) and in permitting of both upland construction and any erosion protection measures that may eventually be required, and 5) management of the coastal ecosystem and its natural resources. Lastly, wave records composed of multiple decades are needed in order to assess past changes in wave climate, and to provide insight into anticipated rise in sea level and changes in global storm climate.

1.2 Available Sources of Long-Term Nearshore Wave Measurements

In situ wave measurements can be collected using a variety of instruments, although the most common are wave-riding surface buoys (based upon accelerometer technology), usually deployed in relatively deep water. These buoys can collect detailed wave energy-frequency spectra, but generally can provide only coarse estimates of wave direction. Although buoys can operate in shallow water, nearshore wave measurements have typically been made using bottom-

mounted instruments, evolving through the years from initially lone pressure transducers (providing only frequency spectra), to combined pressure transducers and electromagnetic current meters, called 'PUVs' (providing frequency and coarse directional spectra), to linear arrays of multiple pressure transducers (providing high-resolution directional spectra). However, bottom-mounted pressure transducers are not capable of accurately resolving the higher frequencies in the wave spectrum. The advent of the Acoustic Doppler Profiler (ADP) in the late 1990s has revolutionized directional wave measurement, particularly in the nearshore because, although bottom-mounted, uses its acoustic technology to range all the way to the free surface. This enables the instrument to measure fully directional spectra at high frequency and directional resolution. ADP instruments also provide water level measurements and vertical profiles of the mean current.

There have been several notable efforts to collect continuous, long-term nearshore *in situ* wave data around the United States in the past, using the variety of instruments described above. Using surface buoys, the Coastal Data Information Program (CDIP) operated by the University of California at San Diego, began wave data collection in California around the 1970's and today includes buoys around the United States, with most stations on the West and East coasts and a few in the Gulf of Mexico (see https://cdip.ucsd.edu/m/deployment/station_view/). However, most buoys are in water deeper than 15 meters, and as such are not usually in the 'nearshore' as defined herein. The Florida Coastal Data Network (FCDN) operated by the University of Florida attempted to set up a series of bottom-mounted nearshore pressure transducers and PUV gauges along the Florida coast. By 1980 six units were installed and two more were proposed, some of which had collected at least 3 years of data (Howell, 1980). In 1986 the U.S. Army

Corps of Engineers deployed their 'Linear Array' of 15 pressure transducers along the 8m depth contour at the Field Research Facility in Duck, North Carolina (Long and Oltmans-Shay, 1991). Although there exists a significant gap in the record from February 2012 to June 2016, this remains the longest record of nearshore wave data in existence. The Florida Institute of Technology began a nearshore wave data collection program at Sebastian Inlet, Florida in 1996, which started with a PUV system and transitioned to an ADP in the early 2000's. However, there are significant gaps in the early wave record, particularly during winter months. Finally, as part of the Florida Coastal Forcing Project (FCFP) conducted by Surfbreak Engineering Sciences, Inc. (see Leadon, Dally, and Osiecki, 2004), a permanent ADP wave gauge station was installed in the nearshore (8.5 m depth, 615m from the beach) at Melbourne Beach, Florida. The station operated for more than 10 years, from August 2001 until November 2011, with a 94% data capture rate.

1.3 Long-Term 'Synthetic' Wave Records

All of these *in situ* data collection efforts were/are expensive to operate and maintain, and as mentioned most of the records contain significant gaps due to equipment breakdowns and/or lapses in funding support. Although several of these projects provided one or more decades of wave measurements, their records still are not of enough duration to be considered 'long-term'. In addition, directly measured wave information for a specific site is seldom available, and almost never collected for a for multiple decades. Due to this lack of measured nearshore wave data, 'synthetic' nearshore wave information is usually developed by transforming an archived deep-water wave 'hindcast' to shallow water at the site(s) of interest. This means that the accuracy of the nearshore wave record depends on 1) the reliability/validity of the model used to

generate the deep-water hindcast, 2) the veracity of the wind record used to drive the hindcast model, 3) the reliability/validity of the wave model used to transform the deep-water waves to the nearshore, and 4) the reliability of the bathymetry used by the nearshore wave transformation model. Different wave models may adopt different underlying physics and different numerical solution techniques, resulting in different nearshore wave records for simulations conducted at the same location. Because the improvement of both wave hindcasting and transformation models is ongoing, the procedure for producing nearshore wave information has not yet been standardized. The Florida Coastal Forcing Project (FCFP) began to address these issues by developing a consistent methodology for producing nearshore wave hindcasts for the Florida Coast, first described by Dally and Osiecki (2006). The purpose of this thesis is to develop, validate, and begin to utilize a sufficiently long-term (60^{+}-year) nearshore wave hindcast for Brevard County, Florida, based upon the procedures developed by Dally and Osiecki (2006) but now including several significant improvements.

1.4 Methodology to be Pursued

As indicated above, the methodology to be used in this study is to develop long-term nearshore wave information by utilizing a long-term offshore hindcast record to drive a wave transformation model to bring the waves to shallow water. Although data from deep-water wave buoys are available to drive the transformation model, 1) the buoy records are generally insufficient in length, 2) most buoys are non-directional and those that are so-equipped can only provide coarse directional estimates, 3) their records often contain lengthy gaps, particularly if the buoy breaks from its mooring during a storm event (just when the data are particularly important/useful), and 4) the buoys themselves are sparsely located and often a suitable one is

not available for a specific stretch of shoreline. Although artificial, most deep-water hindcast 'data' are 1) available in sufficiently long records, 2) validated to data from the buoys across the entire network and, more recently, satellite data, 3) available as fully directional spectra, and 4) consistently derived, continuous records. The wave transformation model is to be locally calibrated for energy losses due to bed friction using a limited amount of *in situ* measured nearshore wave data. Finally, the synthetic nearshore wave record is validated by comparing it to the remainder of the available nearshore measurements.

Selection of the Canaveral Bight as the location in which to develop and test the methodology will be discussed in Chapter 2. Chapter 3 will explore the available deep-water hindcasts in the region, and provide justification for selection of the Oceanweather, Inc. MSC/GROWFAB hindcast for driving the wave transformation model. The selection of the spectral wave transformation model, STWAVE^{+}, used to transform the deep-water wave record to the nearshore will be presented in Chapter 4. Model set-up and calibration of STWAVE^{+} for the Canaveral Bight will be presented in Chapter 5. In Chapter 6, validation of the nearshore synthetic wave record in comparison to the entire record from the FCFP station in Melbourne Beach is first demonstrated, and then supplemented by comparison to the Sebastian Inlet Tax District (SITD) wave data. Chapter 7 will provide analysis, sample applications, and discussion of the resulting long-term near shore synthetic wave record (NSWR), and summary and conclusions will be presented in Chapter 8.

Chapter 2: Selection of the Canaveral Bight for Development and Testing of the Nearshore Synthetic Wave Record Methodology

2.1 The Spessard Nearshore Wave Record

The major reason for selecting the Canaveral Bight in Brevard County, Florida (see Figure 2.1) as the test-bed for the NSWR methodology is the availability of the more than 10 years of nearly continuous, high-quality directional wave spectra from the FCFP site at Spessard Holland North Beach Park, for both calibrating the selected nearshore wave transformation model as well as validating the NSWR to the greatest degree possible. This data record was collected using an RD Instruments 1200 kilohertz Acoustic Doppler Current Profiler (ADCP), deployed near the sea floor on a water-jetted stainless-steel pipe installed on the 9m isobath. The ADCP 'burst' for 20 minutes at 2 hertz once every two hours starting at the top of the hour, as well as measuring water level (via pressure) and current profiles every 10 minutes. The ADCP was a 'real-time' system connected to a shore station via an armored steel cable that provided both power and communication, facilitating monitoring of its status. The shore station also supported a directional anemometer and barometer; however, these data records were approximately only 6½ years in length. Whenever a problem with the real-time ADCP system arose, a second instrument, operating in self-contained mode, was deployed as quickly as possible in order to maintain the data stream, while repairs were made to the real-time system.

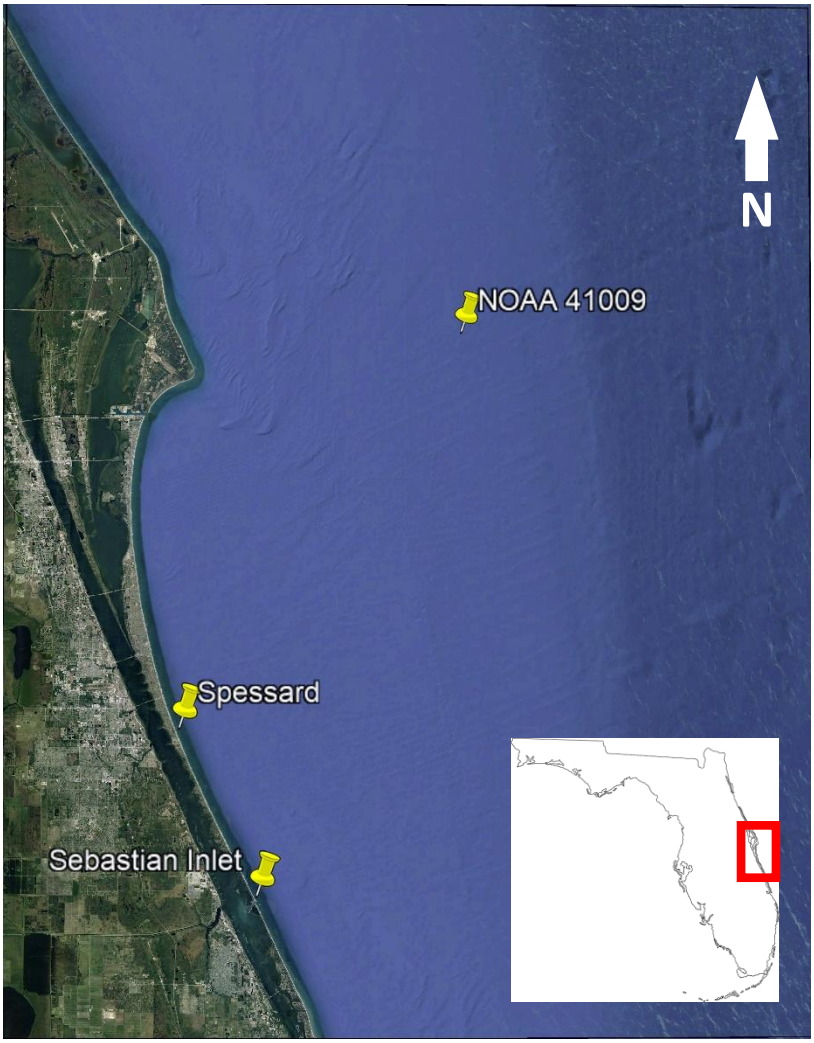

Figure 2.1 – Aerial view of the study area in the Cape Canaveral Bight (not to scale). Deepwater wave measurements are available from NOAA Buoy 41009 (1988 - 2019 in 42 m depth), and nearshore wave measurements are available from an Acoustic Doppler Profiler (ADP) located at Spessard Holland North Beach Park (September 2001 – October 2011 in 8.5 m mean depth), and from various instruments located at Sebastian Inlet (1997 - 2019 in 8.5 m mean depth).

2.2 The NOAA Deepwater Buoy Wave Record

The second benefit to utilizing the Canaveral Bight is the availability of wave and weather information from the nearby NOAA Buoy #41009 (shown in Figure 2.1). This buoy, located 20 nautical miles to the east of Cape Canaveral in 42 m water depth, provided a data record of (non-directional) deep-water wave measurements from 1988 to present. As will become apparent, these data serve a valuable role in establishing the veracity of the deep-water hindcasts available to the study, and in selecting the most appropriate hindcast.

2.3 Nearshore Wave Data Collection at Sebastian Inlet

A third justification for conducting the study in the Canaveral Bight is the availability of the nearshore wave data from the location immediately to the north of Sebastian Inlet (see Figure 2.2). Data collection was conducted here starting in 1996 using a PUV instrument manufactured by the Woods Hole Group, Inc. As noted in the introduction, the pressure response factor dictates that pressure fluctuations are reduced in magnitude through the water column depending on the wave height and frequency. Since high frequency energy is unable to reach the sea floor, energy-based significant wave heights (Hmo) reported are lower than the true significant wave height.

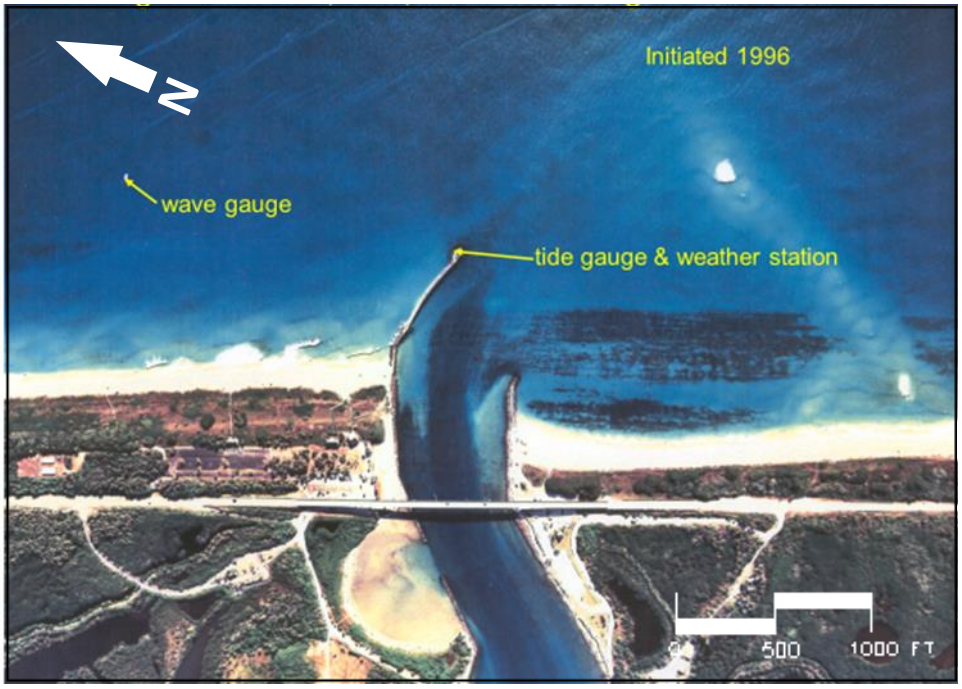

Figure 2.2 – Aerial view of the instrument locations at Sebastian Inlet.

These data provide insight as to the shortcomings of the earlier PUV technology. As a test of the new technology to be used by the FCFP, an ADCP was installed adjacent to the Sebastian PUV for approximately 2 weeks in March 2001, during which a strong nor'easter occurred. Comparison of the significant wave height reported by the two instruments, along with concurrent data from the NOAA buoy 41009 are presented in Figure 2.3. Two issues are immediately apparent. Firstly, significant wave heights are comparable between the PUV and the ADCP only when there is a large swell at the peak of the storm, but otherwise the PUV underpredicts during lesser sea states. For this reason, the Sebastian PUV data is not used for the validation of the methodology to be developed. Data collection was restarted at Sebastian in 2004 using two acoustic instruments, one Acoustic wave and current meter ('AWAC') and an 'Aquadopp' instrument, both manufactured by Nortek USA, Inc., and continued until 2010. A new AWAC system has been in use from 2011 until the present day. Data are collected every

three hours by sampling at 2Hz for 20 minutes at the top of every 3-hour period. These data will be used to supplement the validation of the NSWR methodology.

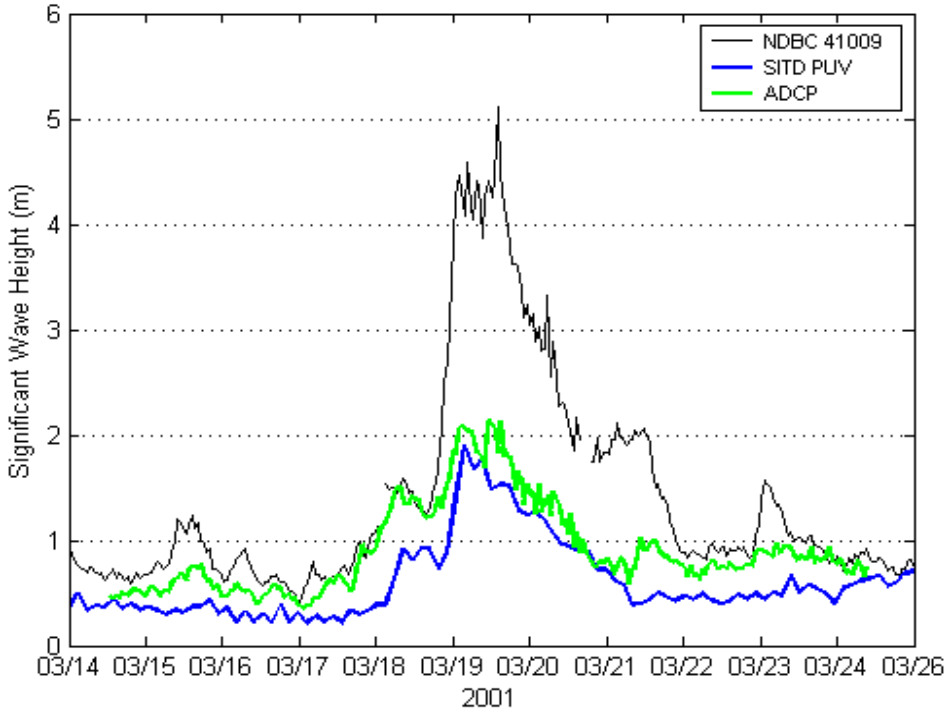

Figure 2.3 – Comparison of deep-water buoy measurements of energy-based significant wave height during a storm in March 2001 with those from a PUV wave gauge and an ADP that were collocated in the nearshore at Sebastian Inlet. Energy losses between deep and shallow water are clearly apparent, as well as the inability of the PUV to capture all wave energy except at the peak of the storm.

The second important issue, clear in Figure 2.3, is the dramatic loss in wave height between the deep-water NOAA buoy and the nearshore instruments, particularly during the peak of the storm. This has been shown to be due to energy losses due to bottom friction as the waves enter shallower water and highlights the necessity of rigorous calibration of the wave transformation model to be used in generating the NSWR.

Chapter 3: Selection of the Deep Water Hindcast

3.1 Deepwater Hindcast Options

Some of the most common deep-water hindcasts available in the Canaveral bight are the Army Corps of Engineers' Wave Information Study (WIS), NOAA's Wavewatch 3 driven hindcast (WW3), and Oceanweather's MSC50 hindcast. WIS is a resource made with compiled information from observations, multi-decade hindcasts and storm event archives (Army Corps of Engineers, 2019). Modeling efforts have improved and been updated since the beginning of this hindcast, the major downside being that updates, instead of being applied to the entire record, are simply appended to the end. The WaveWatch3 hindcast produced by NOAA-NCEP and is made in a consistent manner by using the same type of model and validation methods. There have been improvements to the model and domain so hindcast output is divided by the version of the Wavewatch model used and the version of the grid domain. The latest WaveWatch3 Hindcast information ranges from 2005 to present and is a multi-grid global model. This multi-grid domain includes a fine resolution grid along the Atlantic coast and started being used in 2005. From 2015 to present, a new version of Wavewatch3 is used but the multi-grid domain remains the same. This fine resolution grid that includes the Florida Coast is pictured in Figure 3.1.

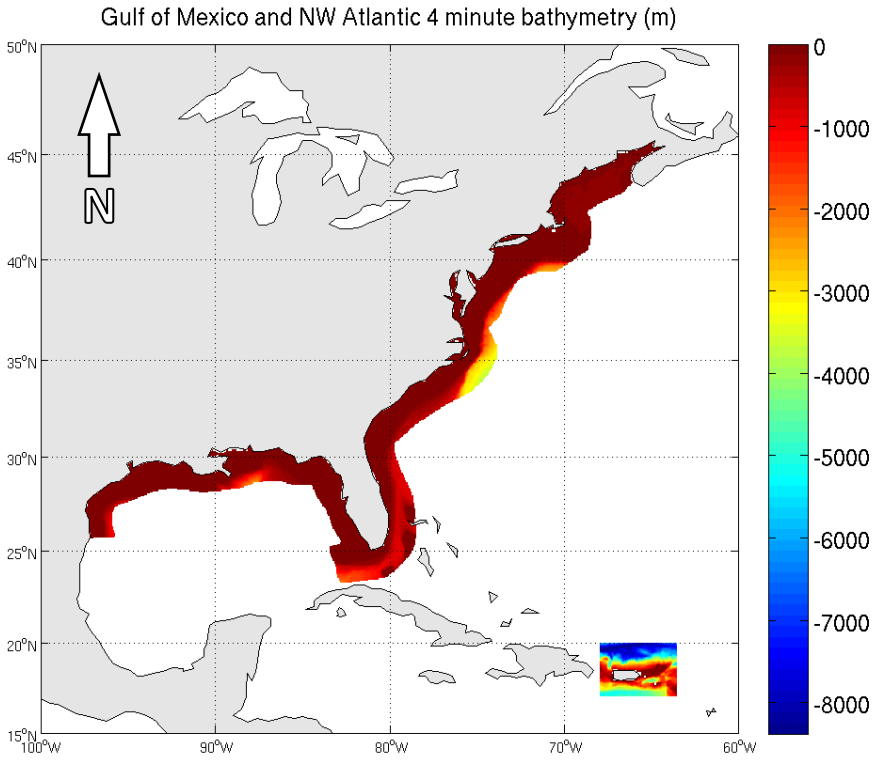

Figure 3.1 - US Eastern Coast fine resolution grid used in the WW3 multigrid set-up (NCEP, 2019)

The MSC50 hindcast uses a WAM (**WA**ve **M**odel)-like model and is produced by Oceanweather(Swail et al., 2006). The focus of this hindcast is the Canadian Coast of the North Atlantic but the domain covers the entire North Atlantic and includes the Florida Coast. Of the three hindcasts, the MSC50 is the most consistently produced hindcast with the longest date range which extends from 1954 to 2015. The MSC50 grid is shown in Figure 3.2.

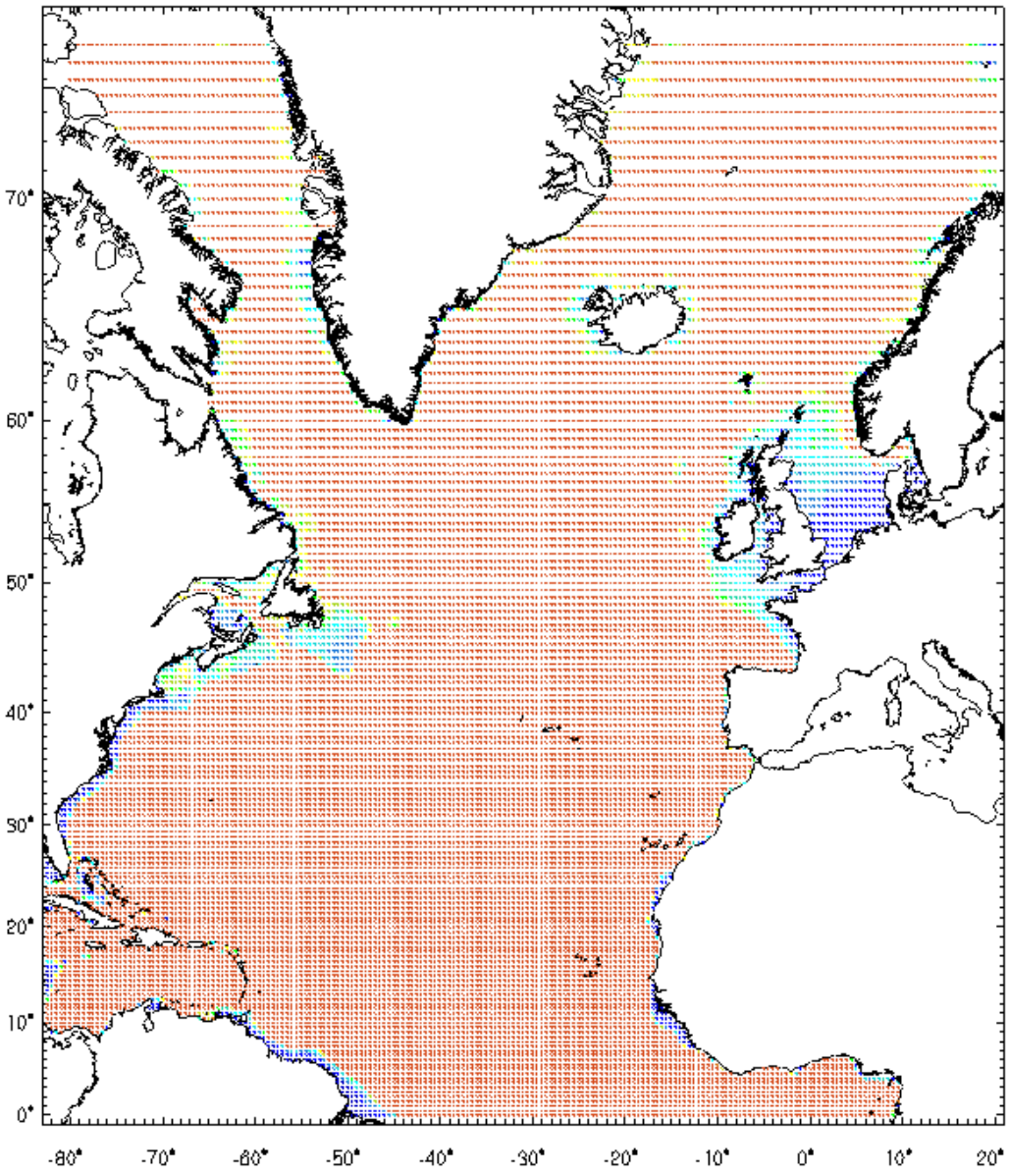

Figure 3.2 - Modeling domain used in the MSC50 hindcast production. (Swail et al., 2006)

In this study, the WW3 portion between 2005 and 2015 will be compared to the MSC50 hindcast. Both hindcasts are similar in that they cover the entire North Atlantic and run third generation spectral wave models.

Equation 3.1 shows the governing equation for third generation models. The left-hand side describes the evolution of the energy density in time and space where Cg represents the group velocity and E represents the variance spectrum. The right-hand side show the source terms: energy input (Sin), non-linear interactions (Snl), and dissipation (Sds).

$$\frac{\partial \mathrm{E}}{\partial \mathrm{t}} + \nabla \cdot \left(C_g E\right) = S_{in} + S_{nl} + S_{ds} \tag{3.1}$$

MSC50 is modeled using OWI-3G which follows the same physics and source terms as the WAM model (WAMDI Group, 1988) with some changes to the numerical implementation. The NOAA hindcast uses the Wavewatch 3 model (WW3DG, 2016). It is important to note that both models use the same formulation for non-linear wave interactions (Hasselmann and Hasselmann, 2002), this is what defines a 'third generation' model. The most significant difference between the two models is the difference in input winds. The WW3 hindcast uses the operational National Centers for Environmental Prediction (NCEP) winds from the Global Forecasting System (GFS) while the MSC50 hindcast uses refined reanalyzed winds with their Interactive Objective Kinematic Analysis (Swail and Cox, 2000). This reanalysis was done to address the systematic errors from NCEP wind fields.

3.2 Comparison to Buoy and ADCP Measurements

The figures 3.4 and 3.5 are scatter plots of the buoy data compared against the MSC50 and WW3 hindcasts. Both model results of significant wave height show fairly good results and have comparable error metrics. The error metrics used are defined in equations 3.1 – 3.5 as Root Mean Squared Error (RMSE), Pearson Correlation Coefficient (R), Bias, Scatter Index (SI), and the Modified Index of Agreement (MIA). In each of these equations M represents the modeled

hindcast results, O represents the observed data and N represents the number of observations. RMSE quantifies how much the model deviates from the data and SI represents how widespread these differences are. BIAS quantifies the existence of a consistent over prediction or underprediction of the model. R quantifies how close is the linear relationship between model results and observations. MIA quantifies, from 0 to 1, the overall agreement of the model results to the data with 1 meaning perfect agreement.

$$RMSE = \left[\frac{1}{N}\sum_{i=1}^{N}(M_i - O_i)^2\right]^{1/2} \quad . \quad . \quad . \quad (3.1)$$

$$\mathrm{R} = \frac{\sum_{i=1}^{N}[(M_i-\bar{M})(O_i-\bar{O})]}{\sqrt{\sum_{i=1}^{N}(M_i-\bar{M})^2}\sqrt{\sum_{i=1}^{N}(O_i-\bar{O})^2}} \quad . \quad .. \quad . \quad (3.2)$$

$$BIAS = \frac{1}{N}\sum_{i=1}^{N}(M_i - O_i) \quad . \quad . \quad . \quad (3.3)$$

$$SI = \frac{RMSE}{\sqrt{\overline{MO}}} \quad . \quad . \quad . \quad . \quad . \quad . \quad (3.4)$$

$$\mathrm{MIA} = 1 - \left\{\frac{\sum_{i=1}^{N}|\mathrm{O_i}-\mathrm{M_i}|}{\sum_{i=1}^{N}(|M_i-\overline{O_i}|+|O_i-\bar{O}_i|)}\right\} \quad . \quad . \quad . \quad (3.5)$$

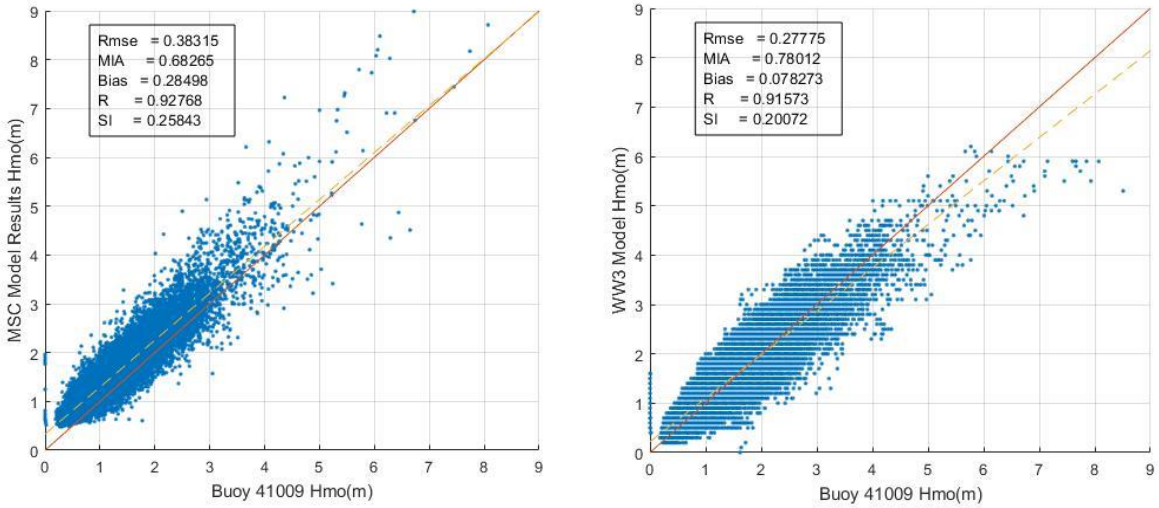

Figure 3.3 – Scatter plots comparing MSC and WW3 hindcasts to data from Buoy 41009 during the time period 2005-2015. The red line shows the ideal fit line and dashed line depicts the linear best fit line.

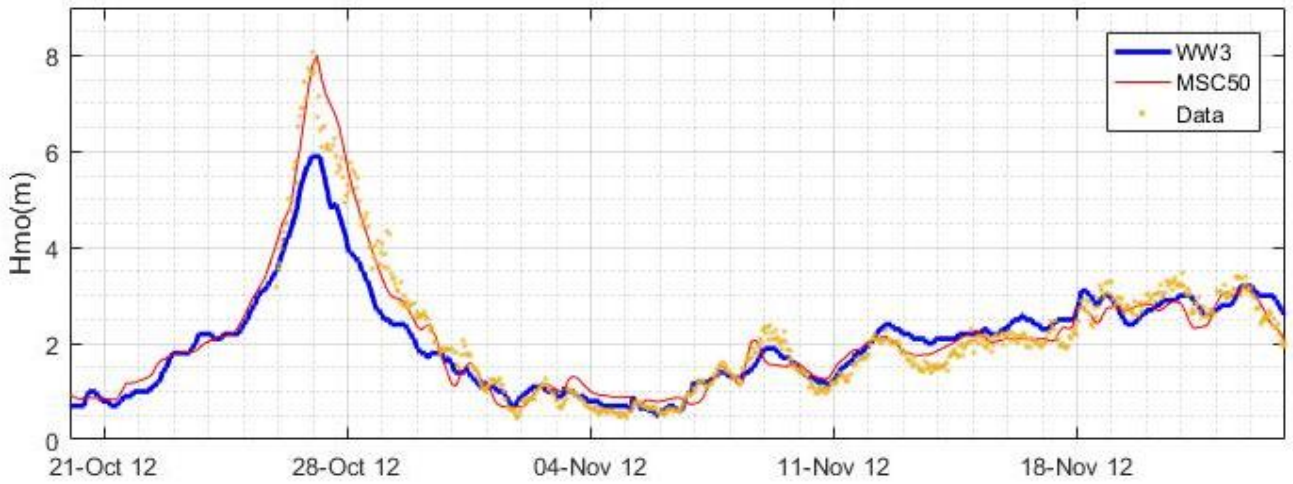

Figure 3.4 – Time series sample of the results for significant wave height from the MSC50 and WW3 hindcasts, in comparison to measurements from Buoy 41009. The peak shown was produced by Hurricane Sandy as it passed offshore.

The specific case in Figure 3.4 depicts the significant weight heights as Hurricane Sandy moved past the Florida Coast. This is one case in which WW3 under performs. Hurricane

waves can be difficult to estimate due to rapidly shifting wind fields (Panigrahi and Misra, 2010). Underpredictions from WW3 in a case like this might be attributed to the wind input resolution (1/2 deg), interpolation or proximity to the coast (Chawla, Spindler, and Tolman, 2013). This can also be caused by mistakes in the input wind field, which would support the need to reanalyze winds that cause extreme wave events as described by the kinematic wind analysis by Swail and Cox (2000).

In a study done by Dally (2018) the MSC50 hindcast was compared directly with measurements from an ADCP installed at the same location as the MSC node just offshore of St. John's County. Comparisons between the ADCP and the MSC50 directional spectra show that results follow the data very closely and recreate wave events in the record for the exception of a few instances. These instances show MSC overpredicting low frequency waves and under predicting high frequency waves. Additionally, MSC results at this location show over predicting of waves coming from the west and from the south. These issues are attributed to the coarseness of the grid and the node's proximity to the coast.

3.3 Final Selection of MSC50 and Analysis

When comparing the two hindcasts against the data from Buoy 41009, the MSC and WW3 show comparable good results. Table 3.1 summarizes the statistics for the significant wave heights of the two offshore hindcasts.

Table 3.1 – Statistics for Offshore Hindcast comparison to Buoy 41009 data

Offshore Hindcast v Buoy 41009					
	RMSE(m)	R	Bias(m)	MIA	SI
MSC	0.383	0.928	0.285	0.683	0.258
WW3	0.278	0.916	0.078	0.780	0.201

WW3 seems to be a better fit with lower rms error and higher index of agreement, but these because these parameters are highly influenced by the, more prominent, lower energy waves, it is essential to visually verify the hindcast. A closer look at the higher wave heights on the scatter plots show that there seems to be some systematic errors. It is very evident from the bin averaged scatter plots in figure 3.5 that there is a significant underprediction of the higher wave events for WW3. It is possible these errors may be addressed with the newest releases of the hindcast as it continues to change and improve.

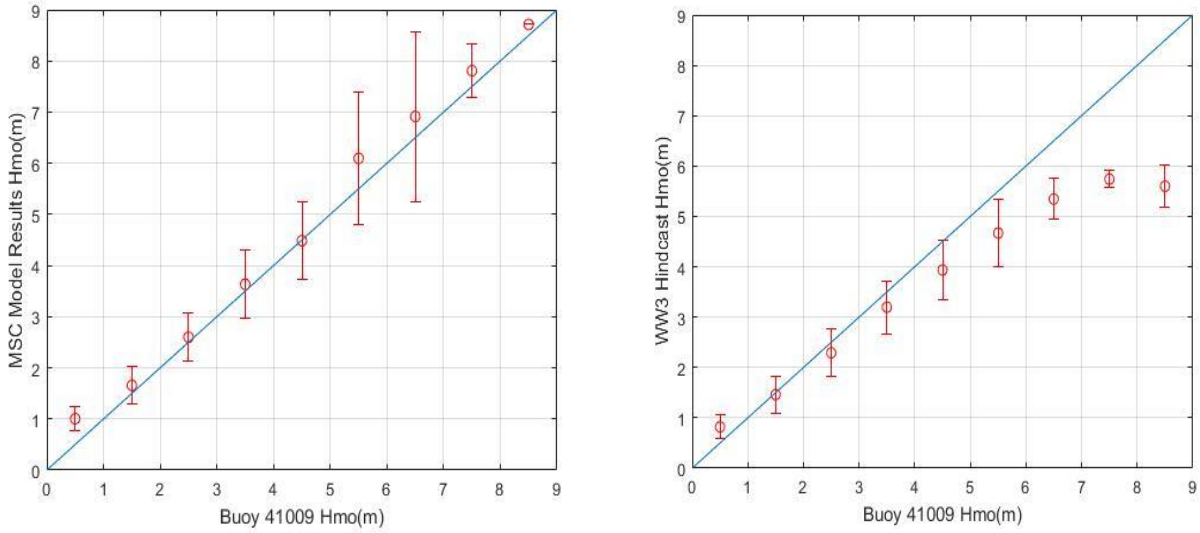

Figure 3.5 – Bin-averaged scatter plots of MSC and WW3 hindcasts compared to Buoy 41009 data. The data/model results have been averaged into 1m bins. The bars represent one standard deviation within the bin average.

The extreme wave events are important when considering extreme value analysis and a long range of time is instrumental for the purposes of a nearshore wave record. Although the MSC50 hindcast has a higher scatter index and rms error, the scatter plots show it captures waves in the higher range and, like WW3, it performs very well in lower wave heights. Another advantage to the MSC50 is the 62 years that were produced in a consistent manner from 1954 to 2016. For these reasons the MSC50 hindcast was chosen as the input to produce the nearshore wave record.

The MSC50 hindcast is studied further by isolating data points into eight different cases. Each case is dependent on the wave direction and wind direction of the buoy data. Figure 3.6 shows the breakdown of the directional windows used to categorize the data, a specific direction

specifies where the wind or waves are ‘coming from’. The largest window being ‘Offshore’ is defined between 160 and 340. The other three are 60-degree windows: ‘From the South’ is defined between 160 and 100 degrees, ‘From the North’ between 340 and 40 degrees, and ‘Onshore’ between 40 and 100 degrees.

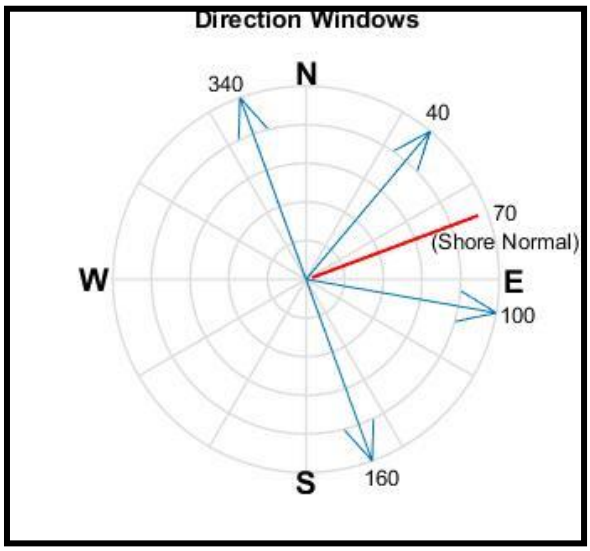

Figure 3.6 – The directional windows used in categorizing the wave data (oceanographic convention).

In the following figures the MSC50 significant wave height results are categorized based on the wind or wave directions at which the data was collected, results are displayed on their respective scatter plots. This categorization of hindcast data shows in what cases the hindcast may be under/over predicting. The wave height scatter plots categorized by wind direction are shown in Figure 3.7 and Table 3.2 summarizes the error metrics for these results.

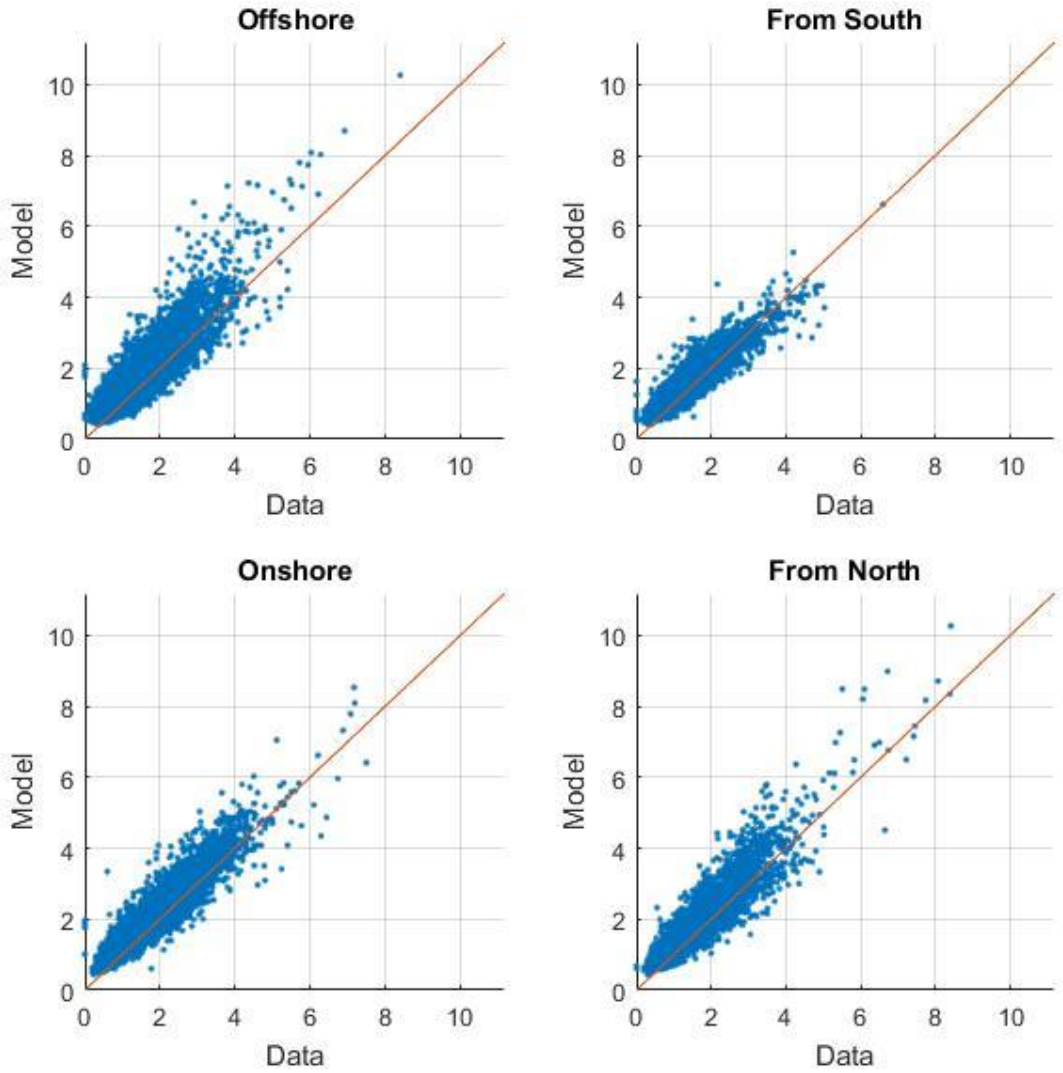

Figure 3.7 – Significant wave height from the MSC hindcast compared to Buoy #41009 categorized by wind direction.

Table 3.2 – Statistics of MSC hindcast categorized by wind direction

MSC Categorized by Wind Direction					
	RMSE (m)	MIA	BIAS (m)	R	SI
Offshore	0.402	0.629	0.301	0.906	0.303
From South	0.307	0.681	0.224	0.927	0.236
Onshore	0.369	0.745	0.253	0.939	0.208
From North	0.409	0.710	0.272	0.922	0.242

Overall, results show similar error metrics with the lowest model agreement when the data winds are pointed offshore with a correlation coefficient of 0.906, rms error of 0.402m and a bias of 0.301.

The same analysis is done using wave direction to categorize the data. The wave height scatter plots categorized by mean wave direction are shown in Figure 3.8.

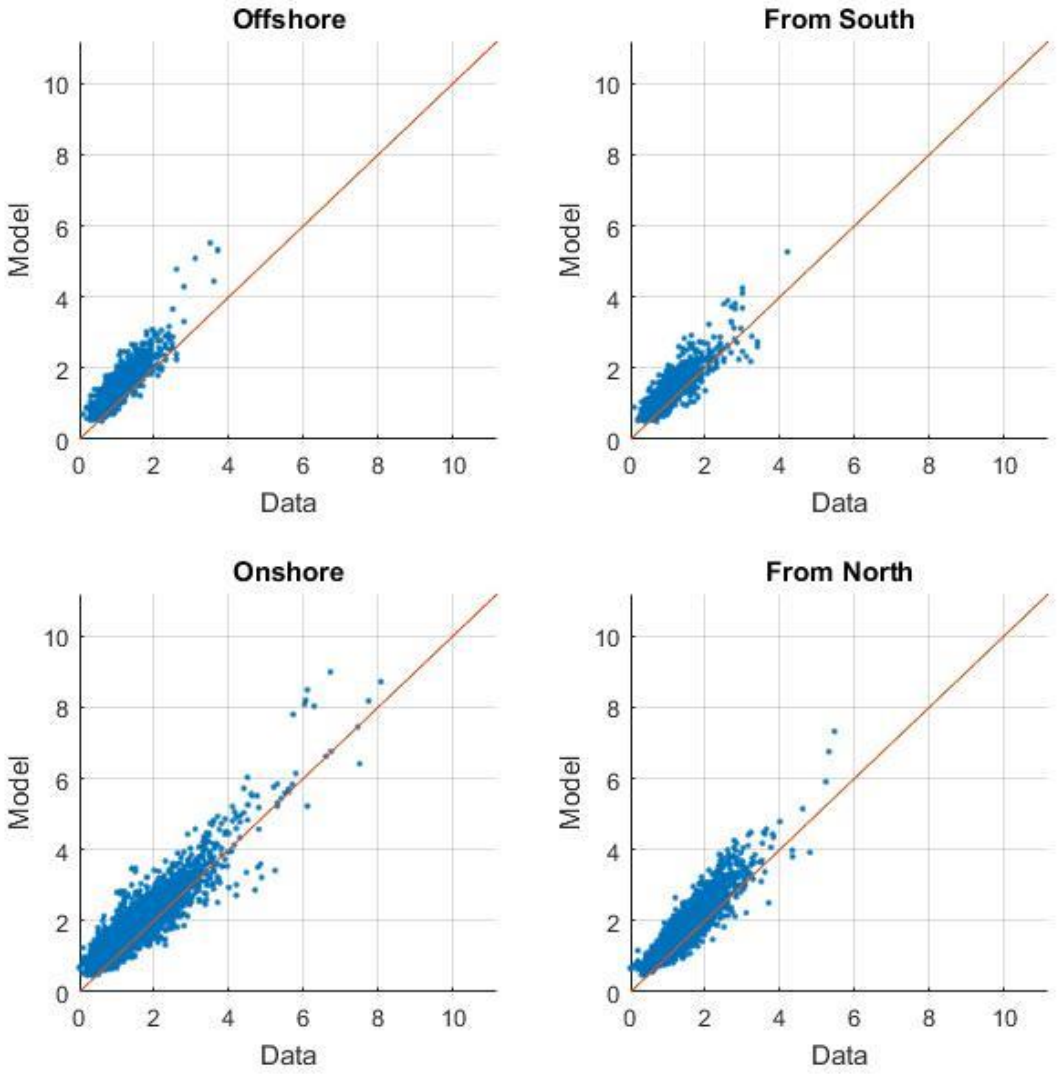

Figure 3.8 – Significant wave height from the MSC hindcast compared to Buoy #41009 categorized by wave direction.

Table 3.3 – Statistics of MSC hindcast results categorized by mean wave direction

MSC Categorized by Wave Direction					
	RMSE (m)	MIA	BIAS(m)	R	SI
Offshore	0.501	0.527	0.420	0.896	0.376
From South	0.381	0.603	0.286	0.884	0.311
Onshore	0.392	0.650	0.301	0.928	0.282
From North	0.439	0.664	0.325	0.918	0.262

Again, all directions have similar performance metrics with the best performance coming from onshore waves. The 'offshore' direction has the lowest model agreement of 0.527 and the greatest rms error 0.501. This supports the claims (Dally, 2018) that near the coast, the MSC hindcast performs best when winds and waves are moving toward the shore.

Chapter 4: Selection of the Spectral Wave Model for Nearshore Wave Transformation

4.1 Wave model options

Three commonly used models are available to simulate nearshore wave transformation, these include MIKE21 (DHI, 2014), SWAN (Booij, Ris, & Holthuijsen, 2002), and STWAVE (Smith et al., 1999). All three models use wave action balance to model the transformation of wave spectra. This is very similar to the energy balance that offshore wave generation models use Equation 3.1, but it is solved for wave action rather than energy. The equation 4.1 shows the relationship between wave energy density and action density, where N is the wave action density, E is the energy density and σ the wave frequency.

$$N = \frac{E}{\sigma} \tag{4.1}$$

MIKE21 and SWAN both solve for wave action density in time and space in their options to run as a fully spectral like a third-generation model. Both models also have an option to run using parameterization of the wave action equation like second generation models. These two models are full plane models, meaning they simulate waves from all directions which is advantageous when modeling waves in a bay or a similar body of water. STWAVE is a steady-state half-plane model that solves for action density along backward traced wave rays. The steady state nature of this model simplifies the computation since the temporal part of the equation is not needed.

4.2 Selection Criteria

For this study, the selection criteria for choosing the nearshore model are: accuracy, ease of use, stability, and computation time. All three models have been compared in a study by Fonseca, Gonçalves, & Soares (2017). The study shows that all three models perform similarly and are statistically comparable. If they are carefully calibrated and studied, the full plane models are very useful, yet it is very common to encounter numerical instabilities leading to inaccuracies while using the SWAN model (Zijlema & van der Westhuysen, 2005). Of the three models, STWAVE is the simplest to implement since there is no tuning coefficients, this also makes the model very stable.

These features in STWAVE make it robust, easy to implement and time efficient. In a study that compared the two models, computer time required for STWAVE was 80% less than that of a SWAN simulation on the same domain (Gonçalves, Rusu, & Soares, 2015).

4.3 Final Selection of STWAVE+

STWAVE was the model of choice to simulate the nearshore results because of its robustness and time efficiency. This study used STWAVE^{+}, a modified version of STWAVE that includes a simple bottom friction model simulating bed stress with equation 4.2. In this equation, $\vec{\tau}$ represents the turbulent shear stress, ρ is the density of water, Cf is the friction coefficient, and $\vec{u}$ is the velocity immediately outside the bottom boundary layer.

$$\vec{\tau} = \rho\, C_f \vec{u}\, |\vec{u}| \tag{4.2}$$

The predecessor to this study used this formulation for bottom friction and obtained the bottom friction coefficient using data available from the dissipation between offshore and nearshore ADCP measurements (Dally & Osiecki, 2005). In their study, Dally and Osiecki calibrated the bottom friction using a screening threshold of an estimated dissipation rate per planform area. Although the best bottom friction coefficient was found to be 0.026, this value is recalibrated using a different approach which includes an entire year of data and model simulations.

Chapter 5: STWAVE+ Set-Up and Calibration for Wave Energy Losses due to Bed Friction

5.1 Configuration of STWAVE+ for the Canaveral Bight

A set of nested grids were set up to take the offshore information and transform it to the nearshore. The offshore domain is an 86x244 grid with a 500m resolution and the nearshore domain is 183 x 610 grid with a 150m resolution. This replicates the setup produced for the Florida Coastal Forcing Project.

Winds and wave spectra from the MSC50 hindcast were applied to the nearshore grid. Wave spectra were assumed to be uniform at the offshore edge of the grid. Similarly, winds were assumed to be uniform across the model domain. Tidal adjustment was made using the Trident Pier NOAA CO-OPS station. The bottom friction grid is assumed to have a uniform sandy bottom with a uniform bottom friction coefficient. Lastly, the bathymetry files were produced using data from NGDC (National Geophysical Data Center). Figure 5.1 shows the nested grids and bathymetry used for the model.

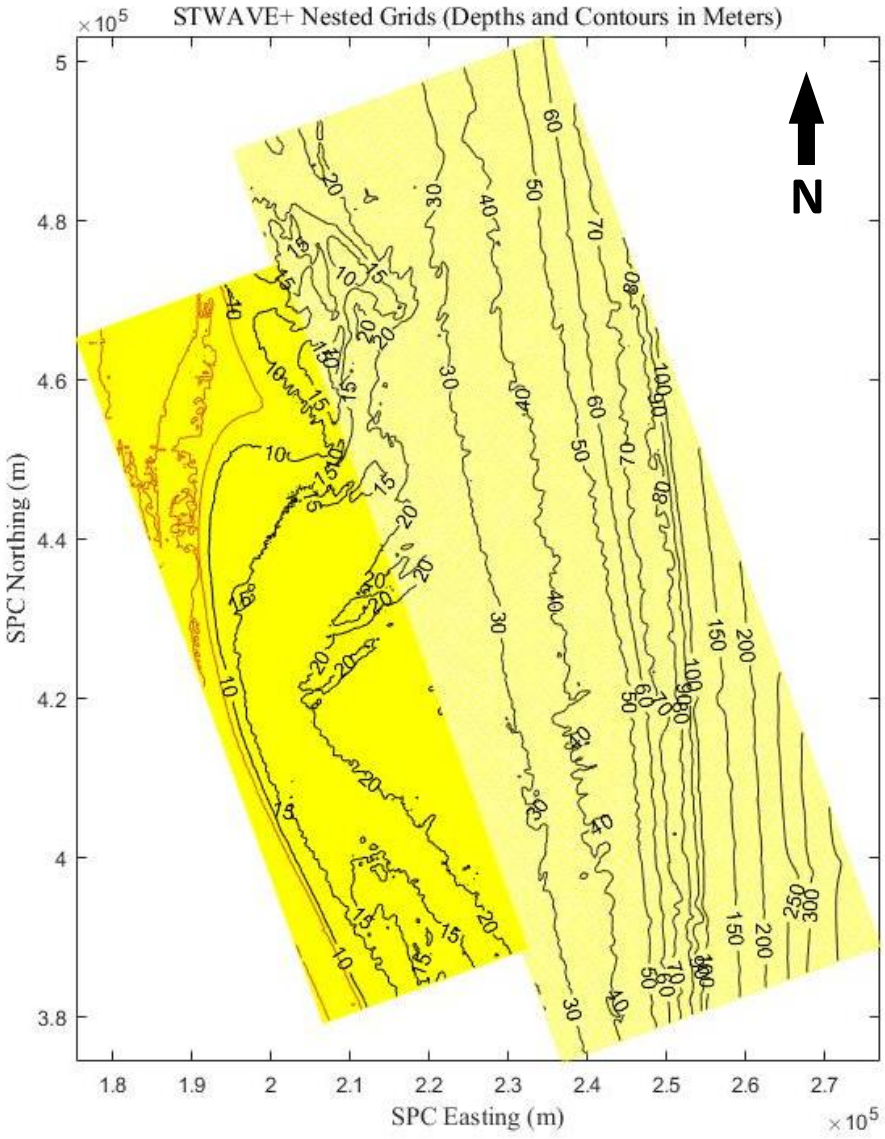

Figure 5.1 – Conjoined grids used in the STWAVE^{+} wave transformation modeling, projected in the state Plane Coordinate System (NAD83). The offshore grid has a 500m resolution, whereas the nearshore grid has a 150m resolution. Contours are mean water depths in meters.

Since STWAVE is a half plane model, only wave energy propagating in the onshore direction is simulated. Therefore, input spectra must be trimmed to the 175-degree window in

the shore-normal direction and interpolated to 5-degree angle bands. Frequency bins were kept the same as the input spectra from the MSC50 spectra.

5.2 Calibration Using Spessard ADCP Data

Calibration for the friction model was performed by running STWAVE+ with four different friction coefficients, each run was compared to data from the 2004 year. The first run was simulated with no bottom friction. The other three runs used 0.01, 0.015, and 0.02 as the friction coefficients. High wave energy was needed for the calibration since these are the waves that are affected the most by bottom friction. Since 2004 had a very active hurricane season with large swell affecting the area of study, this year was chosen to calibrate the bottom friction. Scatter and Q-Q plots were produced to visualize the performance of each run and error metrics were calculated. The following figures show scatter plots and quantile plots for the different runs used to calibrate the nearshore STWAVE+ model.

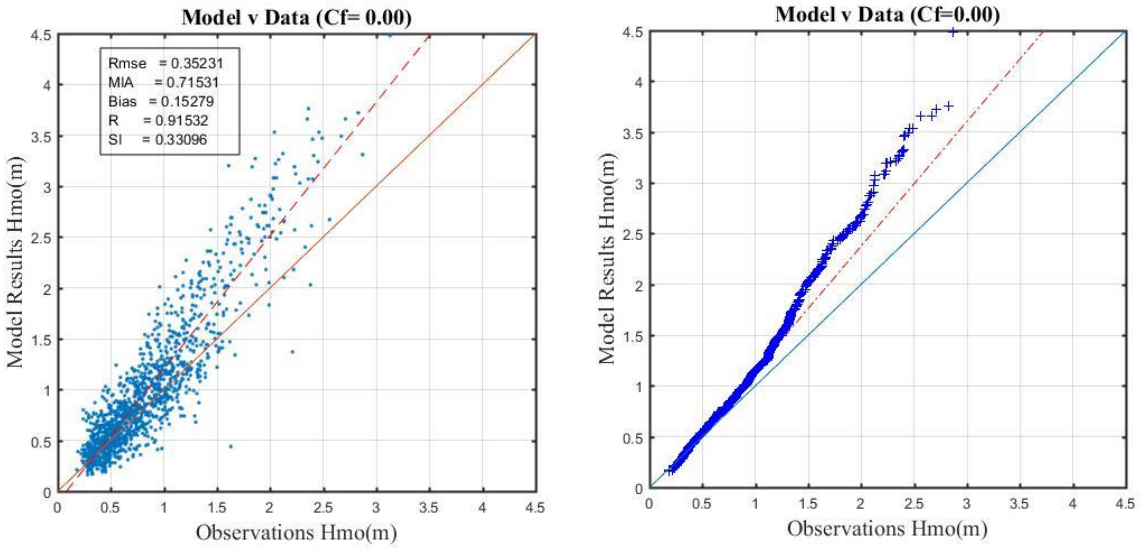

Figure 5.2 – Scatter plots and Quantile-Quantile plots of STWAVE^{+} results, without losses due to bottom friction ($C_f = 0$), versus the Spessard ADP measurements for 2004 (model calibration year). The solid line represents perfect agreement and the dashed line is the linear best-fit.

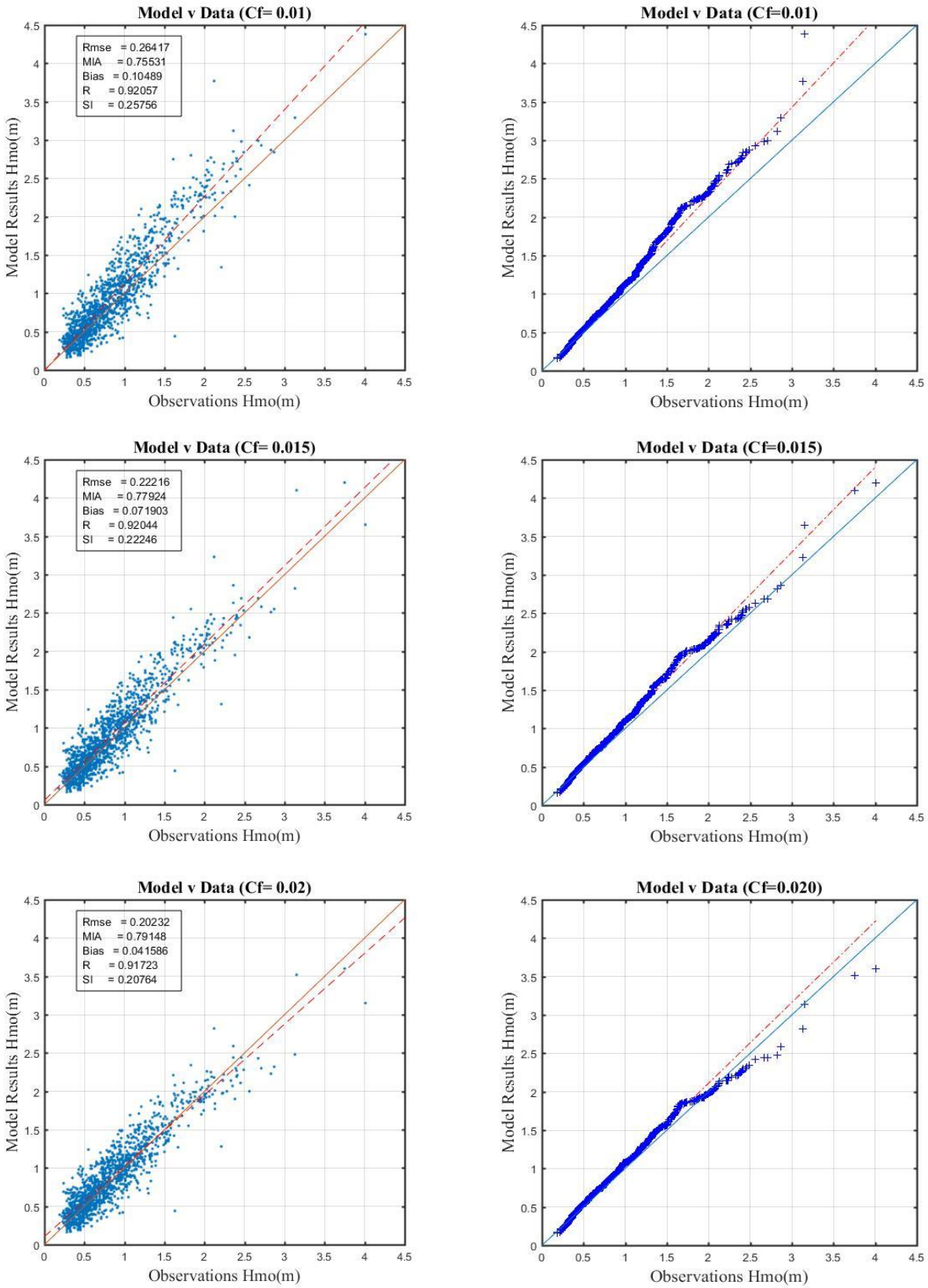

Figure 5.3 – Scatter plots and Quantile-Quantile plots of STWAVE^{+} results for $C_f = 0.01$, 0.015, and 0.02 as bottom friction coefficients, versus the Spessard ADP measurements for 2004 (model calibration year). The solid lines represent perfect agreement, and the dashed lines are linear best-fits.

Table 5.1 – Statistics for calibration runs.

Calibration Runs						
Run #	Cf	RMSE (m)	R	BIAS (m)	MIA	SI
1	0.000	0.352	0.915	0.153	0.715	0.331
2	0.010	0.264	0.921	0.105	0.755	0.258
3	0.015	0.222	0.920	0.072	0.779	0.222
4	0.020	0.202	0.917	0.042	0.791	0.208

Without bottom friction, the model significantly over estimates the data with an overall bias and exceeding values by up to two meters in larger wave events demonstrating the need for bottom friction. The three different tests show that as you increase the friction coefficient RMSE, SI values improve. From the scatter plots and statistics, the run with a coefficient of 0.02 shows the least amount of rms error and scatter index with 0.202 and 0.208 respectively. Moreover, using a coefficient of 0.015 shows very similar numbers with a rms error of 0.222 and a scatter index of 0.222. The q-q plots show that using 0.02 begins to under estimate large values, because of this no larger coefficients were studied. A time series of a large wave event is used as a visual verification since the calculated values are heavily influenced by the bulk of the data points in the lower range. Figure 5.4 shows the time series of significant wave heights from Hurricane Jeanne and the comparison between coefficients 0.020 and 0.015. The run with a coefficient of 0.015 captures the peak wave energy better than the run with the 0.020 coefficient. Figures 5.5 and 5.6 show more peaks within the year used in calibration.

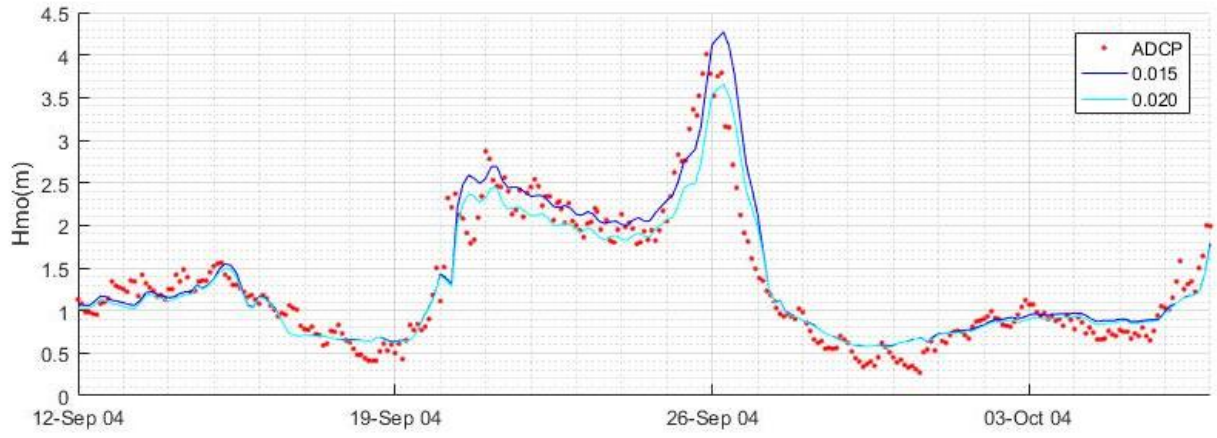

Figure 5.4 – Sample time series of STWAVE^{+} results using $C_f = 0.015$ and $C_f = 0.020$ compared to Spessard ADCP data during Hurricane Jeanne, September 21-27, 2004, showing the underprediction by using $C_f = 0.020$.

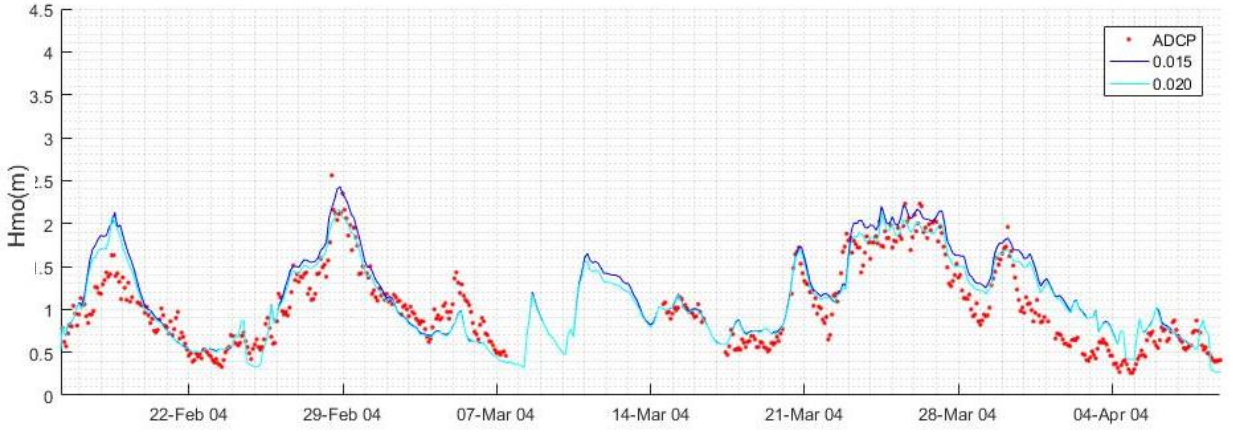

Figure 5.5 – Sample time series of STWAVE^{+} results using $C_f = 0.015$ and $C_f = 0.020$ compared to Spessard ADCP data between Feb. and Apr. 2004, showing several other peaks, most likely nor'easters, in the record where both coefficients have almost identical results.

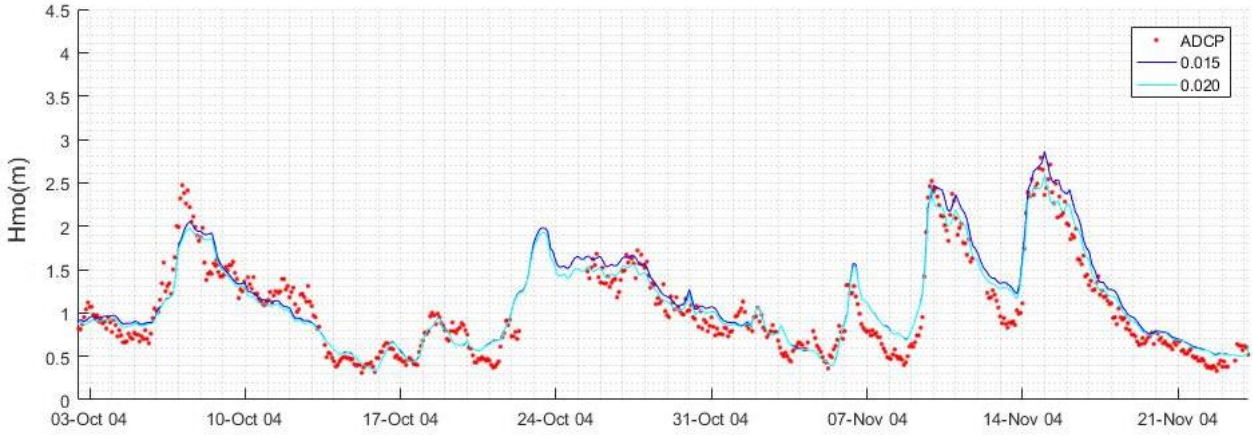

Figure 5.6 - Time series of results using Cf= 0.015 and Cf= 0.020 compared to Spessard ADCP data between Oct. and Nov. 2004, showing additional peaks where both coefficients have similar results.

The time series show that bottom friction has a smaller effect on lower energy seas so there is a small difference between the two model runs. This highlights the importance of extreme wave events, like Hurricane Jeanne, in the process of calibrating bottom friction.

With the given statistics, q-q plots and time series the calibration runs show that 0.015 is a good value to use since 0.020 begins to under predict values in the higher range. This is confirmed further in the following chapter.

Chapter 6: Validation

To validate that the model is appropriately calibrated, results are compared with the data that was not used for calibration (2001-2003 and 2005-2011). Hmo is compared one more time between the two best performing friction coefficients. Along with the previous figures, the scatter plots in Figure 6.1 show that using 0.020 as the friction coefficient dampens too much of the energy in large wave events. Table 6.1 shows the error metrics calculated from the validation results.

Table 6.1 – Statistics for comparing Cf= 0.015 and Cf= 0.020 using the validation data set (2001-2003, 2005-2011)

Cf	RMSE(m)	R	BIAS(m)	MIA	SI
0.015	0.272	0.861	0.132	0.697	0.278
0.020	0.251	0.859	0.104	0.712	0.262

Like in the calibration data, Cf=0.015 and Cf=0.020 had very similar values for correlation, index of agreement and scatter index but, once again, the q-q plots show that 0.020 under estimates values in the higher range. It is unclear, from studying these values, which is the better coefficient of friction until the scatter data is plotted. This further emphasizes the importance and utility of including scatter and q-q plots in the analysis.

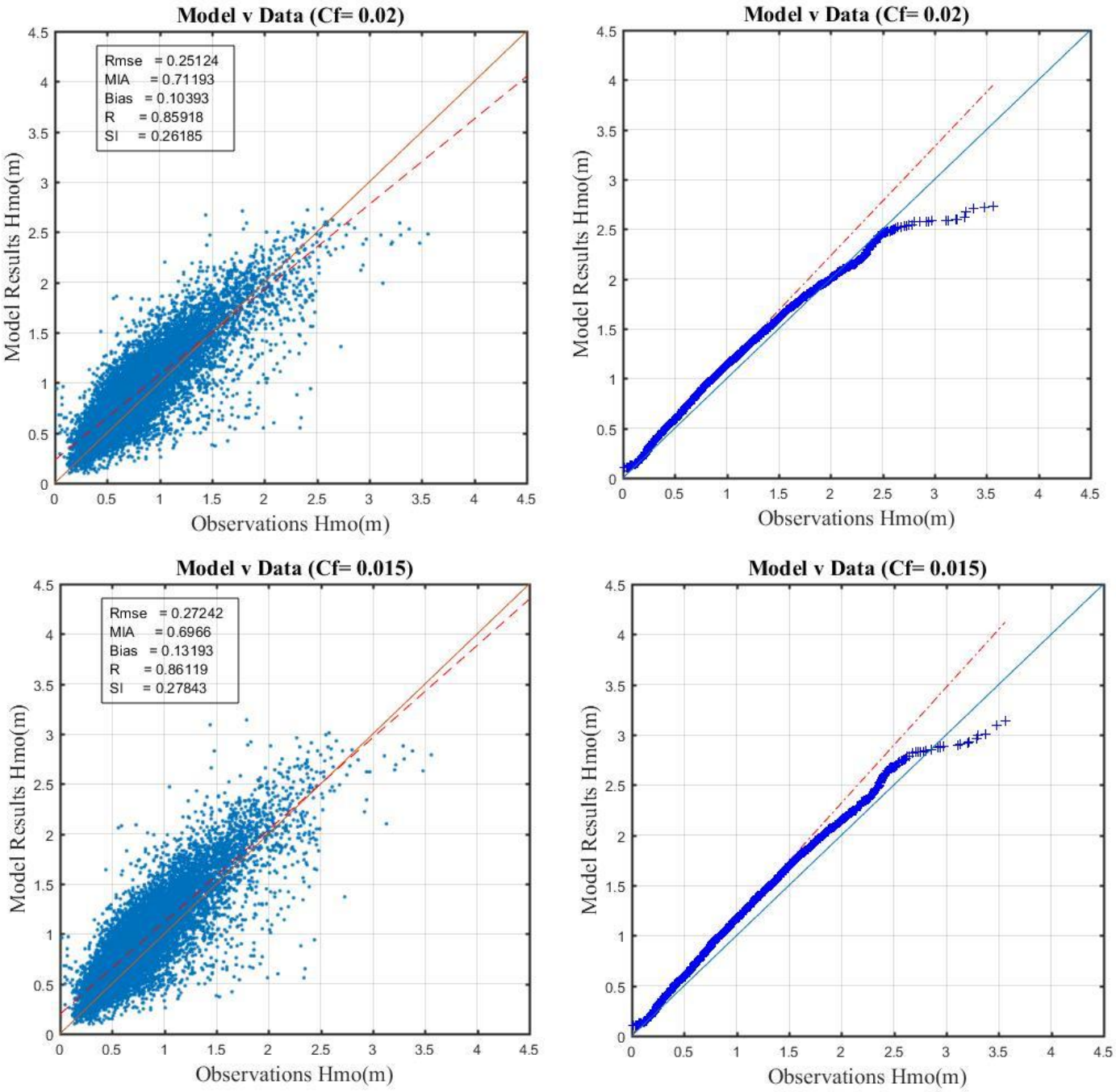

Figure 6.1 – Scatter Plots and Quantile-Quantile plots for results using Cf = 0.015 and Cf = 0.020. The solid lines represent the perfect agreement line and the dashed lines are the linear best fit line. Results are compared to Spessard ADCP data collected between 2001 and 2011 excluding 2004.

Figure 6.2 shows the Hmo time series of two notable swell events in 2011. The first is Hurricane Sandy with a peak around August 26, the second is Hurricane Katia with a peak around September 9. Hurricane Sandy reinforces the case for using 0.015 as the friction coefficient. The Hurricane Katia swell is an anomaly in the record that was picked up by the offshore, nearshore models and in the Sebastian inlet ADCP, but the swell did not register on the ADCP data from Spessard. An in-depth investigation should be performed on this anomaly as it is only isolated to this event.

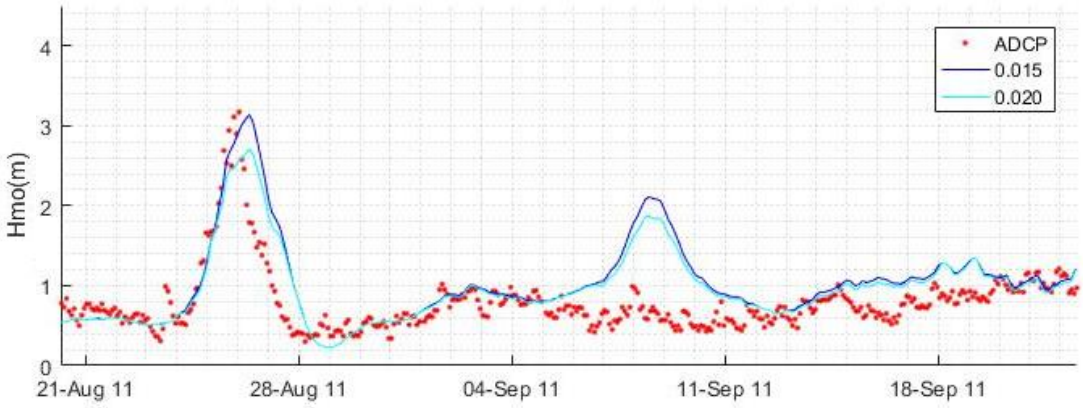

Figure 6.2 - Time series of results using $C_f = 0.015$ and $C_f = 0.020$ compared to Spessard ADCP data. The first storm peak depicts Hmo during Hurricane Sandy, and the second depicts Hurricane Katia (a solitary anomaly in the data record.)

Although 0.02 has better statistics, the Q-Q plots and bin averaged plots show that 0.015 has a better agreement during large wave events in the wave record. Therefore 0.015 is a good medium between having relatively good statistics and capturing the peaks in the data. Because

of this, the following analysis and discussion will use the simulation that had 0.015 set as the coefficient of friction while noting that medium range waves may be slightly over estimated.

The nearshore synthetic wave record was then validated against the long-term data record collected by FIT near Sebastian Inlet. Figure 6.3 shows the comparison of model to the FIT data. Statistics show that the model underperforms in this location and this can be attributed partly to the data having 'noise' at two times in the record. This comparison resulted with a relatively large scatter index of 0.336, a root mean squared error of 0.317 and a modified index of agreement of 0.646.

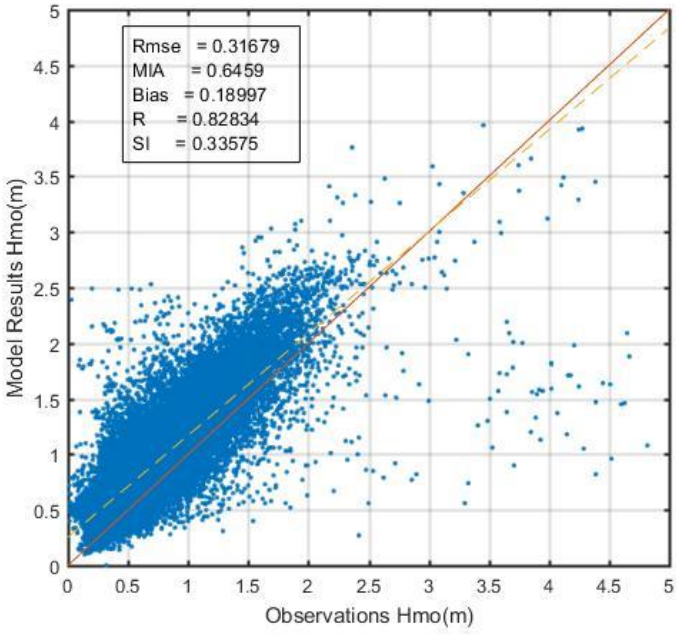

Figure 6.3 – Scatter plot of model results using C_f= 0.015 compared to ADP data available at Sebastian Inlet. The solid line represents perfect agreement and the dashed line is the linear best-fit. Scatter plot exhibits similar behavior to the comparison in Spessard, with similar error metrics. Data points that appear to severely under predict represent an anomaly in the data record.

Figure 6.4 below displays the instances where the model appears to severely under estimate the observations. It is important to note that this apparent 'noise' only occurs twice in this data record and both are pictured. Although the data record is useful to validate some of the model results, it is evident that the data set needs further quality control, therefore only figures and error metrics are generated for significant wave height.

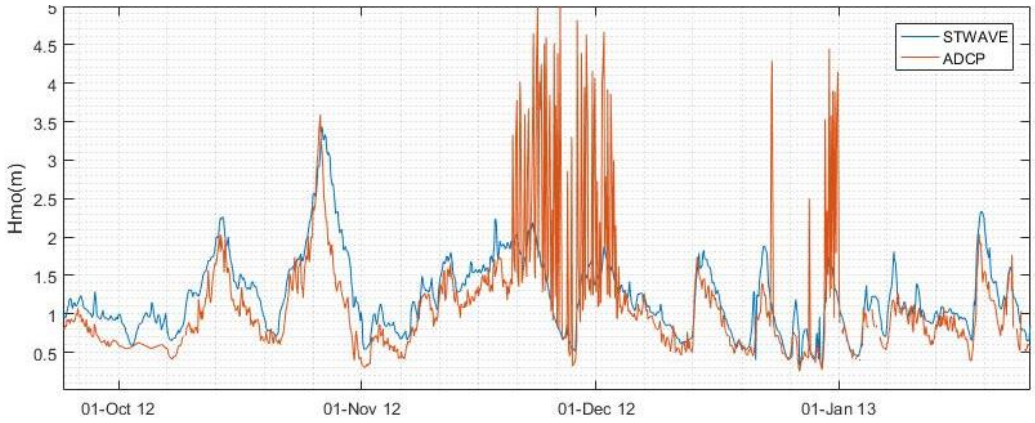

Figure 6.4 – Sample of Hmo time series of STWAVE^{+} results compared to ADP data collected at Sebastian Inlet. Pictured are the two instances of 'noise' in the data record around December 1, 2012 and January 1, 2013, indicating a need to further quality control this data record.

Figure 6.5 displays both scatter plots for the nearshore record's performance in respect with mean period and mean wave direction. The scatter for wave direction demonstrates the model's exclusion of wave energy with high incident angles as well as locally generated waves travelling along shore. For the bulk of the data the model appears to simulate direction well with an apparent bias toward the south (model > observation). With respect to mean wave period, model results appear to under-predict high periods (> ~10s) and over predict the lower periods (<~4s). This trend in modeled wave periods is introduced by the deep-water hindcast and it is unclear how much error is contributed by the nearshore model.

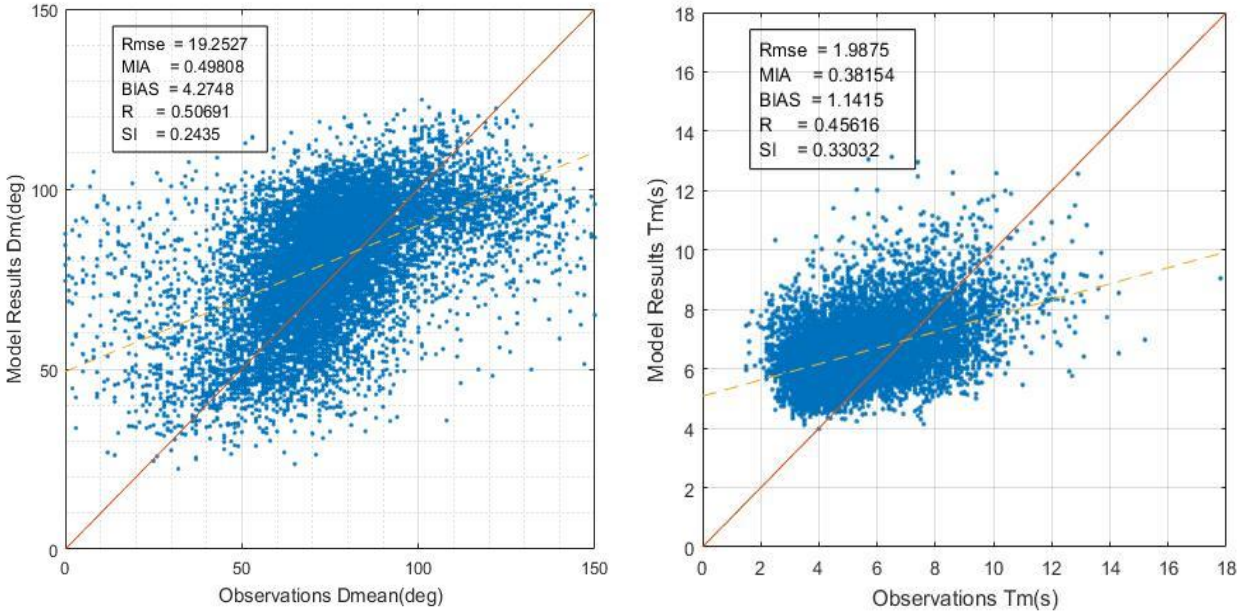

Figure 6.5 - Scatter plots of model results compared to Spessard ADCP data for mean period and mean wave direction. The solid lines represent perfect agreement and the dashed lines are linear best-fits.

The synthetic nearshore record results are summarized in Table 6.2. The Spessard data set provided data to compare between significant wave height, mean period and mean wave direction, while the Sebastian Inlet only included significant wave height. Both mean period and mean wave direction show large error metrics due to errors in the deep-water hindcast and the fact that minor discrepancies between wave spectra can affect the value of these bulk parameters. Although there could be improvements made with the period and wave direction, the good performance of significant wave heights indicate that the models adequately simulate the total wave energy.

Table 6.2 - Validation statistics for Spessard and Sebastian inlet

	RMSE	R	BIAS	MIA	SI
Spessard					
Hmo (m)	0.272	0.861	0.132	0.697	0.278
Tm (s)	1.99	0.382	1.14	0.382	0.330
Dm (deg)	19.25	0.507	4.275	0.498	0.244
Sebastian Inlet					
Hmo (m)	0.317	0.828	0.190	0.646	0.336

Chapter 7: Analysis and Discussion

7.1 Nearshore Record Analysis

The 62-year long nearshore hindcast was analyzed for the wave climate, extreme waves and long-term trends. Wave roses were produced for each calendar year, these are found in Appendix A. As expected, the wave roses show the majority of waves incoming south of shore normal and the higher wave heights incoming north of shore normal. This balance between south and north wave incidence is useful in historical sediment transport studies.

Fast Fourier Transform (FFT) analysis was used to find if multi-decadal oscillating trends exist in Hmo. Figure 7.1 show an FFT analysis of the significant wave height record, where the peaks reveal strong cyclical patterns.

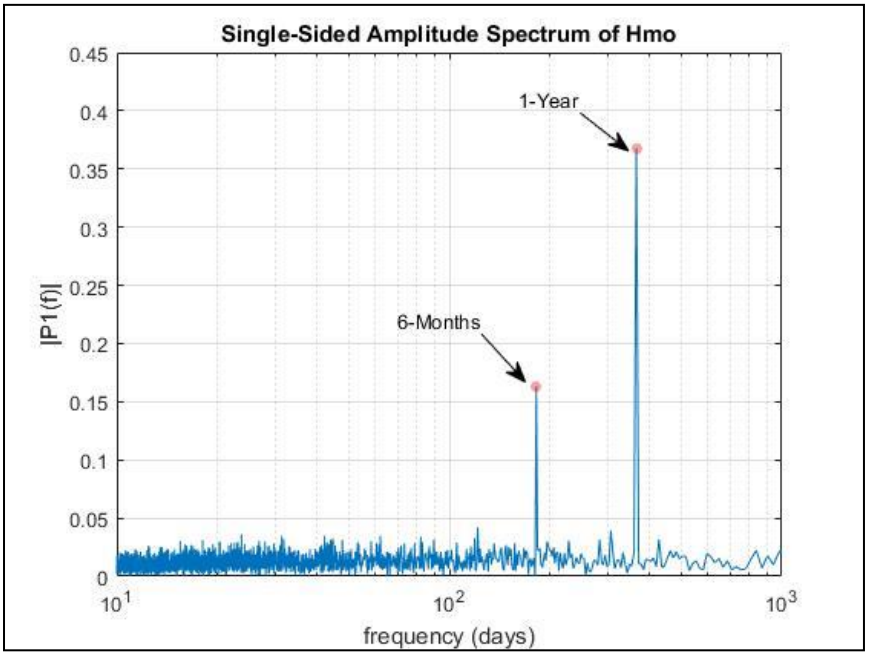

Figure 7.1 – Results of the Fast Fourier Transform analysis of H_{mo} from the 62-year long Nearshore Synthetic Wave Record (NSWR) generated at Spessard, exhibiting significant peaks at only the expected yearly and six-month (seasonal) cycles; i.e. other, longer-term cycles are not evident.

The only two peaks that show up in the figure are at a frequency of one year and 6-months, no other cyclical patterns were identified. If there are long term trends, it is possible that the record is not yet long enough to detect cyclical trends longer than a year.

Extreme wave analysis included a Return Period analysis and Points-Over-Threshold analysis. Both extreme wave analyses used the definition of a storm with a peak greater than 2.5 meters with peaks at least 36 hours apart. Figure 7.2 shows the "storm count" for each year, based on how many peaks pass over the threshold of 2.5m. The latter part of the record exhibits an increase in number of storms.

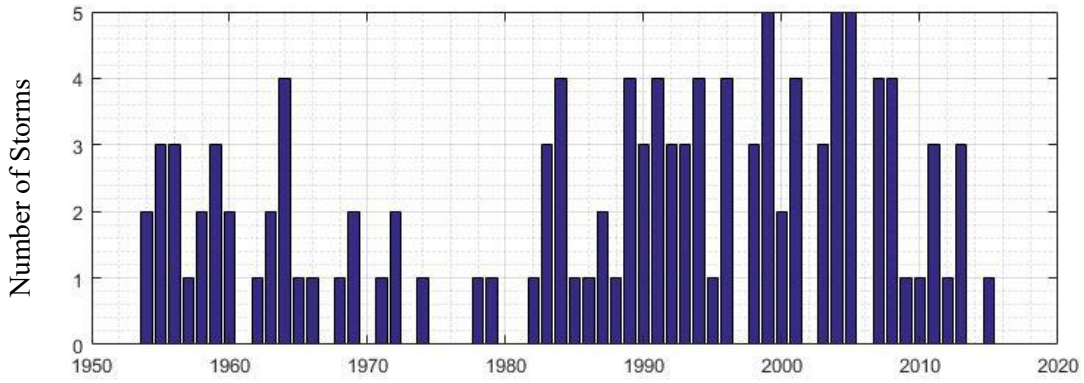

Figure 7.2 – Results of a point-over-threshold analysis using H_{mo} = 2.5m to define a 'storm' indicate an increase in the number of storms during the latter part of the NSWR.

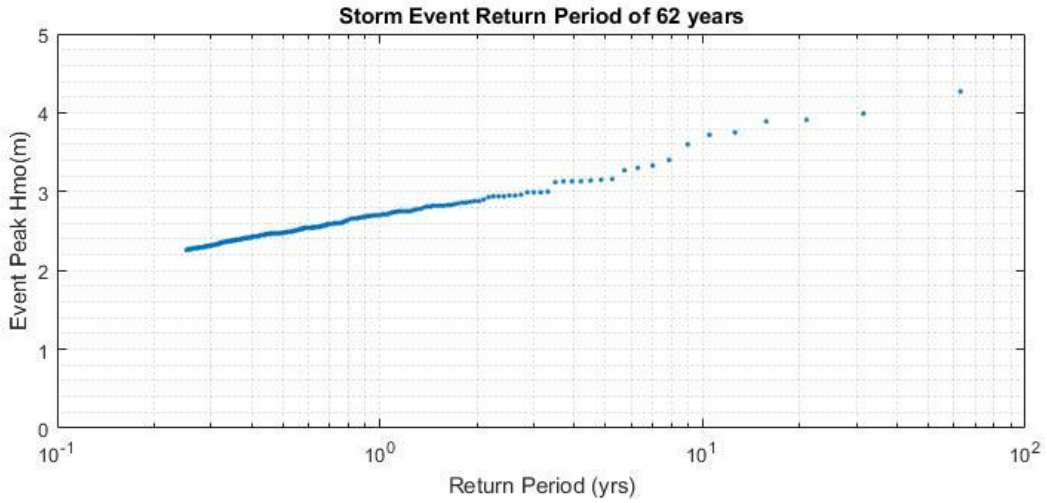

Figure 7.3 – The return period as plotted for every peak within the 62 year-long NSWR, shows that a predicted 100-yr storm would have wave heights of around 4.5m at the 8.5m meter contour.

Based on a straight-line method, the 100-year storm at the 8.5m contour would be approximately 4.5 meters. Table 7.1 shows the most extreme peaks in the wave information record. Hurricane Jeanne ranks as number one in the list, making landfall in Stuart, FL as a category 3 storm, about 100km south of the study area.

Table 7.1 – Top ten peak events throughout wave record

	Peak Date	Hs (m)	Tp (s)	Dm (deg)
1	09/26/04	4.27	14.4	256
2	09/15/99	3.99	14.4	252
3	09/05/04	3.91	13.1	256
4	09/04/79	3.89	13.1	262
5	10/16/99	3.75	11.9	257
6	09/09/64	3.72	14.4	249
7	10/27/12	3.6	14.4	250
8	03/11/96	3.4	13.1	248
9	09/08/65	3.33	11.9	254
10	11/14/94	3.3	10.8	249

Chapter 8: Summary and Conclusion

A nearshore synthetic wave record was updated for Brevard County, Florida for a continuous run length of 62 years (1954–2015). A novel approach was used to validate and calibrate this type of data included using quantile-quantile plots and bin-averaged scatter plots in addition to the commonly used statistical error metrics. Since most data points are lower in wave height the statistics are mostly representative of those points, so the addition of these visual aids allows for the higher wave heights to be considered in the analysis. The flow chart in figure 8.1 shows the steps to consider when following the methodology used herein. Part a describes the selection process of a deep-water hindcast, and part b describes the process of calibrating and validating the nearshore wave model.

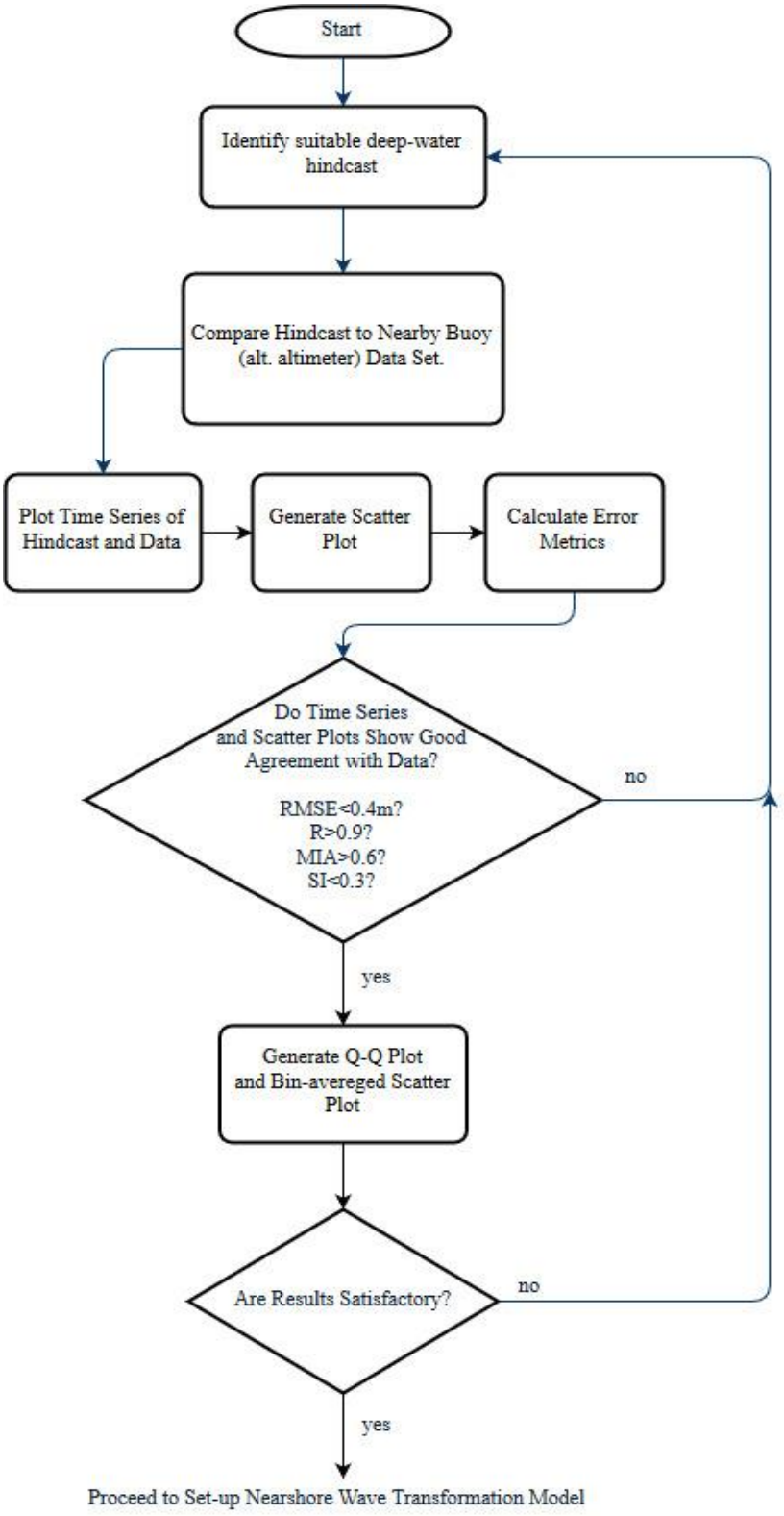

Figure 8.1(a) – Flow chart describing the methodology used. Part (a) describes the selection process of a deep-water hindcast.

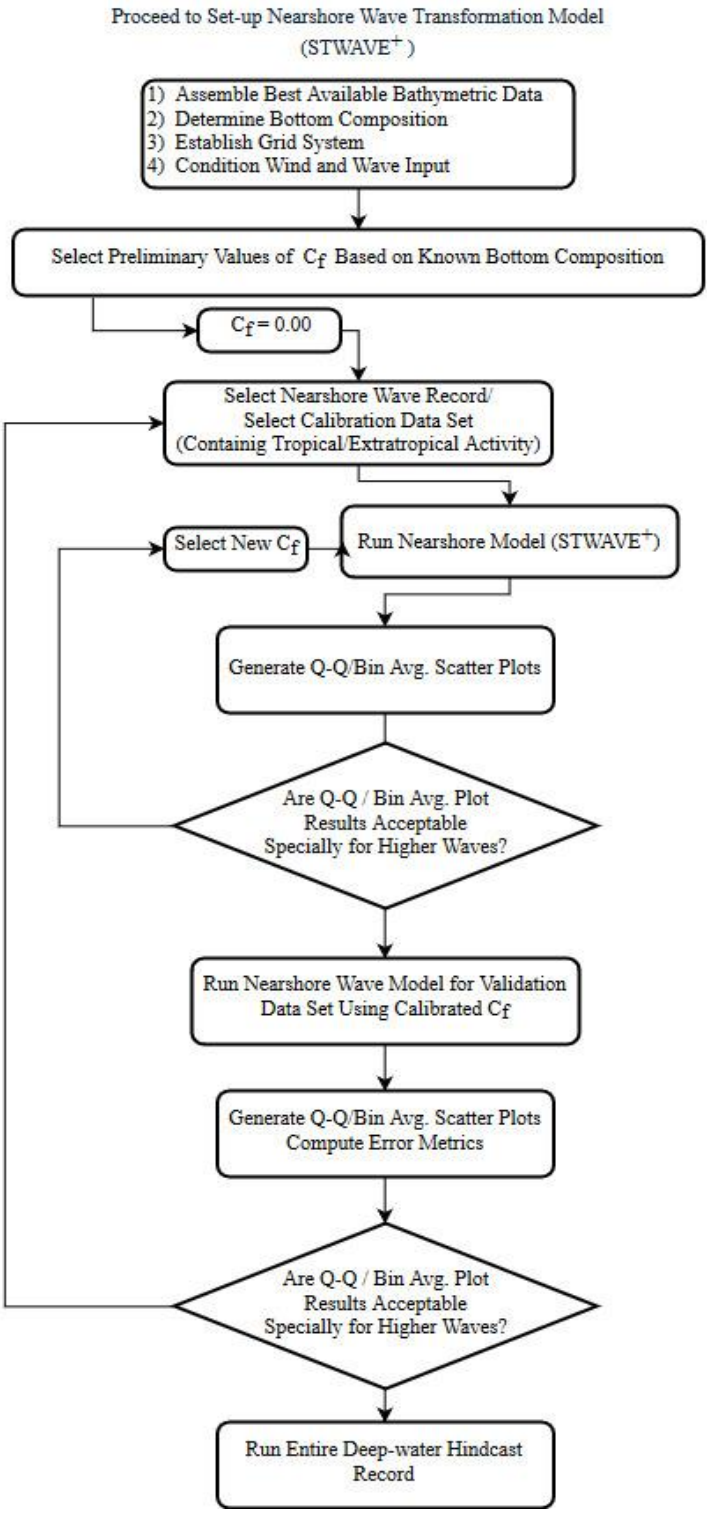

Figure 8.1(b) – Flow chart describing the methodology used. Part (b) describes the process of calibrating and validating the nearshore wave model.

Two Deepwater hindcasts, MCS50 and WW3, were compared against buoy data. While the WW3 hindcast showed better performance in the statistical comparison, the quantile plot exposed its apparent systemic error underpredicting the higher waves at this location. Although the MSC hindcast exhibited more scatter and bias, the quantile plot demonstrated that it performed better at predicting the larger waves, so it was selected as the deep-water hindcast to use as input for the nearshore.

At the nearshore STWAVE proves to be a simple, robust and fast way to create a nearshore wave record. Boundary conditions consisted of offshore hindcast waves and wind as input, nearshore water levels, bottom friction and bathymetry. Bottom friction was calibrated using a range of coefficient values and the approach as discussed above. The record was validated against two continuous data collection efforts located at Spessard Holland State Park and Sebastian Inlet near 9 meters of depth with a root mean squared error of 0.272m-0.317m and modified index of agreement of 0.697-0.646. Comparison to the validation data set showed that the model performed well for significant wave heights at Spessard and Sebastian Inlet. Relatively large deviations in the mean periods (2s rmse) and mean wave directions (19 deg rmse) were expected because of slight differences between actual and modeled wave spectra as well as the model error introduced by the deep-water hindcast.

Possible future improvements could be made to the produced record in two ways: modifying the offshore hindcast and studying the bottom friction further. Issues with the scatter in the hindcast could be addressed by producing an offshore hindcast with better grid resolution,

like WW3, while still using the MSC50's reanalyzed winds. Further studies into different friction models may also help improve some of the results It is important to note that further study and calibration on the friction model needs to be done using measured data as input, rather than a modeled hindcast record. This would help isolate and quantify how much model deviation is introduced by either the offshore hindcast or caused by the nearshore model.

Overall, the use of the MSC50 hindcast, to drive STWAVE at the nearshore, exhibits good agreement with ADCP data. Results analyzed for significant wave heights showed no strong multi-decadal trend in wave climate at this location, and more years into the record may be needed to detect this type of trend. Furthermore, the half plane feature of STWAVE allows for a robust and time efficient way to produce long-term nearshore records. With the parameters given in this study, one year's worth of simulated time was simulated in four days real time. Finally, given that extreme values were well simulated by the MSC50-STWAVE combination, the extreme value analysis for Hmo can be used with confidence.

References

Army Corps of Engineers. (2019, 04 20). Wave Information Studies. Retrieved from http://frf.usace.army.mil/wis/

Booij, N., Ris, R. C., & Holthuijsen, L. H. (2002). A third-generation wave model for coastal regions. Journal of Geophysical Research: Oceans, 104(C4), 7649–7666. https://doi.org/10.1029/1998jc900123

Chawla, A., Spindler, D. M., & Tolman, H. L. (2013). Validation of a thirty-year wave hindcast using the Climate Forecast System Reanalysis winds. *Ocean Modelling*, *70*, 189-206.

Dally, W. R., & Osiecki, D. A. (2006). Development & validation of hindcast-driven nearshore wave information. In *Proceedings of the 9th International Workshop on Wave Hindcasting and Forecasting*.

Dean, R. G., & Dalrymple, R. A. (2004). *Coastal processes with engineering applications*. Cambridge University Press.

DHI, M. (2014). A Modelling System for Rivers and Channels, Reference Manual. Horsholm, DenmarN.

Donelan, M., LeMéhauté, B., & Hanes, D. (1990). Air-sea interaction, the sea: Ocean engineering science. edited by BL Mehaute and DM Hanes, 239-292.

Fonseca, R. B., Gonçalves, M., & Soares, C. G. (2017). Comparing the Performance of Spectral Wave Models for Coastal Areas. Journal of Coastal Research, 33(2), 331–346. https://doi.org/10.2112/jcoastres-d-15-00200.1

Gonçalves, M., Rusu, E., & Soares, C. G. (2015). Evaluation of Two Spectral Wave Models in Coastal Areas. Journal of Coastal Research, 31(2), 326–339. https://doi.org/10.2112/JCOASTRES-D-12-00226.1

Hasselmann, S., & Hasselmann, K. (2002). Computations and Parameterizations of the Nonlinear Energy Transfer in a Gravity-Wave Spectrum. Part I: A New Method for Efficient Computations of the Exact Nonlinear Transfer Integral. *Journal of Physical Oceanography*. https://doi.org/10.1175/1520-0485(1985)015<1369:capotn>2.0.co;2

Howell, G. (1980). Florida coastal data network. *Coastal Engineering Proceedings*, *1*(17).

Leadon, M. E., Dally, W. R., & Osiecki, D. A. (2004). The Florida coastal forcing project. In *Proceedings of the 17th National Conference on Beach Preservation Association*.

Long, C. E., & Oltman-Shay, J. M. (1991). *Directional characteristics of waves in shallow water* (No. CERC-TR-91-1). COASTAL ENGINEERING RESEARCH CENTER VICKSBURG MS.

NCEP. (2019, April 30). WAVEWATCH III Production Hindcast, Multigrid: Feb 2005 to Mar 2019. Retrieved from https://polar.ncep.noaa.gov/waves/hindcasts/prod-multi_1.php

Panigrahi, J. K., & Misra, S. K. (2010). Numerical hindcast of extreme waves. *Natural Hazards*. https://doi.org/10.1007/s11069-009-9438-4

Smith, J. M., Resio, D. T., Zundel, A. K., Resio, J. M., Zundel, D. T., & Alan, K. (1999). STWAVE : Steady-State Spectral Wave Model Report 1 User's Manual for STWAVE Version 2.0.

Swail, V. R., Cardone, V. J., Ferguson, M., Gummer, D. J., Harris, E. L., Orelup, E. A., & Cox, A. T. (2006). The MSC50 Wind and Wave Reanalysis. In *International Workshop On Wave Hindcasting and Forecasting*.

Swail, V. R., & Cox, A. T. (2000). On the use of NCEP-NCAR reanalysis surface marine wind fields for a long-term North Atlantic wave hindcast. *Journal of Atmospheric and Oceanic Technology*, *17*(4), 532–545. https://doi.org/10.1175/1520-0426(2000)017<0532:OTUONN>2.0.CO;2

WAMDI Group, T. (1988). The WAM model - A third generation ocean wave prediction model. *Journal of Physical Oceanography*. https://doi.org/10.1175/1520-0485(1988)018<1775:TWMTGO>2.0.CO;2

The WAVEWATCH III Development Group (WW3DG). (2016). User manual and system documentation of WAVEWATCH III version 5.16. Tech. Note 329, NOAA/NWS/NCEP/MMAB, College Park, MD, USA. *Technical Note, MMAB Contribution*. https://doi.org/10.3390/ijerph2006030011

Zijlema, M., & van der Westhuysen, A. J. (2005). On convergence behaviour and numerical accuracy in stationary SWAN simulations of nearshore wind wave spectra. Coastal Engineering, 52(3), 237–256. https://doi.org/10.1016/j.coastaleng.2004.12.006

Appendix A – Annual Wave Roses

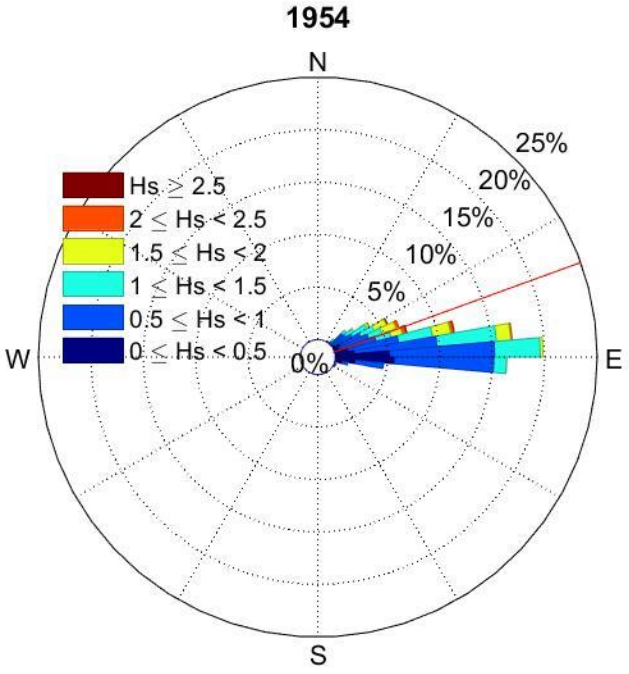
1954
N
S
W
E
25%
20%
15%
10%
5%
0%
Hs ≥ 2.5
2 ≤ Hs < 2.5
1.5 ≤ Hs < 2
1 ≤ Hs < 1.5
0.5 ≤ Hs < 1
0 ≤ Hs < 0.5

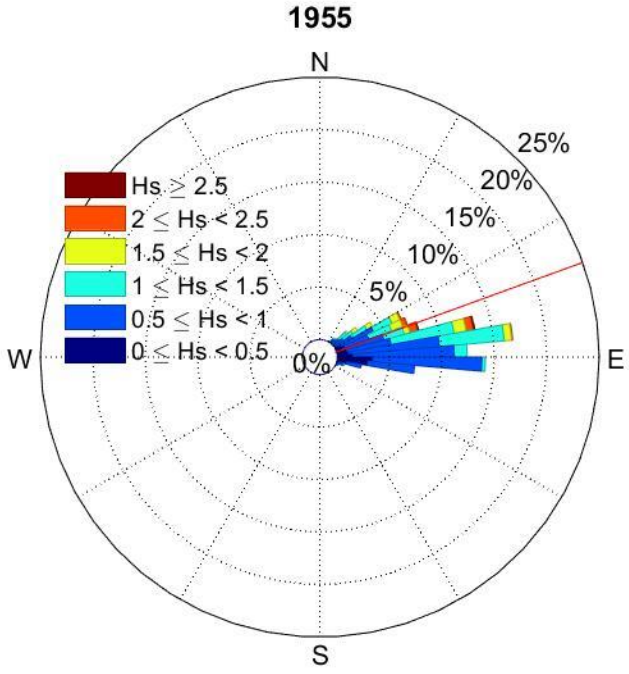
1955
N
S
W
E
25%
20%
15%
10%
5%
0%
Hs ≥ 2.5
2 ≤ Hs < 2.5
1.5 ≤ Hs < 2
1 ≤ Hs < 1.5
0.5 ≤ Hs < 1
0 ≤ Hs < 0.5

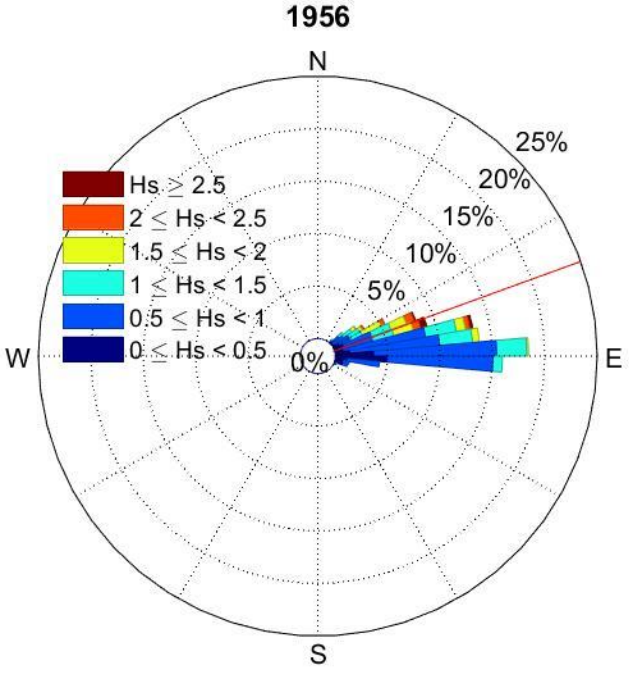
1956
N
S
W
E
25%
20%
15%
10%
5%
0%
Hs ≥ 2.5
2 ≤ Hs < 2.5
1.5 ≤ Hs < 2
1 ≤ Hs < 1.5
0.5 ≤ Hs < 1
0 ≤ Hs < 0.5

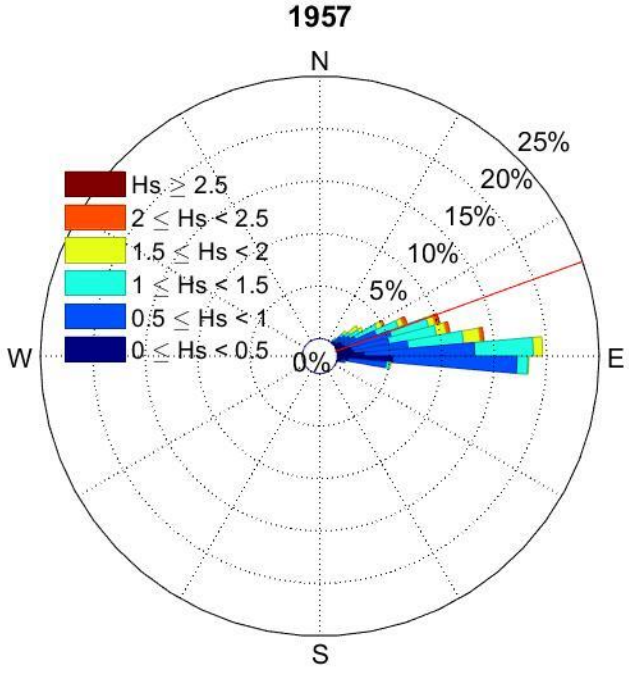
1957
N
S
W
E
25%
20%
15%
10%
5%
0%
Hs ≥ 2.5
2 ≤ Hs < 2.5
1.5 ≤ Hs < 2
1 ≤ Hs < 1.5
0.5 ≤ Hs < 1
0 ≤ Hs < 0.5

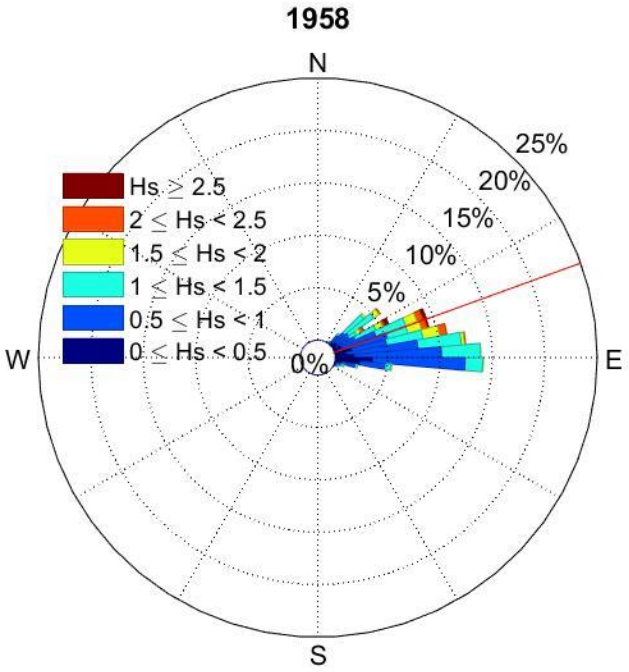
1958
N
E
S
W
25%
20%
15%
10%
5%
0%
Hs ≥ 2.5
2 ≤ Hs < 2.5
1.5 ≤ Hs < 2
1 ≤ Hs < 1.5
0.5 ≤ Hs < 1
0 ≤ Hs < 0.5

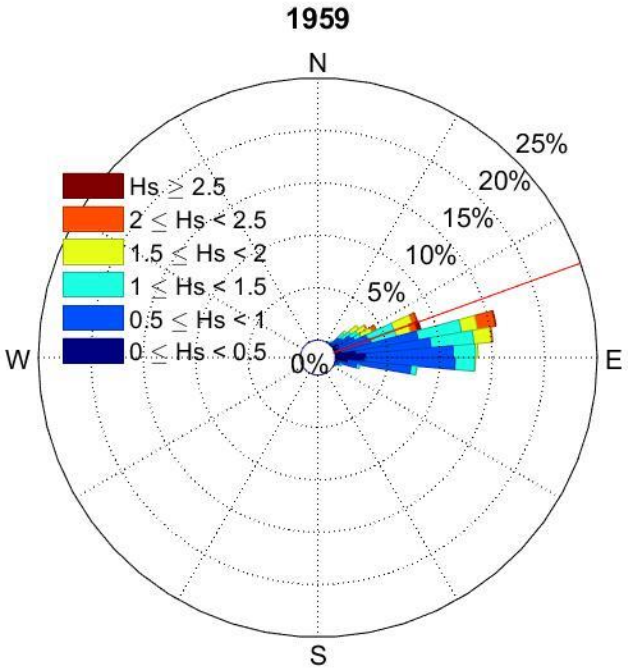
1959
N
E
S
W
25%
20%
15%
10%
5%
0%
Hs ≥ 2.5
2 ≤ Hs < 2.5
1.5 ≤ Hs < 2
1 ≤ Hs < 1.5
0.5 ≤ Hs < 1
0 ≤ Hs < 0.5

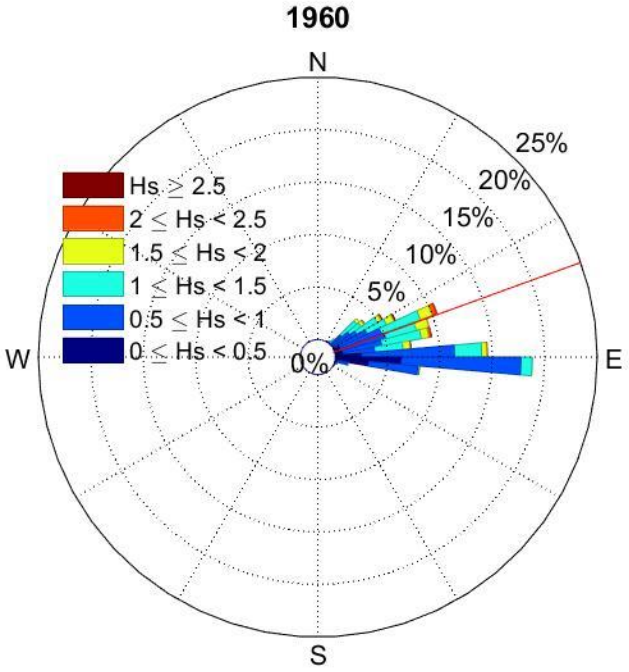
1960
N
E
S
W
25%
20%
15%
10%
5%
0%
Hs ≥ 2.5
2 ≤ Hs < 2.5
1.5 ≤ Hs < 2
1 ≤ Hs < 1.5
0.5 ≤ Hs < 1
0 ≤ Hs < 0.5

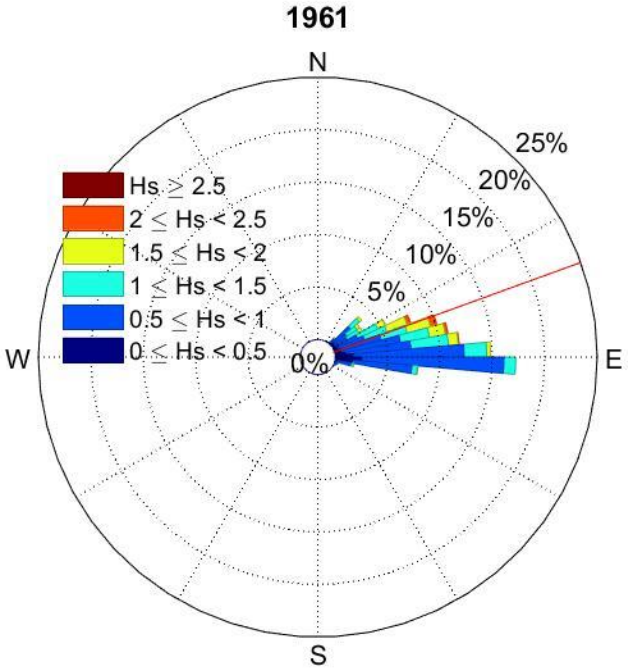
1961
N
E
S
W
25%
20%
15%
10%
5%
0%
Hs ≥ 2.5
2 ≤ Hs < 2.5
1.5 ≤ Hs < 2
1 ≤ Hs < 1.5
0.5 ≤ Hs < 1
0 ≤ Hs < 0.5

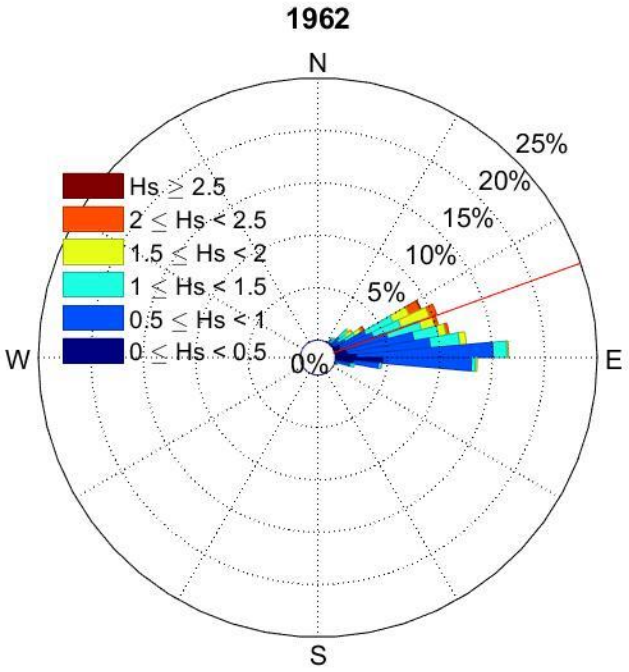
1962
N
E
S
W
25%
20%
15%
10%
5%
0%
Hs ≥ 2.5
2 ≤ Hs < 2.5
1.5 ≤ Hs < 2
1 ≤ Hs < 1.5
0.5 ≤ Hs < 1
0 ≤ Hs < 0.5

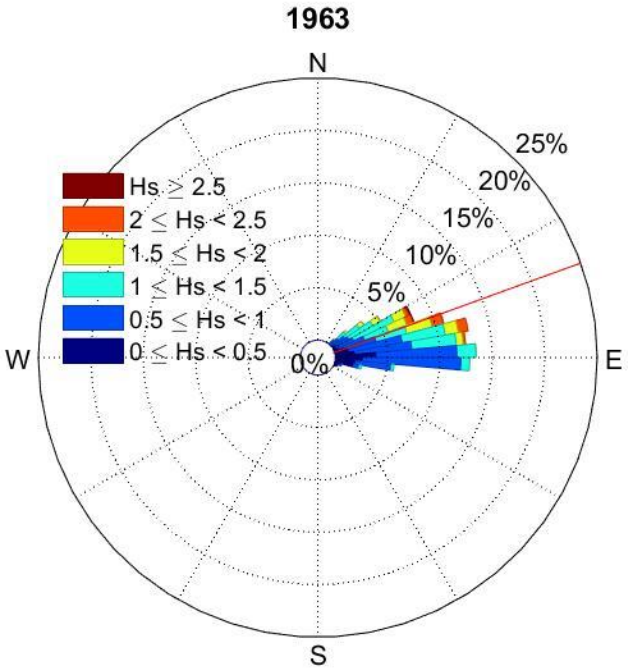
1963
N
E
S
W
25%
20%
15%
10%
5%
0%
Hs ≥ 2.5
2 ≤ Hs < 2.5
1.5 ≤ Hs < 2
1 ≤ Hs < 1.5
0.5 ≤ Hs < 1
0 ≤ Hs < 0.5

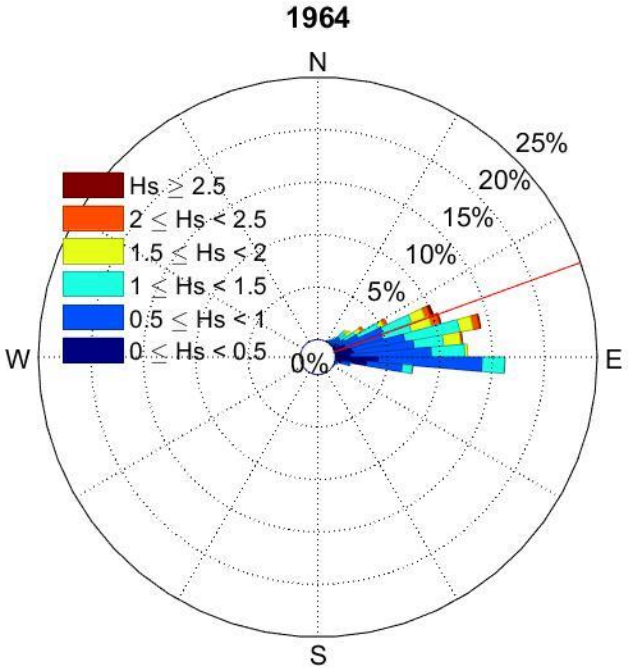
1964
N
E
S
W
25%
20%
15%
10%
5%
0%
Hs ≥ 2.5
2 ≤ Hs < 2.5
1.5 ≤ Hs < 2
1 ≤ Hs < 1.5
0.5 ≤ Hs < 1
0 ≤ Hs < 0.5

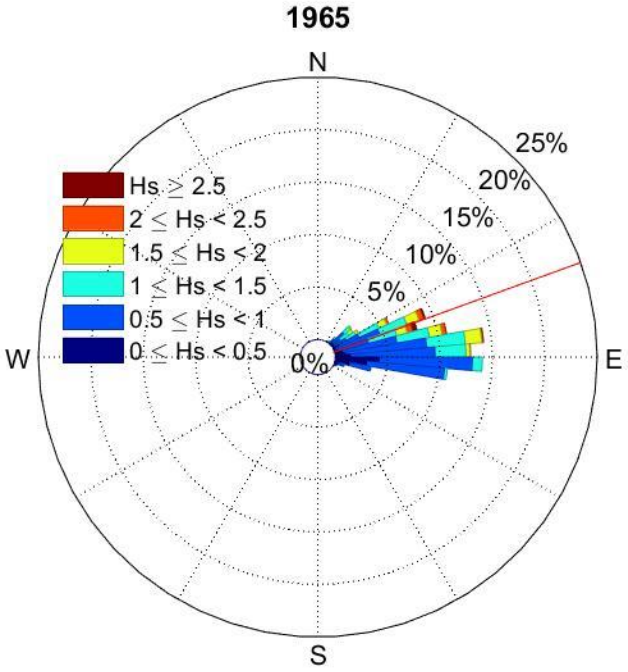
1965
N
E
S
W
25%
20%
15%
10%
5%
0%
Hs ≥ 2.5
2 ≤ Hs < 2.5
1.5 ≤ Hs < 2
1 ≤ Hs < 1.5
0.5 ≤ Hs < 1
0 ≤ Hs < 0.5

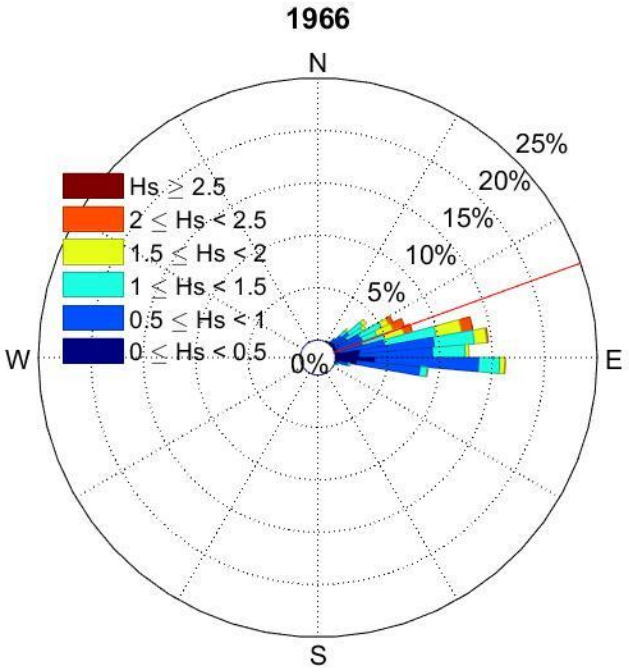
1966
N
S
W
E
25%
20%
15%
10%
5%
0%
Hs ≥ 2.5
2 ≤ Hs < 2.5
1.5 ≤ Hs < 2
1 ≤ Hs < 1.5
0.5 ≤ Hs < 1
0 ≤ Hs < 0.5

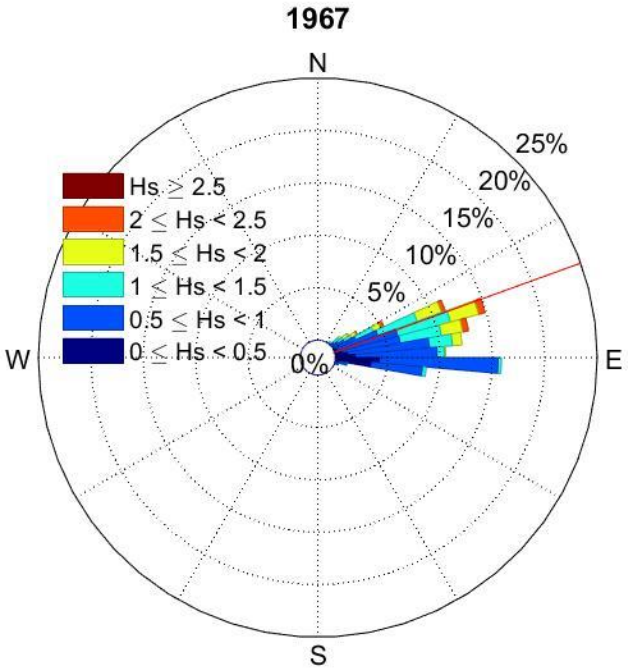
1967
N
S
W
E
25%
20%
15%
10%
5%
0%
Hs ≥ 2.5
2 ≤ Hs < 2.5
1.5 ≤ Hs < 2
1 ≤ Hs < 1.5
0.5 ≤ Hs < 1
0 ≤ Hs < 0.5

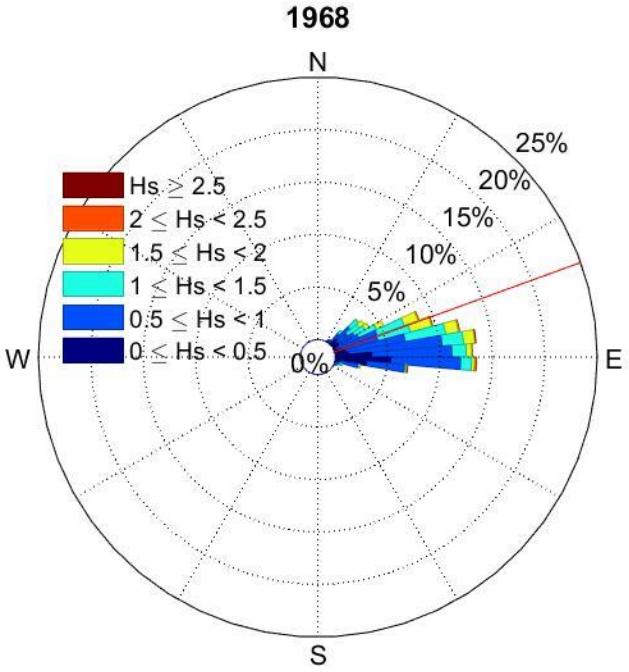
1968
N
S
W
E
25%
20%
15%
10%
5%
0%
Hs ≥ 2.5
2 ≤ Hs < 2.5
1.5 ≤ Hs < 2
1 ≤ Hs < 1.5
0.5 ≤ Hs < 1
0 ≤ Hs < 0.5

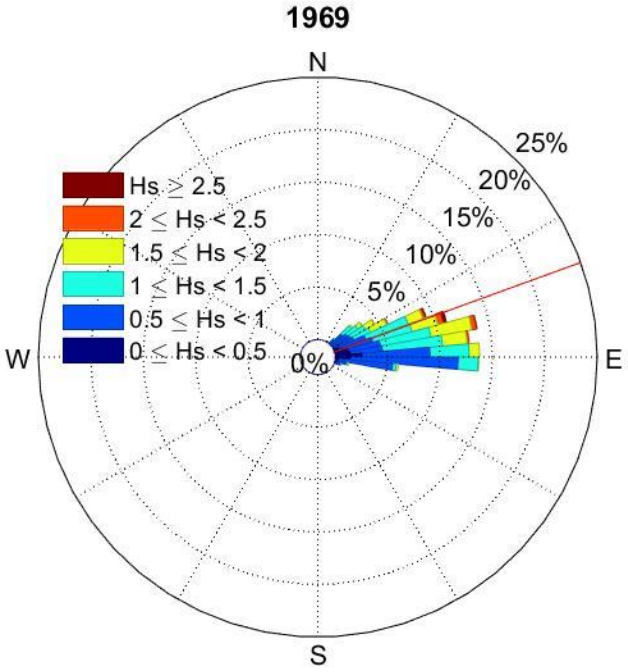
1969
N
S
W
E
25%
20%
15%
10%
5%
0%
Hs ≥ 2.5
2 ≤ Hs < 2.5
1.5 ≤ Hs < 2
1 ≤ Hs < 1.5
0.5 ≤ Hs < 1
0 ≤ Hs < 0.5

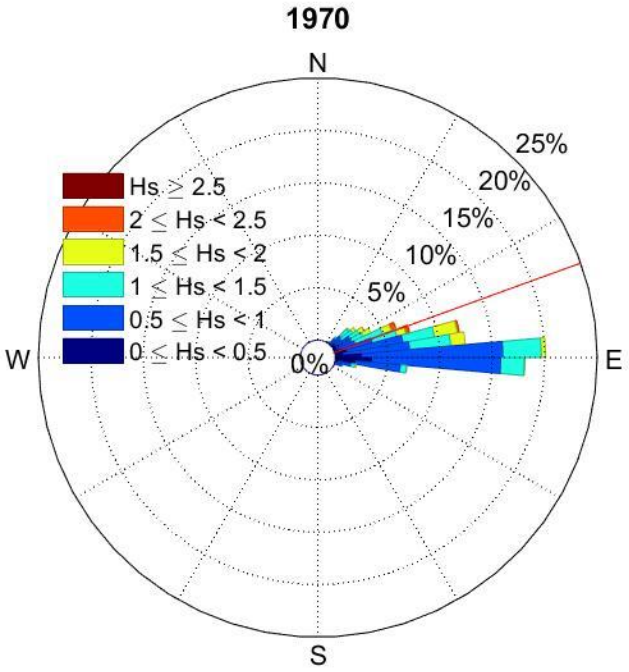
1970
N
E
S
W
25%
20%
15%
10%
5%
0%
Hs ≥ 2.5
2 ≤ Hs < 2.5
1.5 ≤ Hs < 2
1 ≤ Hs < 1.5
0.5 ≤ Hs < 1
0 ≤ Hs < 0.5

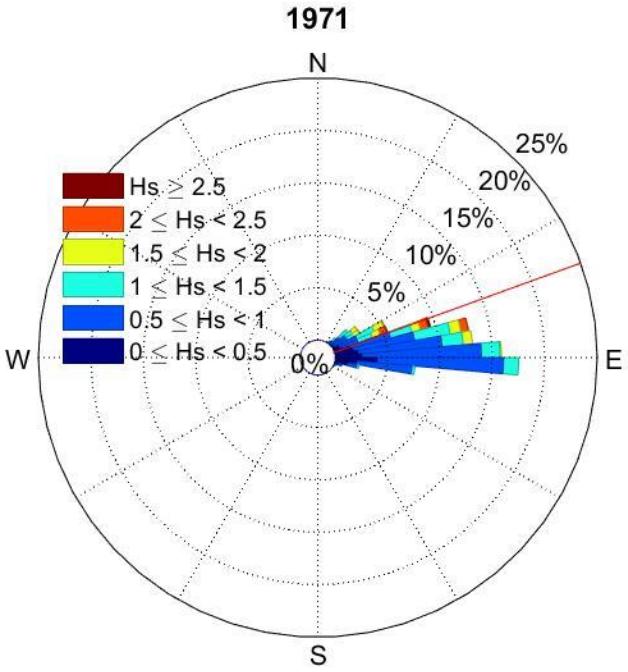
1971
N
E
S
W
25%
20%
15%
10%
5%
0%
Hs ≥ 2.5
2 ≤ Hs < 2.5
1.5 ≤ Hs < 2
1 ≤ Hs < 1.5
0.5 ≤ Hs < 1
0 ≤ Hs < 0.5

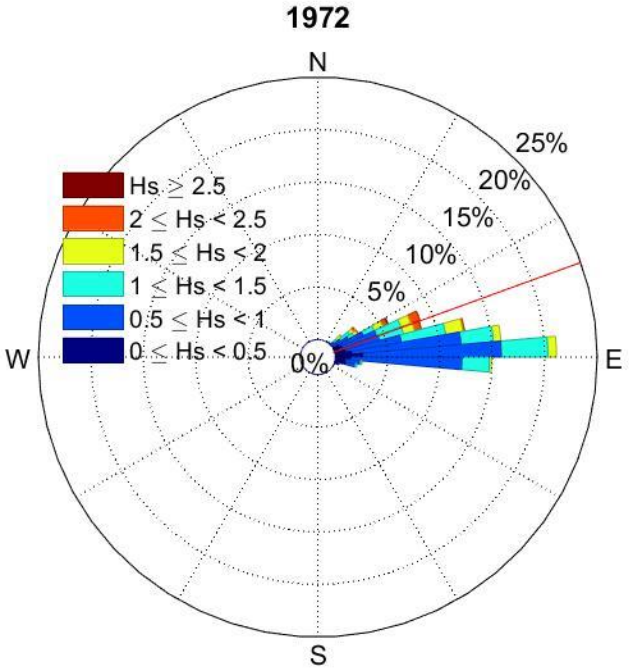
1972
N
E
S
W
25%
20%
15%
10%
5%
0%
Hs ≥ 2.5
2 ≤ Hs < 2.5
1.5 ≤ Hs < 2
1 ≤ Hs < 1.5
0.5 ≤ Hs < 1
0 ≤ Hs < 0.5

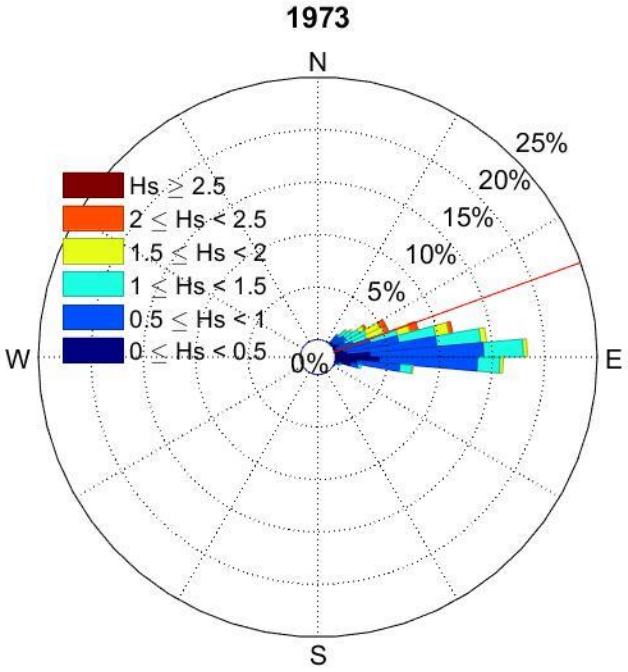
1973
N
E
S
W
25%
20%
15%
10%
5%
0%
Hs ≥ 2.5
2 ≤ Hs < 2.5
1.5 ≤ Hs < 2
1 ≤ Hs < 1.5
0.5 ≤ Hs < 1
0 ≤ Hs < 0.5

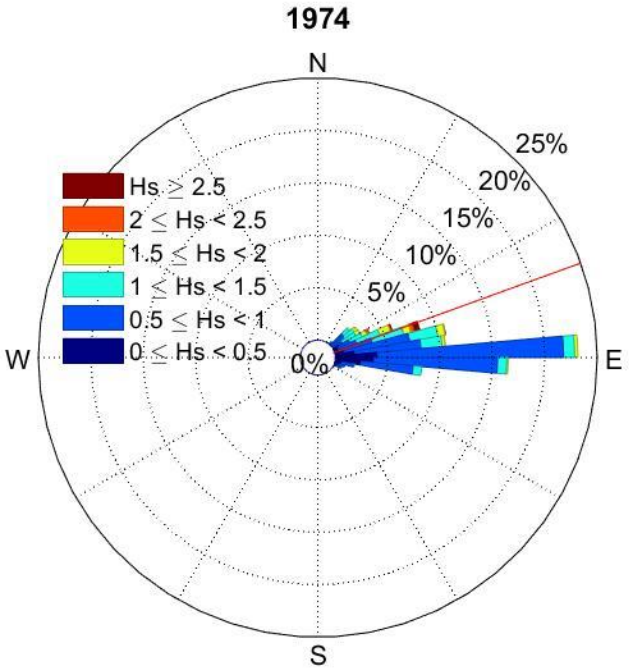
1974
N
E
S
W
25%
20%
15%
10%
5%
0%
Hs ≥ 2.5
2 ≤ Hs < 2.5
1.5 ≤ Hs < 2
1 ≤ Hs < 1.5
0.5 ≤ Hs < 1
0 ≤ Hs < 0.5

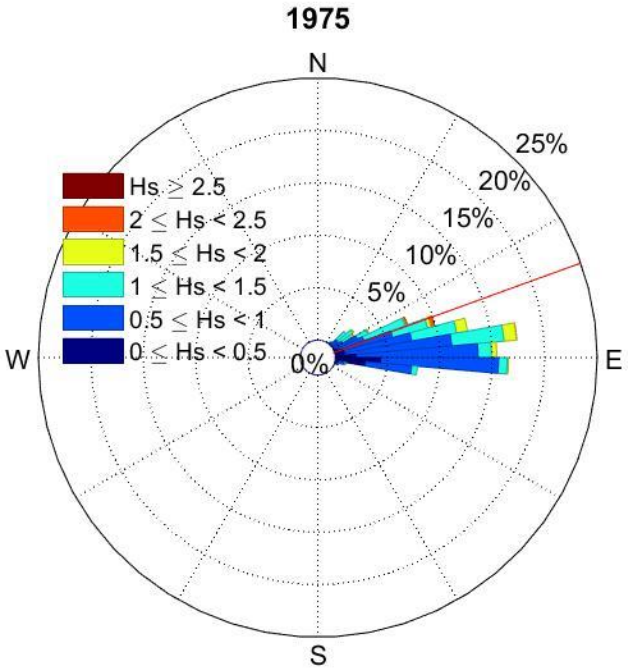
1975
N
E
S
W
25%
20%
15%
10%
5%
0%
Hs ≥ 2.5
2 ≤ Hs < 2.5
1.5 ≤ Hs < 2
1 ≤ Hs < 1.5
0.5 ≤ Hs < 1
0 ≤ Hs < 0.5

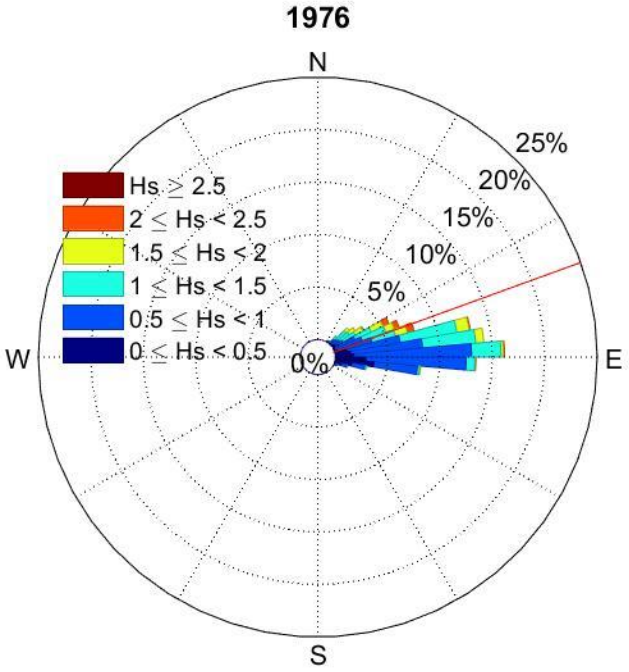
1976
N
E
S
W
25%
20%
15%
10%
5%
0%
Hs ≥ 2.5
2 ≤ Hs < 2.5
1.5 ≤ Hs < 2
1 ≤ Hs < 1.5
0.5 ≤ Hs < 1
0 ≤ Hs < 0.5

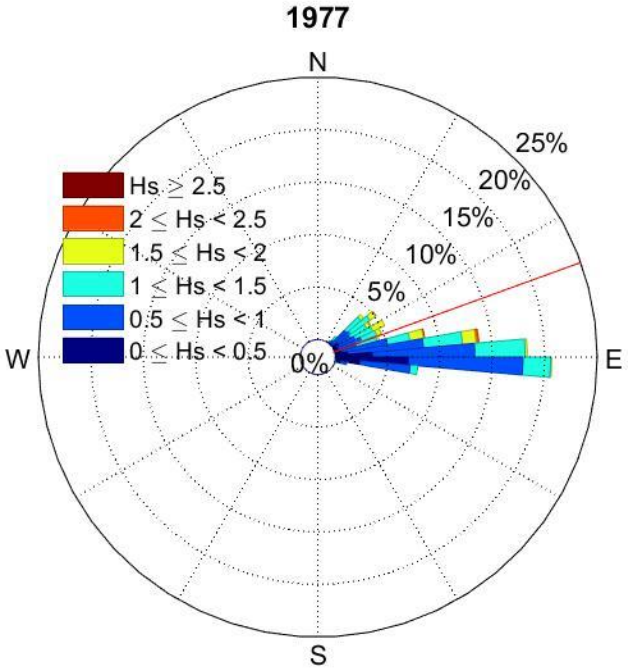
1977
N
E
S
W
25%
20%
15%
10%
5%
0%
Hs ≥ 2.5
2 ≤ Hs < 2.5
1.5 ≤ Hs < 2
1 ≤ Hs < 1.5
0.5 ≤ Hs < 1
0 ≤ Hs < 0.5

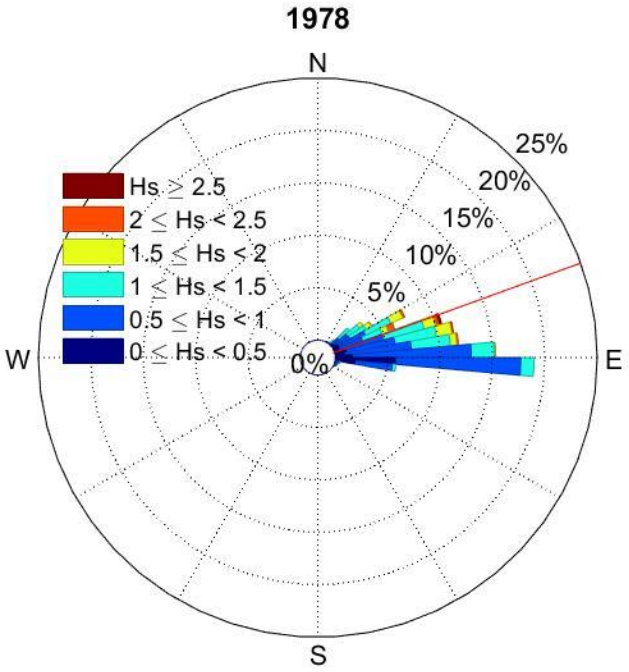
1978
N
S
W
E
25%
20%
15%
10%
5%
0%
Hs ≥ 2.5
2 ≤ Hs < 2.5
1.5 ≤ Hs < 2
1 ≤ Hs < 1.5
0.5 ≤ Hs < 1
0 ≤ Hs < 0.5

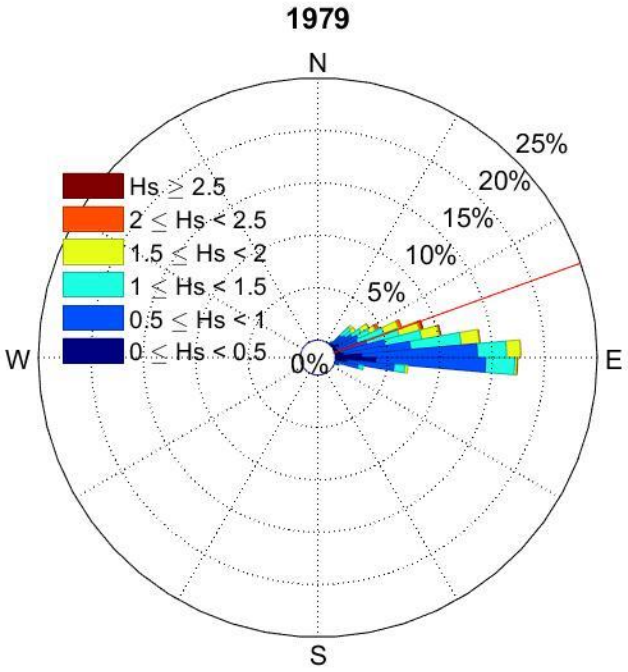
1979
N
S
W
E
25%
20%
15%
10%
5%
0%
Hs ≥ 2.5
2 ≤ Hs < 2.5
1.5 ≤ Hs < 2
1 ≤ Hs < 1.5
0.5 ≤ Hs < 1
0 ≤ Hs < 0.5

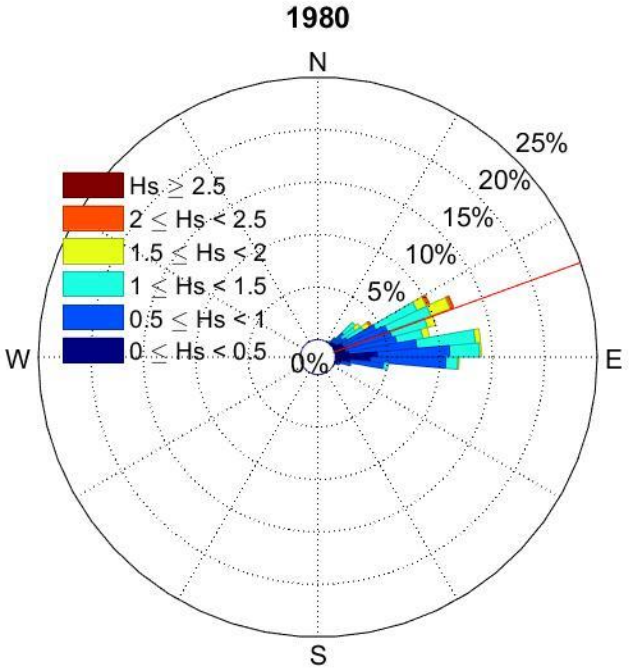
1980
N
S
W
E
25%
20%
15%
10%
5%
0%
Hs ≥ 2.5
2 ≤ Hs < 2.5
1.5 ≤ Hs < 2
1 ≤ Hs < 1.5
0.5 ≤ Hs < 1
0 ≤ Hs < 0.5

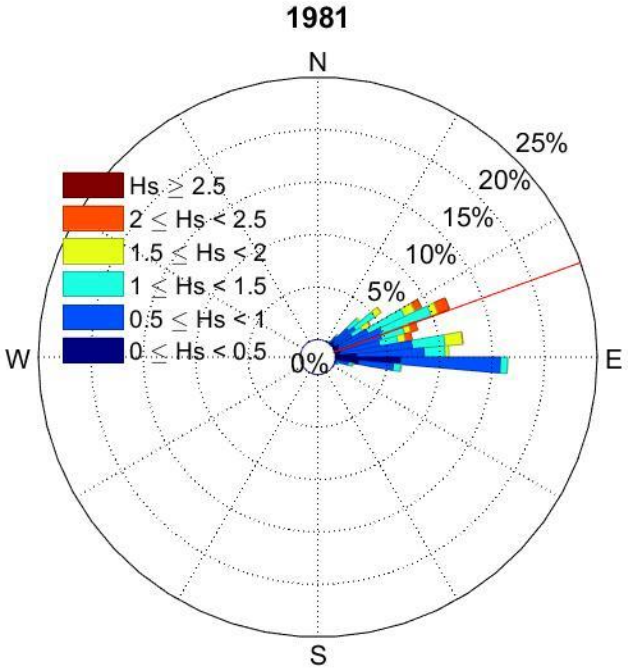
1981
N
S
W
E
25%
20%
15%
10%
5%
0%
Hs ≥ 2.5
2 ≤ Hs < 2.5
1.5 ≤ Hs < 2
1 ≤ Hs < 1.5
0.5 ≤ Hs < 1
0 ≤ Hs < 0.5

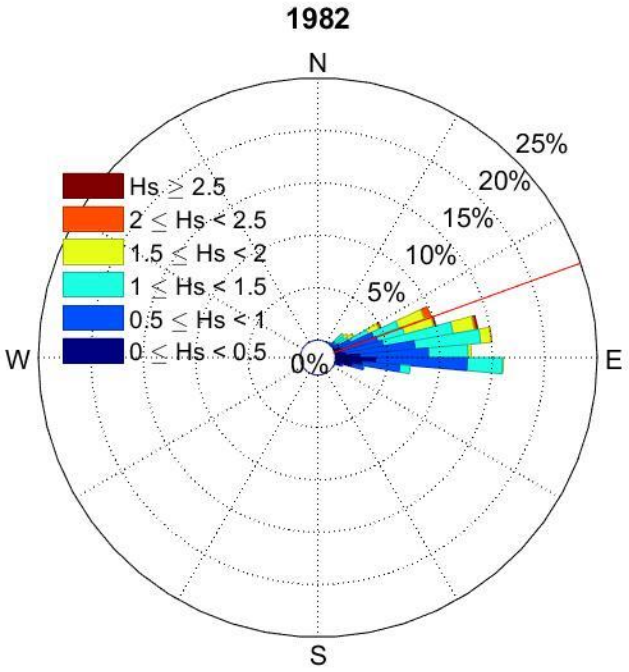
1982
N
E
S
W
25%
20%
15%
10%
5%
0%
Hs ≥ 2.5
2 ≤ Hs < 2.5
1.5 ≤ Hs < 2
1 ≤ Hs < 1.5
0.5 ≤ Hs < 1
0 ≤ Hs < 0.5

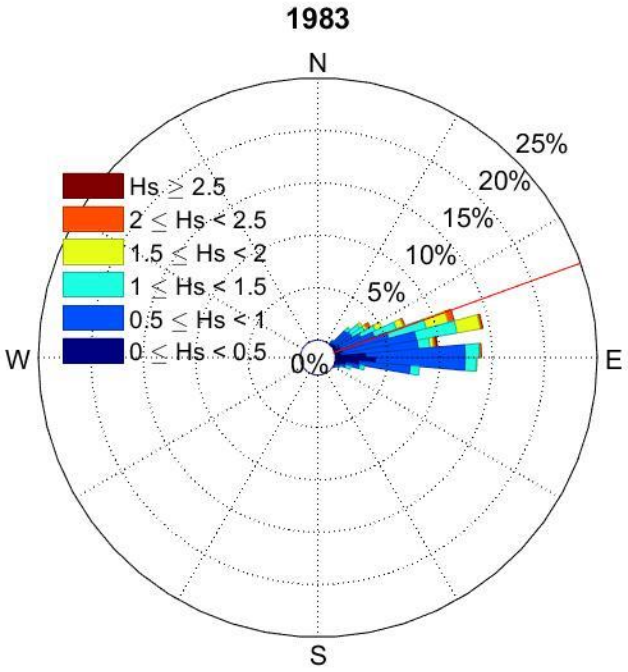
1983
N
E
S
W
25%
20%
15%
10%
5%
0%
Hs ≥ 2.5
2 ≤ Hs < 2.5
1.5 ≤ Hs < 2
1 ≤ Hs < 1.5
0.5 ≤ Hs < 1
0 ≤ Hs < 0.5

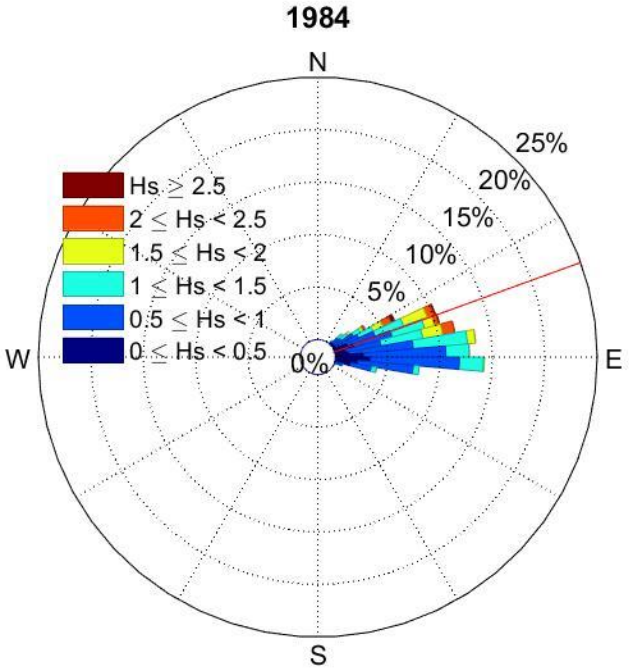
1984
N
E
S
W
25%
20%
15%
10%
5%
0%
Hs ≥ 2.5
2 ≤ Hs < 2.5
1.5 ≤ Hs < 2
1 ≤ Hs < 1.5
0.5 ≤ Hs < 1
0 ≤ Hs < 0.5

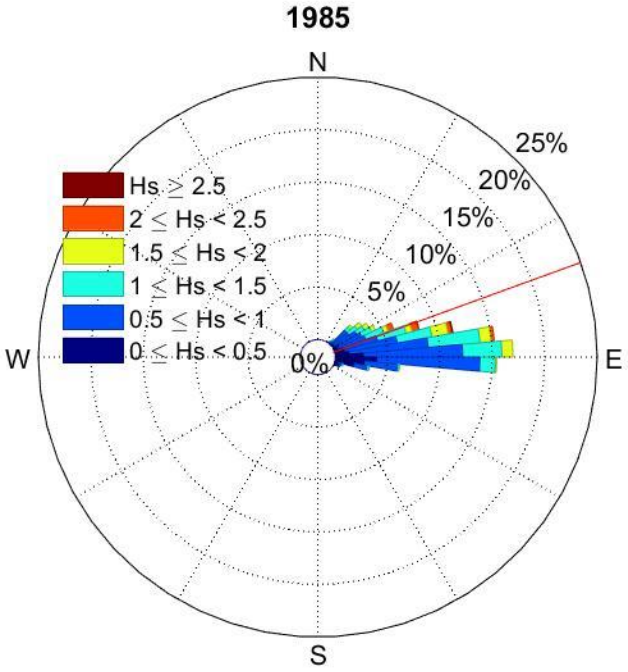
1985
N
E
S
W
25%
20%
15%
10%
5%
0%
Hs ≥ 2.5
2 ≤ Hs < 2.5
1.5 ≤ Hs < 2
1 ≤ Hs < 1.5
0.5 ≤ Hs < 1
0 ≤ Hs < 0.5

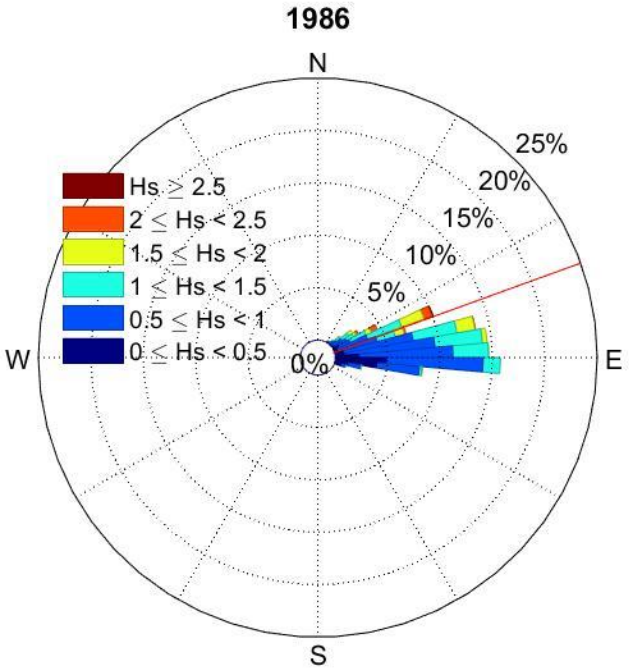
1986
N
S
W
E
25%
20%
15%
10%
5%
0%
Hs ≥ 2.5
2 ≤ Hs < 2.5
1.5 ≤ Hs < 2
1 ≤ Hs < 1.5
0.5 ≤ Hs < 1
0 ≤ Hs < 0.5

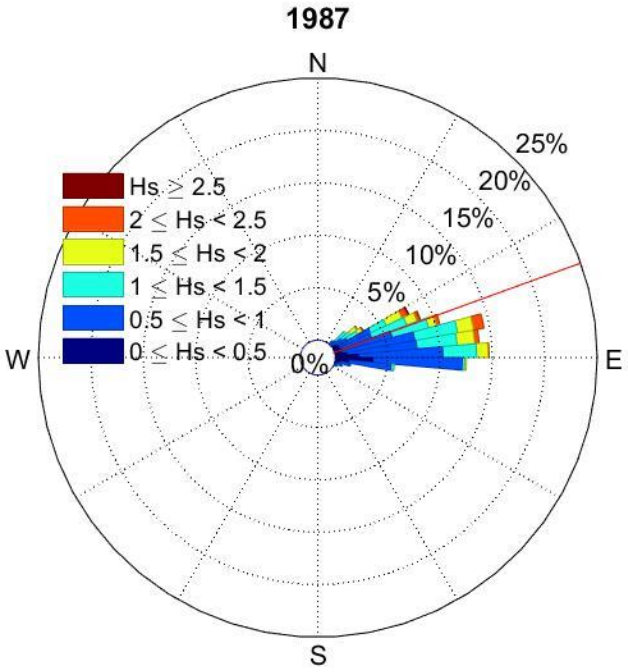
1987
N
S
W
E
25%
20%
15%
10%
5%
0%
Hs ≥ 2.5
2 ≤ Hs < 2.5
1.5 ≤ Hs < 2
1 ≤ Hs < 1.5
0.5 ≤ Hs < 1
0 ≤ Hs < 0.5

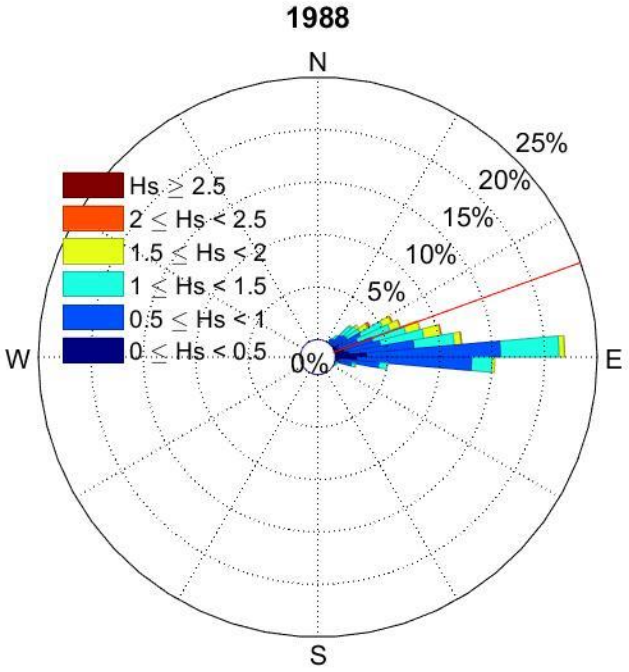
1988
N
S
W
E
25%
20%
15%
10%
5%
0%
Hs ≥ 2.5
2 ≤ Hs < 2.5
1.5 ≤ Hs < 2
1 ≤ Hs < 1.5
0.5 ≤ Hs < 1
0 ≤ Hs < 0.5

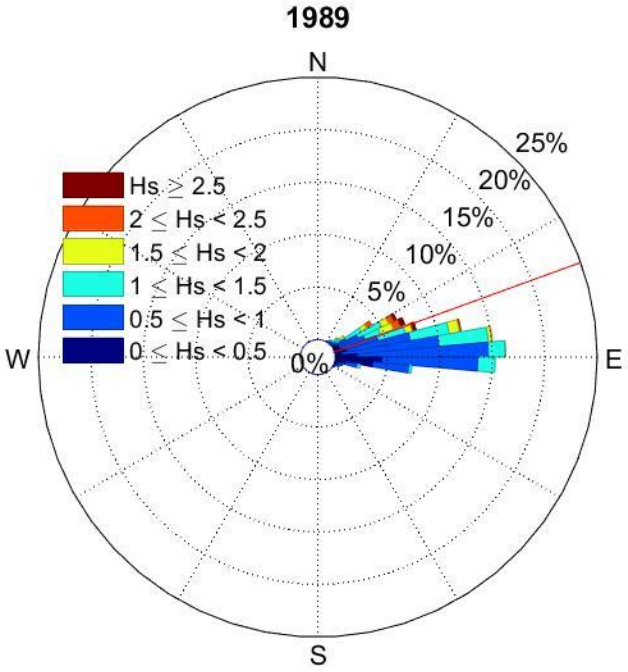
1989
N
S
W
E
25%
20%
15%
10%
5%
0%
Hs ≥ 2.5
2 ≤ Hs < 2.5
1.5 ≤ Hs < 2
1 ≤ Hs < 1.5
0.5 ≤ Hs < 1
0 ≤ Hs < 0.5

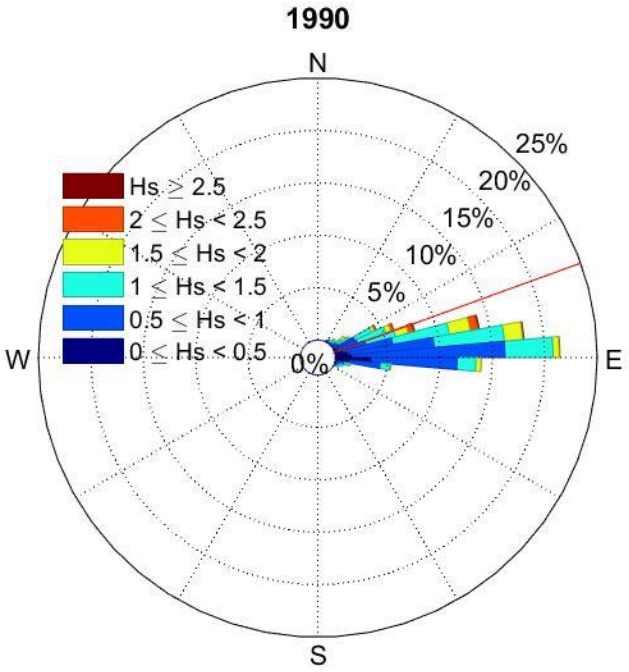
1990
N
S
W
E
25%
20%
15%
10%
5%
0%
Hs ≥ 2.5
2 ≤ Hs < 2.5
1.5 ≤ Hs < 2
1 ≤ Hs < 1.5
0.5 ≤ Hs < 1
0 ≤ Hs < 0.5

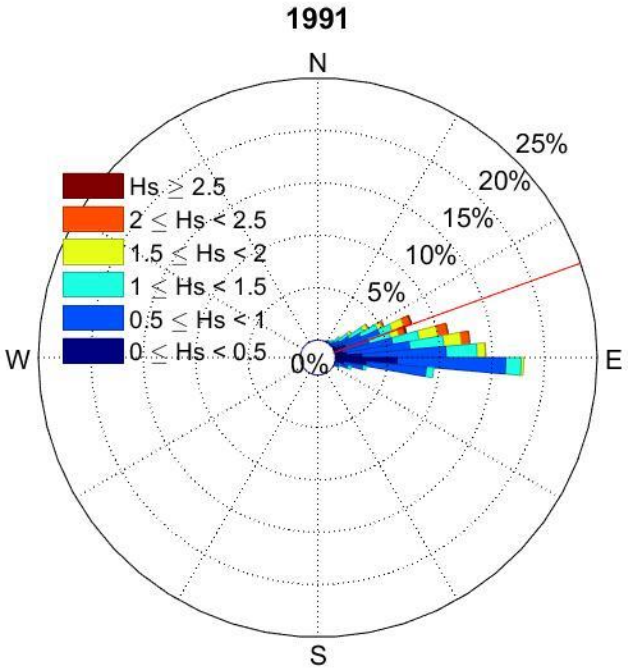
1991
N
S
W
E
25%
20%
15%
10%
5%
0%
Hs ≥ 2.5
2 ≤ Hs < 2.5
1.5 ≤ Hs < 2
1 ≤ Hs < 1.5
0.5 ≤ Hs < 1
0 ≤ Hs < 0.5

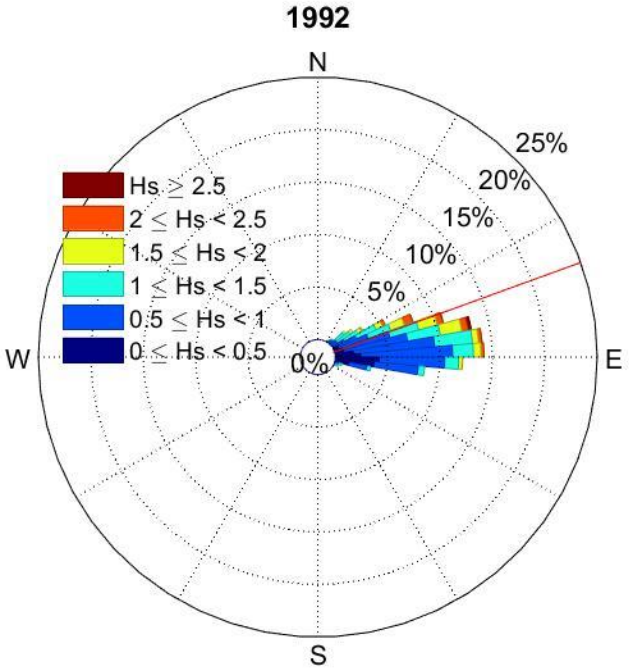
1992
N
S
W
E
25%
20%
15%
10%
5%
0%
Hs ≥ 2.5
2 ≤ Hs < 2.5
1.5 ≤ Hs < 2
1 ≤ Hs < 1.5
0.5 ≤ Hs < 1
0 ≤ Hs < 0.5

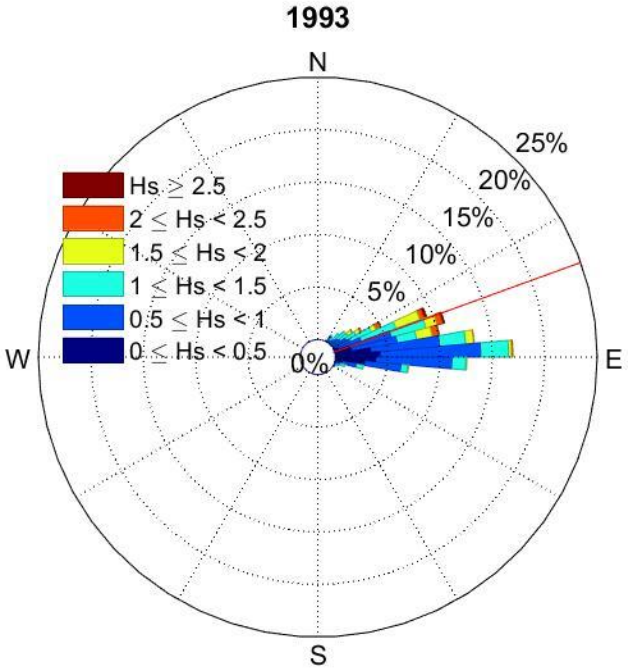
1993
N
S
W
E
25%
20%
15%
10%
5%
0%
Hs ≥ 2.5
2 ≤ Hs < 2.5
1.5 ≤ Hs < 2
1 ≤ Hs < 1.5
0.5 ≤ Hs < 1
0 ≤ Hs < 0.5

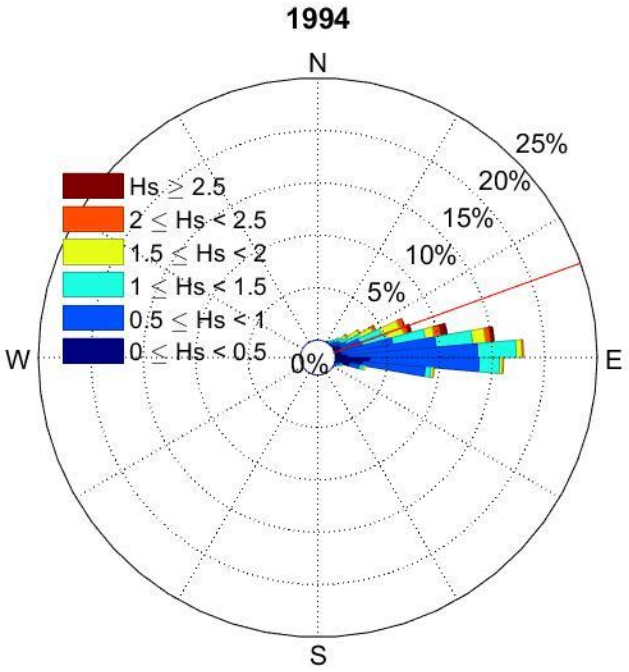
1994
N
S
W
E
25%
20%
15%
10%
5%
0%
Hs ≥ 2.5
2 ≤ Hs < 2.5
1.5 ≤ Hs < 2
1 ≤ Hs < 1.5
0.5 ≤ Hs < 1
0 ≤ Hs < 0.5

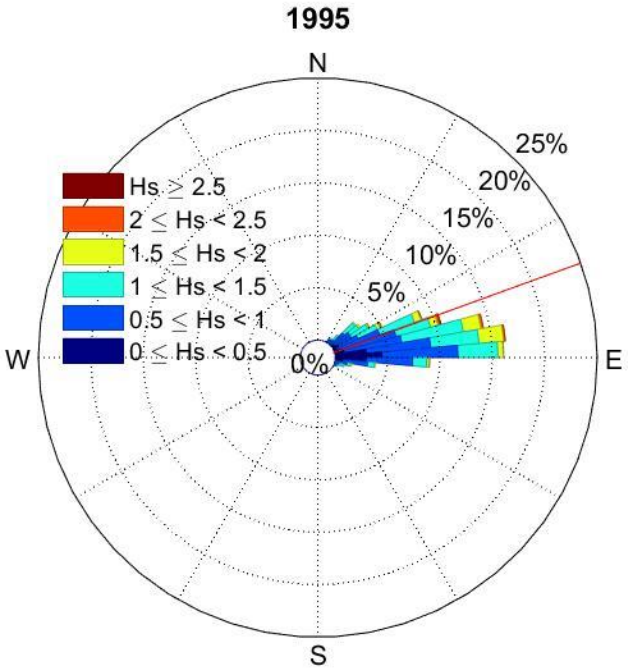
1995
N
S
W
E
25%
20%
15%
10%
5%
0%
Hs ≥ 2.5
2 ≤ Hs < 2.5
1.5 ≤ Hs < 2
1 ≤ Hs < 1.5
0.5 ≤ Hs < 1
0 ≤ Hs < 0.5

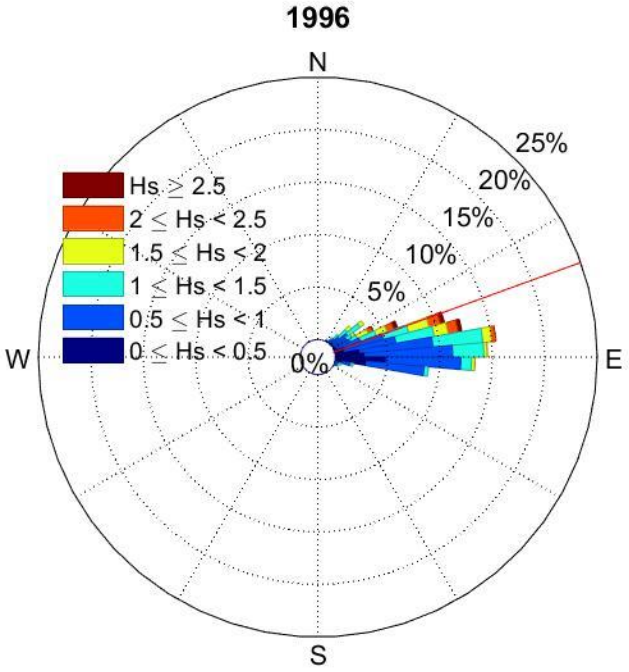
1996
N
S
W
E
25%
20%
15%
10%
5%
0%
Hs ≥ 2.5
2 ≤ Hs < 2.5
1.5 ≤ Hs < 2
1 ≤ Hs < 1.5
0.5 ≤ Hs < 1
0 ≤ Hs < 0.5

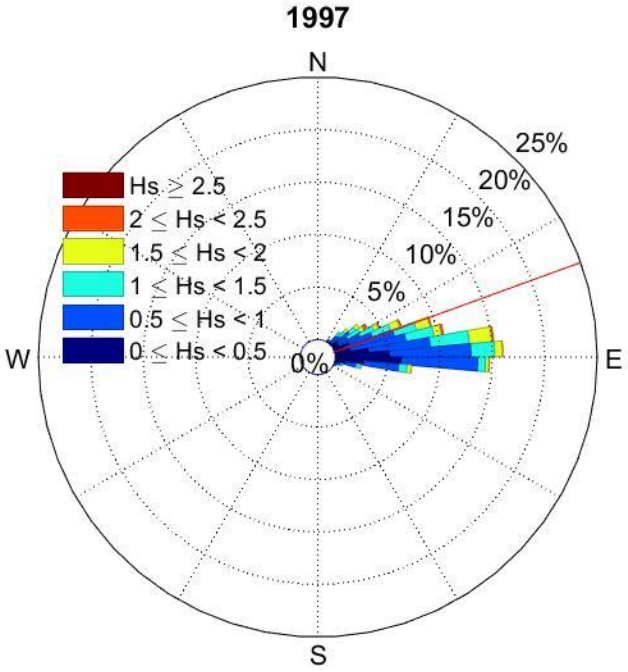
1997
N
S
W
E
25%
20%
15%
10%
5%
0%
Hs ≥ 2.5
2 ≤ Hs < 2.5
1.5 ≤ Hs < 2
1 ≤ Hs < 1.5
0.5 ≤ Hs < 1
0 ≤ Hs < 0.5

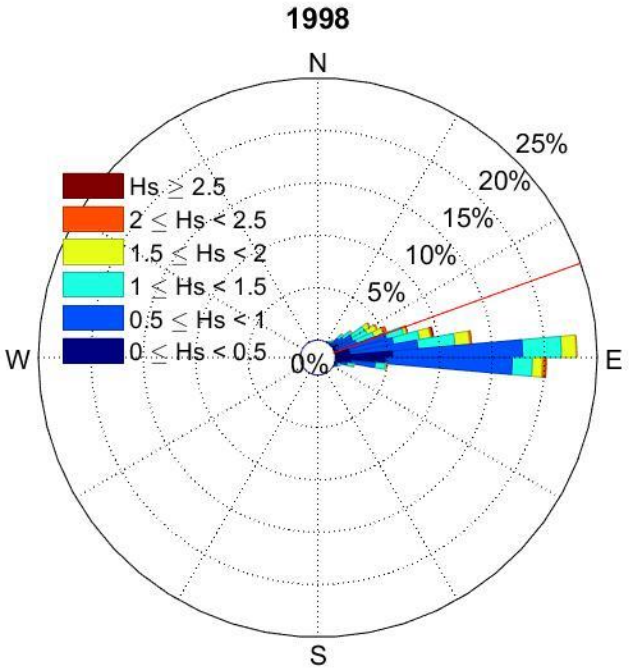
1998
N
E
S
W
25%
20%
15%
10%
5%
0%
Hs ≥ 2.5
2 ≤ Hs < 2.5
1.5 ≤ Hs < 2
1 ≤ Hs < 1.5
0.5 ≤ Hs < 1
0 ≤ Hs < 0.5

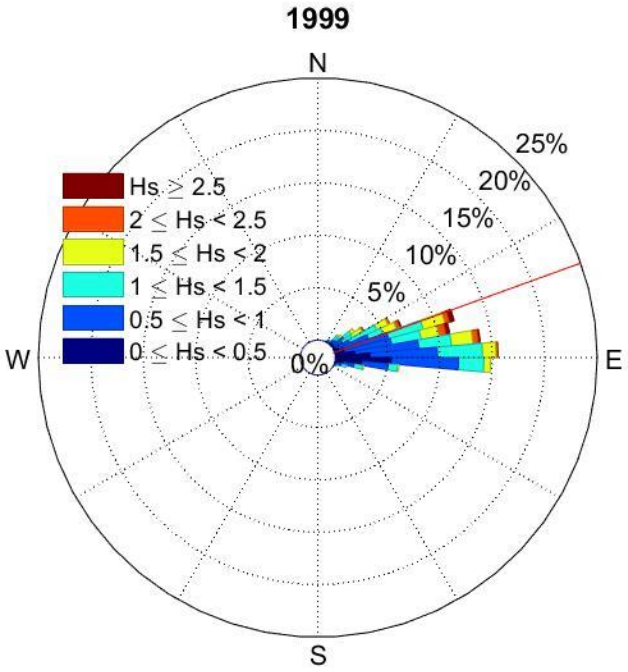
1999
N
E
S
W
25%
20%
15%
10%
5%
0%
Hs ≥ 2.5
2 ≤ Hs < 2.5
1.5 ≤ Hs < 2
1 ≤ Hs < 1.5
0.5 ≤ Hs < 1
0 ≤ Hs < 0.5

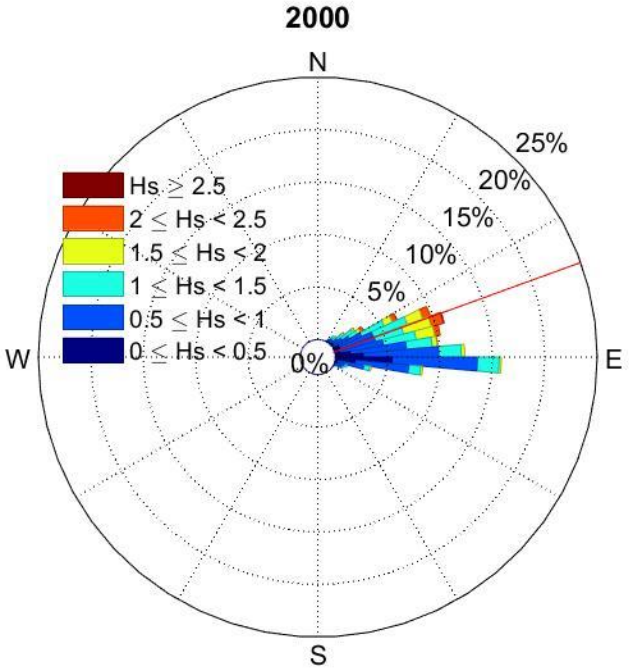
2000
N
E
S
W
25%
20%
15%
10%
5%
0%
Hs ≥ 2.5
2 ≤ Hs < 2.5
1.5 ≤ Hs < 2
1 ≤ Hs < 1.5
0.5 ≤ Hs < 1
0 ≤ Hs < 0.5

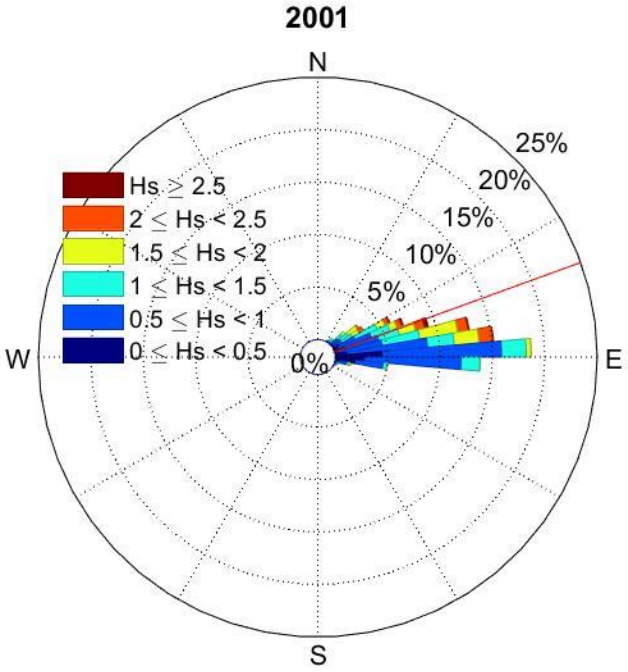
2001
N
E
S
W
25%
20%
15%
10%
5%
0%
Hs ≥ 2.5
2 ≤ Hs < 2.5
1.5 ≤ Hs < 2
1 ≤ Hs < 1.5
0.5 ≤ Hs < 1
0 ≤ Hs < 0.5

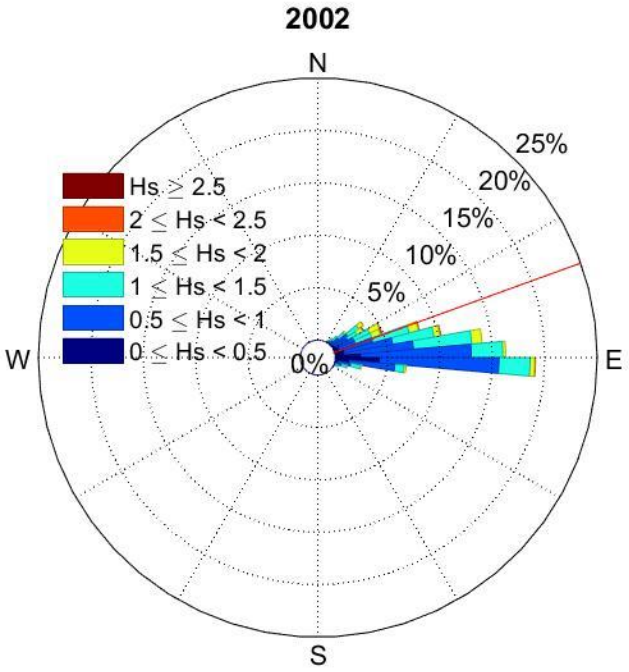
2002
N
E
S
W
25%
20%
15%
10%
5%
0%
Hs ≥ 2.5
2 ≤ Hs < 2.5
1.5 ≤ Hs < 2
1 ≤ Hs < 1.5
0.5 ≤ Hs < 1
0 ≤ Hs < 0.5

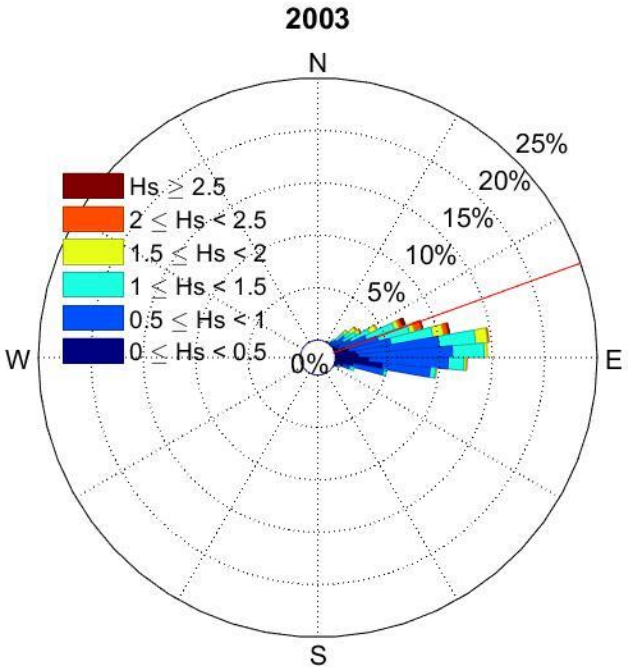
2003
N
E
S
W
25%
20%
15%
10%
5%
0%
Hs ≥ 2.5
2 ≤ Hs < 2.5
1.5 ≤ Hs < 2
1 ≤ Hs < 1.5
0.5 ≤ Hs < 1
0 ≤ Hs < 0.5

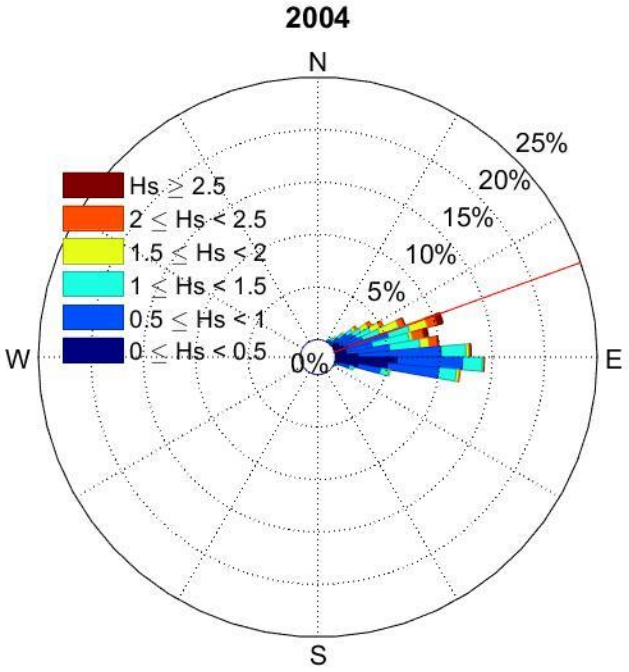
2004
N
E
S
W
25%
20%
15%
10%
5%
0%
Hs ≥ 2.5
2 ≤ Hs < 2.5
1.5 ≤ Hs < 2
1 ≤ Hs < 1.5
0.5 ≤ Hs < 1
0 ≤ Hs < 0.5

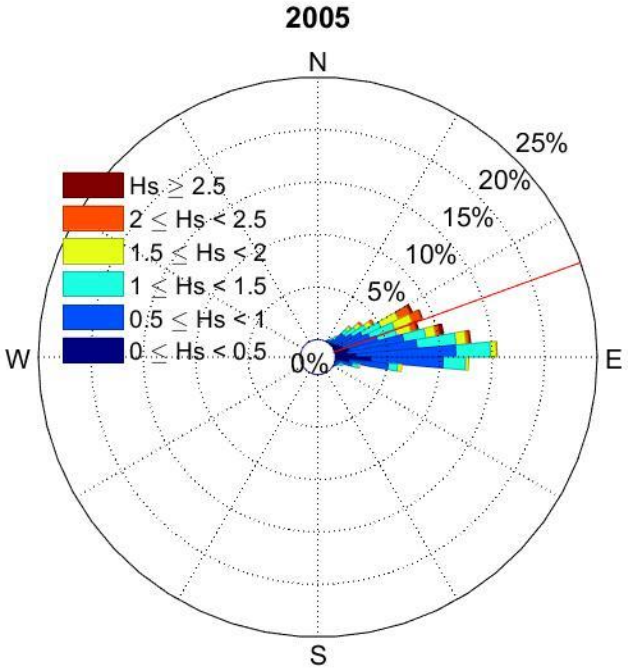
2005
N
E
S
W
25%
20%
15%
10%
5%
0%
Hs ≥ 2.5
2 ≤ Hs < 2.5
1.5 ≤ Hs < 2
1 ≤ Hs < 1.5
0.5 ≤ Hs < 1
0 ≤ Hs < 0.5

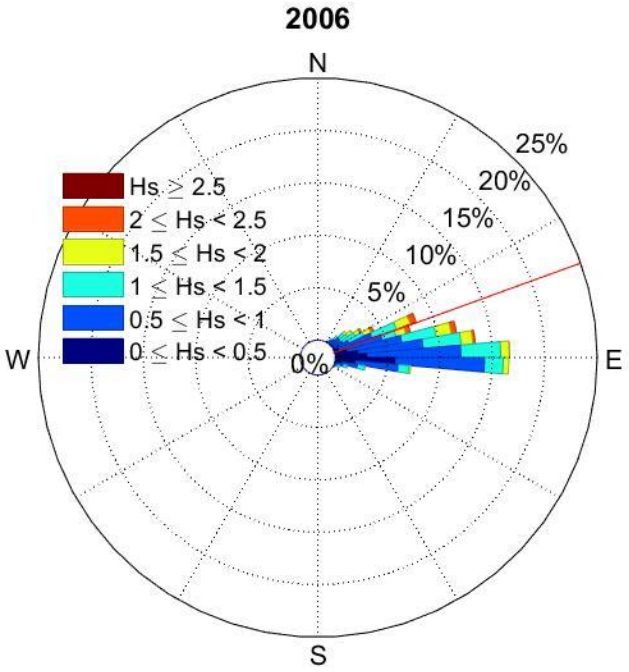
2006
N
E
S
W
25%
20%
15%
10%
5%
0%
Hs ≥ 2.5
2 ≤ Hs < 2.5
1.5 ≤ Hs < 2
1 ≤ Hs < 1.5
0.5 ≤ Hs < 1
0 ≤ Hs < 0.5

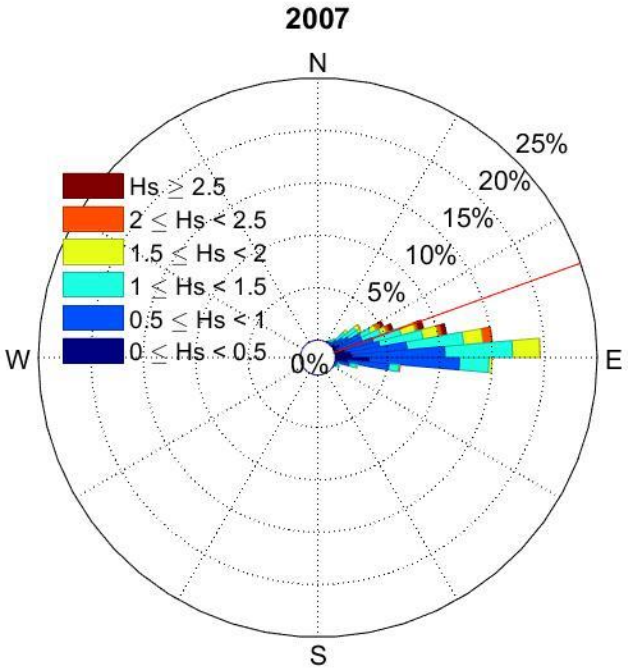
2007
N
E
S
W
25%
20%
15%
10%
5%
0%
Hs ≥ 2.5
2 ≤ Hs < 2.5
1.5 ≤ Hs < 2
1 ≤ Hs < 1.5
0.5 ≤ Hs < 1
0 ≤ Hs < 0.5

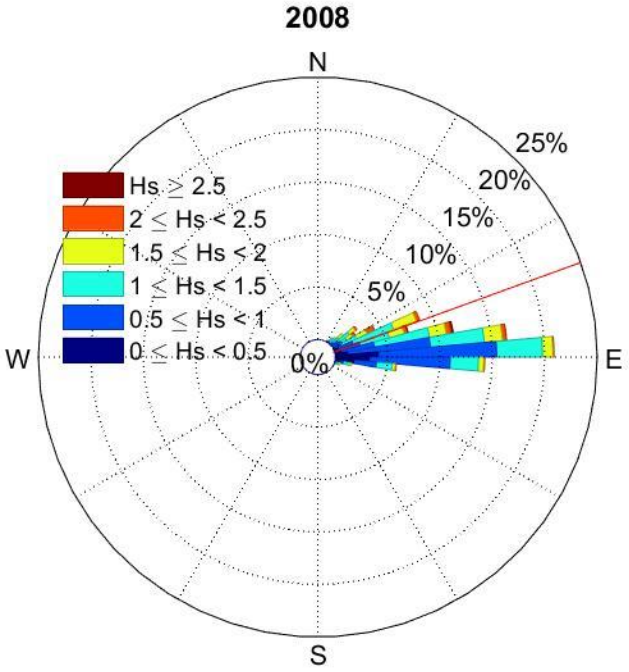
2008
N
E
S
W
25%
20%
15%
10%
5%
0%
Hs ≥ 2.5
2 ≤ Hs < 2.5
1.5 ≤ Hs < 2
1 ≤ Hs < 1.5
0.5 ≤ Hs < 1
0 ≤ Hs < 0.5

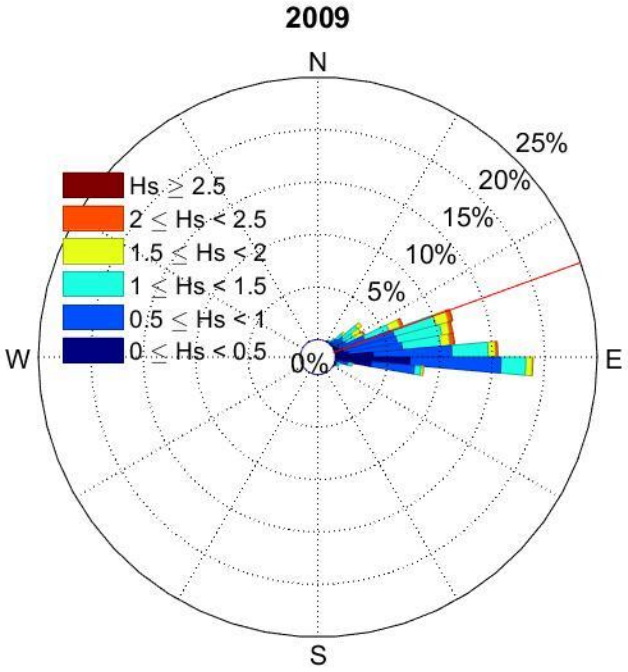
2009
N
E
S
W
25%
20%
15%
10%
5%
0%
Hs ≥ 2.5
2 ≤ Hs < 2.5
1.5 ≤ Hs < 2
1 ≤ Hs < 1.5
0.5 ≤ Hs < 1
0 ≤ Hs < 0.5

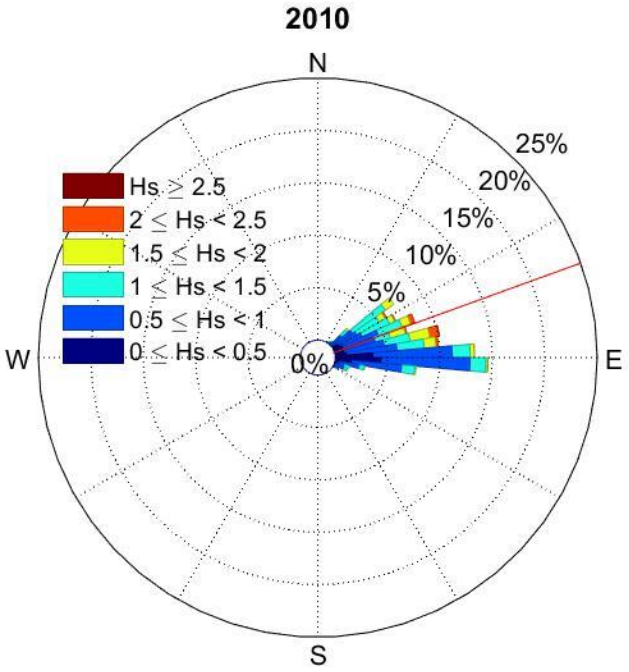
2010
N
E
S
W
25%
20%
15%
10%
5%
0%
Hs ≥ 2.5
2 ≤ Hs < 2.5
1.5 ≤ Hs < 2
1 ≤ Hs < 1.5
0.5 ≤ Hs < 1
0 ≤ Hs < 0.5

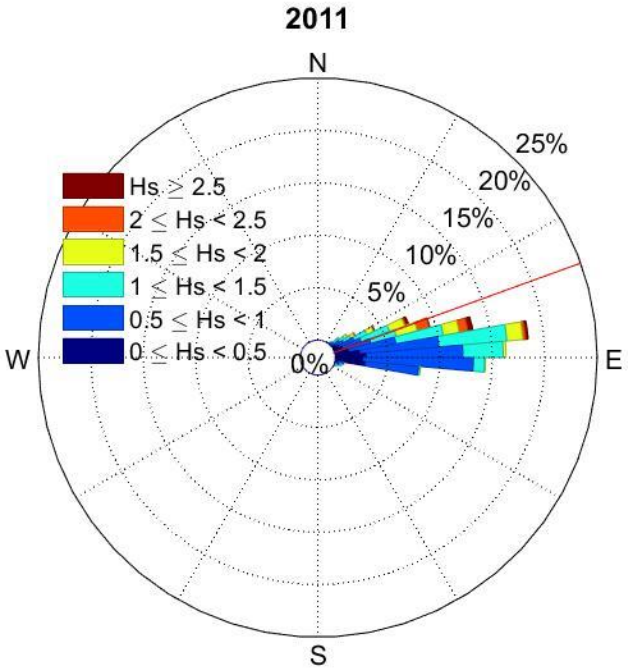
2011
N
E
S
W
25%
20%
15%
10%
5%
0%
Hs ≥ 2.5
2 ≤ Hs < 2.5
1.5 ≤ Hs < 2
1 ≤ Hs < 1.5
0.5 ≤ Hs < 1
0 ≤ Hs < 0.5

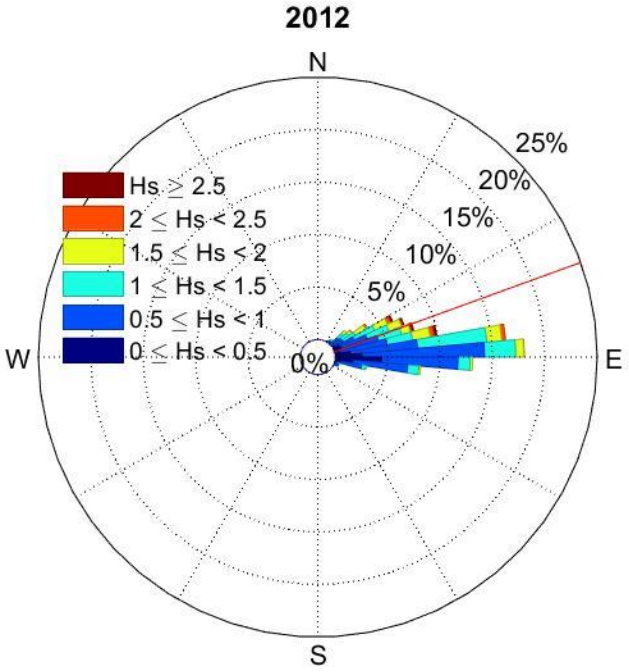
2012
N
E
S
W
25%
20%
15%
10%
5%
0%
Hs ≥ 2.5
2 ≤ Hs < 2.5
1.5 ≤ Hs < 2
1 ≤ Hs < 1.5
0.5 ≤ Hs < 1
0 ≤ Hs < 0.5

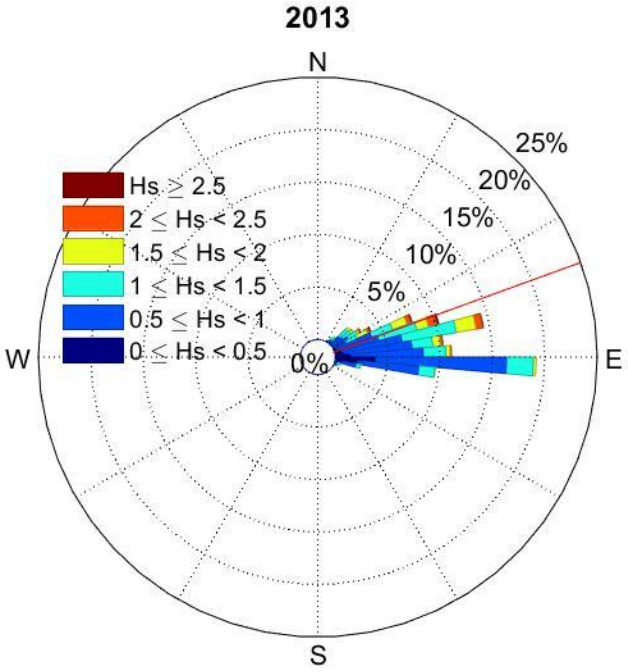
2013
N
E
S
W
25%
20%
15%
10%
5%
0%
Hs ≥ 2.5
2 ≤ Hs < 2.5
1.5 ≤ Hs < 2
1 ≤ Hs < 1.5
0.5 ≤ Hs < 1
0 ≤ Hs < 0.5

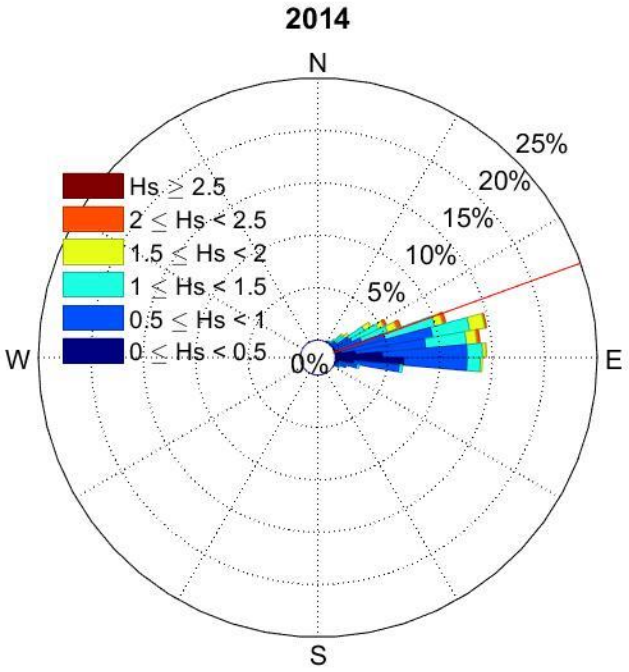
2014
N
E
S
W
25%
20%
15%
10%
5%
0%
Hs ≥ 2.5
2 ≤ Hs < 2.5
1.5 ≤ Hs < 2
1 ≤ Hs < 1.5
0.5 ≤ Hs < 1
0 ≤ Hs < 0.5

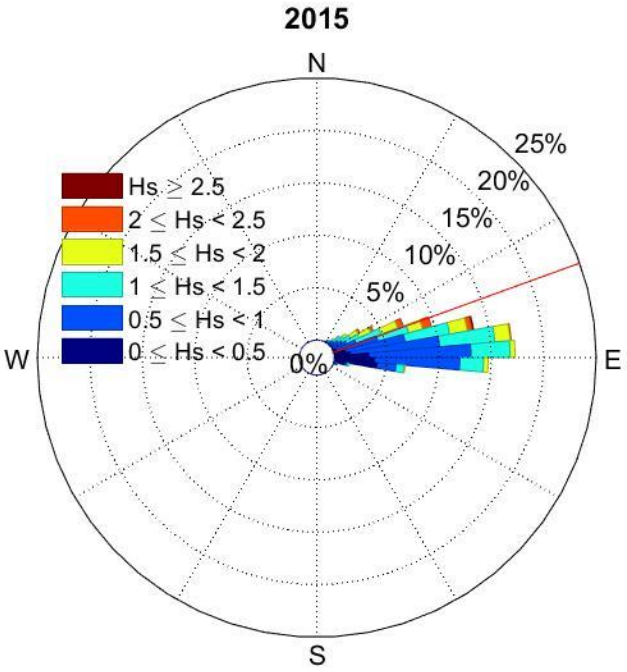
2015
N
E
S
W
25%
20%
15%
10%
5%
0%
Hs ≥ 2.5
2 ≤ Hs < 2.5
1.5 ≤ Hs < 2
1 ≤ Hs < 1.5
0.5 ≤ Hs < 1
0 ≤ Hs < 0.5

Appendix B – Annual Time Series of Offshore MSC50 Hindcast, Nearshore STWAVE+ Results, and Spessard ADCP Data

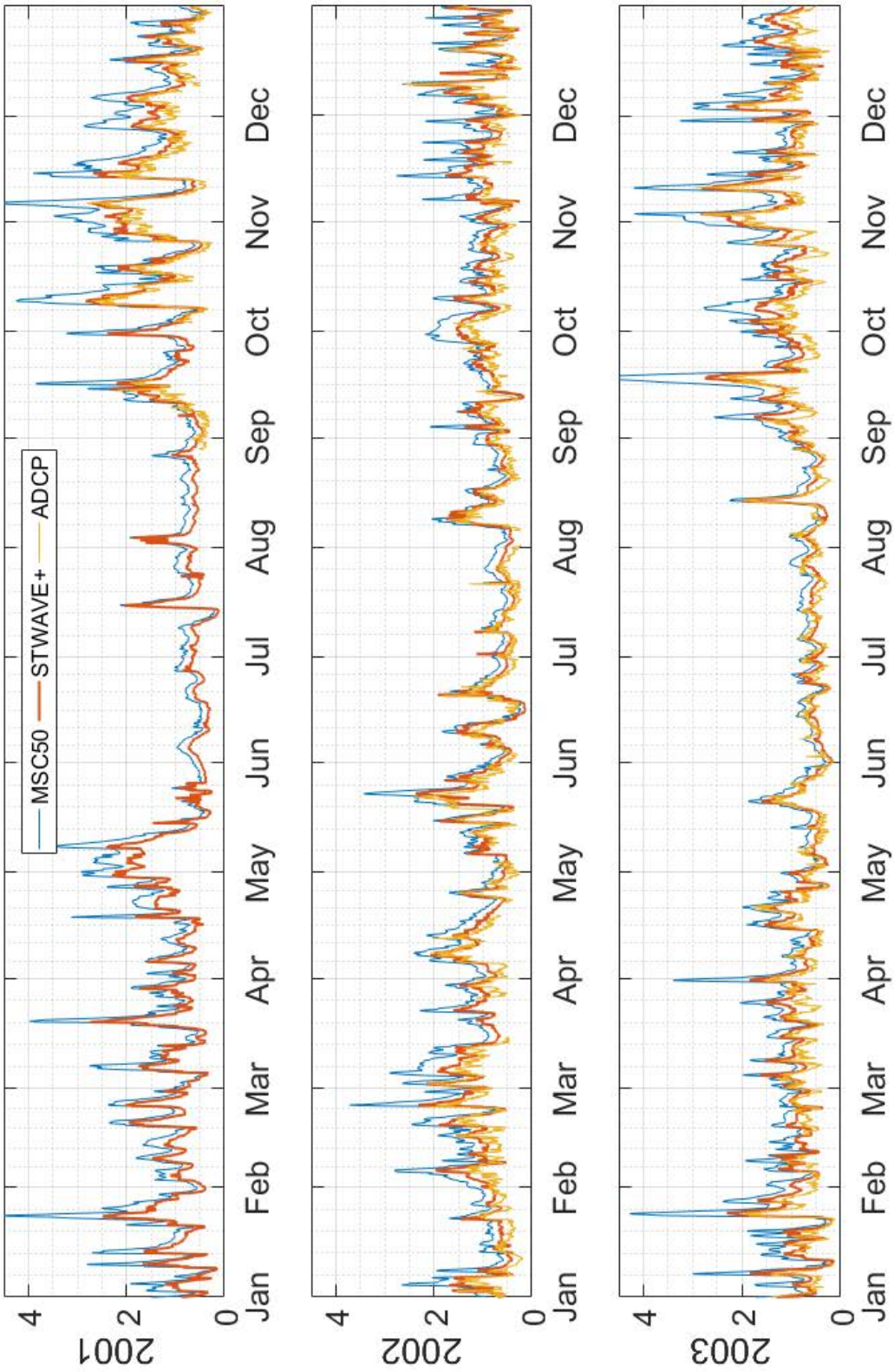
MSC50
STWAVE+
ADCP
2001
2002
2003
0
2
4
Jan
Feb
Mar
Apr
May
Jun
Jul
Aug
Sep
Oct
Nov
Dec

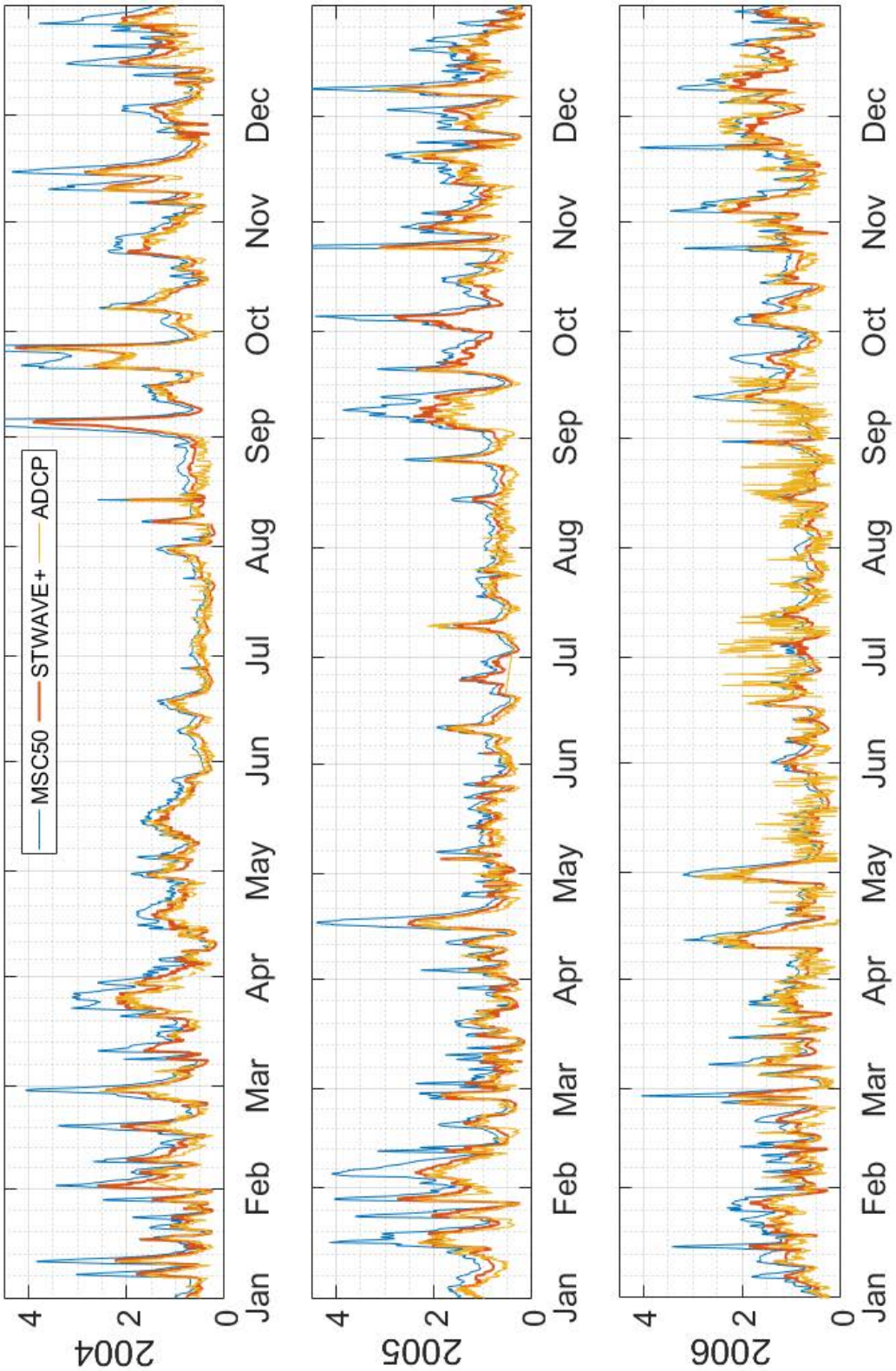
MSC50
STWAVE+
ADCP
2004
2005
2006
0
2
4
Jan
Feb
Mar
Apr
May
Jun
Jul
Aug
Sep
Oct
Nov
Dec

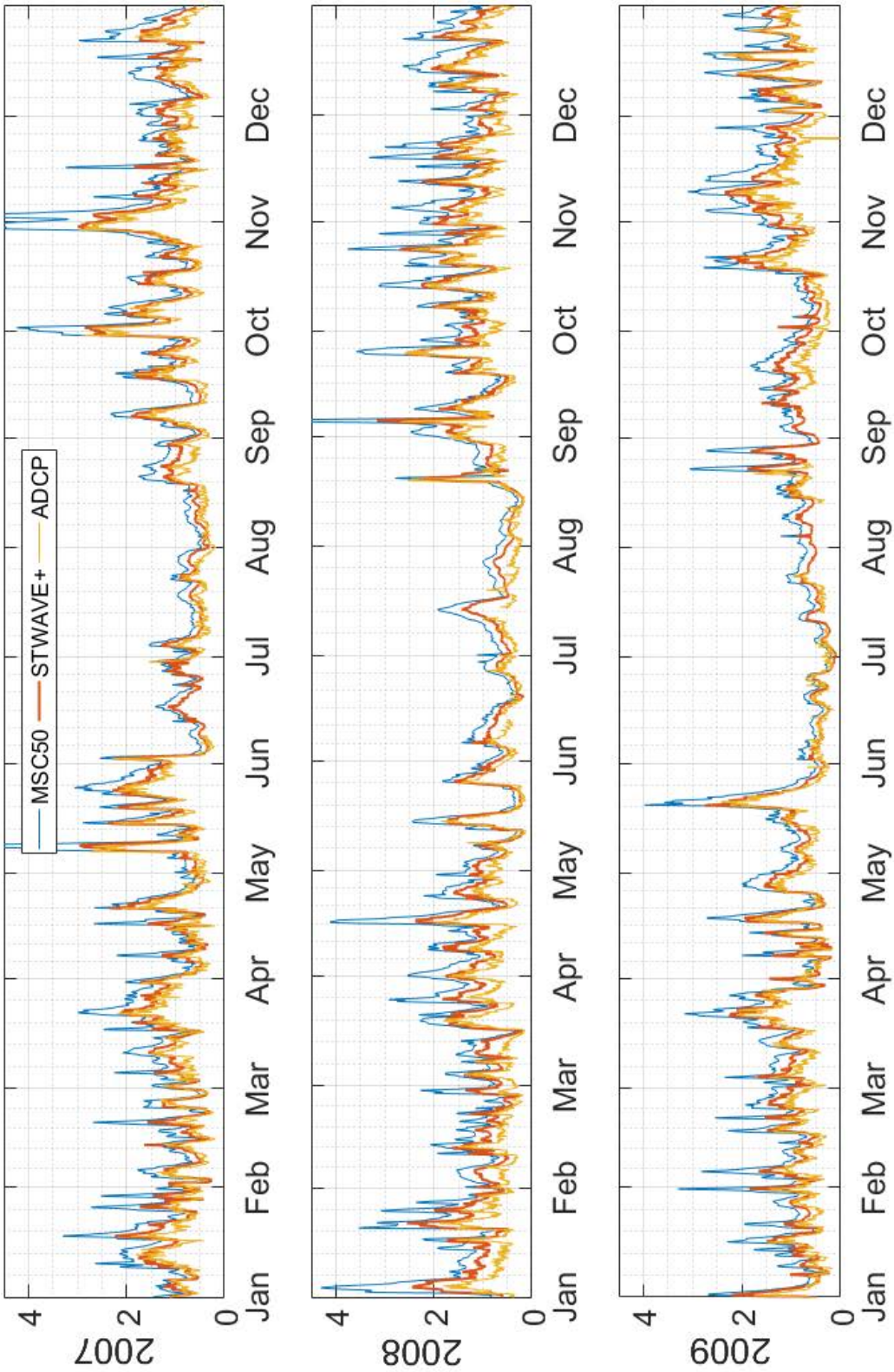
MSC50
STWAVE+
ADCP
2007
2008
2009
0
2
4
Jan
Feb
Mar
Apr
May
Jun
Jul
Aug
Sep
Oct
Nov
Dec

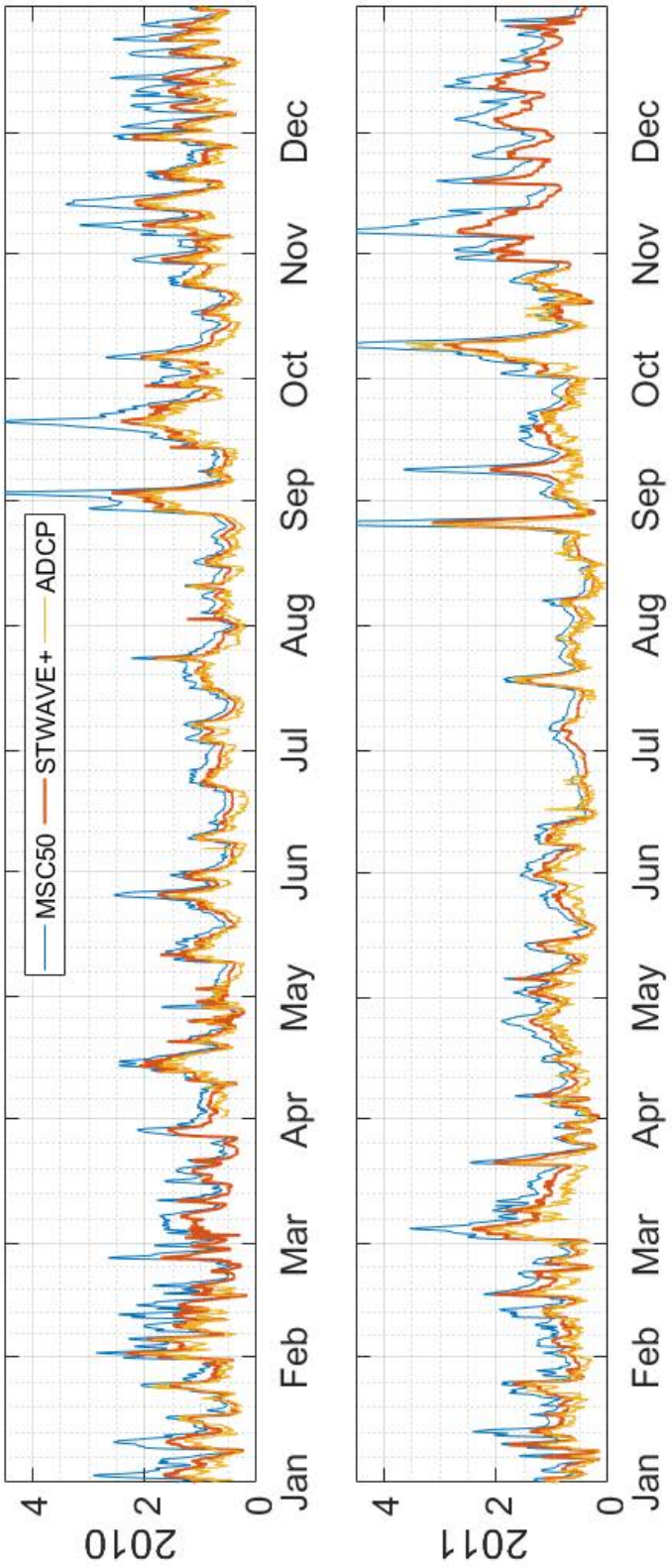
MSC50
STWAVE+
ADCP
2010
2011
0
2
4
Jan
Feb
Mar
Apr
May
Jun
Jul
Aug
Sep
Oct
Nov
Dec